HAPTIC DEVICE DESIGN

A THESIS SUBMITTED TO
THE GRADUATE SCHOOL OF NATURAL AND APPLIED SCIENCES
OF
MIDDLE EAST TECHNICAL UNIVERSITY

BY

ÖZGÜR BAŞER

IN PARTIAL FULFILLMENT OF THE REQUIREMENTS
FOR
THE DEGREE OF MASTER OF SCIENCE
IN
MECHANICAL ENGINEERING DEPARTMENT

JANUARY 2006

Approval of the Graduate School of Natural and Applied Sciences

_____

Prof. Dr. Canan ÖZGEN

Director

I certify that this thesis satisfies all the requirements as a thesis for the degree of Master of Science.

_____

Prof. Dr. S. Kemal İDER

Head of Department

This is to certify that we have read this thesis and that in our opinion it is fully adequate, in scope and quality, as a thesis for the degree of Master of Science.

_____	_____
Asst. Prof. Dr. Buğra KOKU	Asst. Prof. Dr. E. İlhan KONUKSEVEN
Co-Supervisor	Supervisor

Examining Committee Members

Prof. Dr. Kemal ÖZGÖREN (METU, ME) _____

Asst. Prof. Dr. E. İlhan KONUKSEVEN (METU, ME) _____

Prof. Dr. TUNA BALKAN (METU, ME) _____

Asst. Prof. Dr. Buğra KOKU (METU, ME) _____

Asst. Prof. Dr. Afşar SARANLI (METU, EE) _____

I hereby declare that all information in this document has been obtained and presented in accordance with academic rules and ethical conduct. I also declare that, as required by these rules and conduct, I have fully cited and referenced all materials and results that are not original to this work.

Name, Last name : Özgür BAŞER

Signature :

ABSTRACT

HAPTIC DEVICE DESIGN

BAŞER, Özgür

MS., Department of Mechanical Engineering
Supervisor: Asst. Prof. Dr. E. İlhan KONUKSEVEN
Co-Supervisor: Asst. Prof. Dr. Buğra KOKU

January 2006, 119 pages

Haptic devices are used to provide multi-modal data transfer between haptic users and computers in virtual reality applications. They enable humans to take force and tactile feedback from any virtual or remote objects. Haptic devices also facilitate the use of data collected from a real object in the virtual environment.

Usage of the haptic devices increase more and more in industrial, educational and medical applications in parallel with development of virtual reality technology. As virtual reality technology requires interdisciplinary study with related to its application areas, it creates a lot of different specific working areas (Haptic interface design, freeform model, surgical operations in virtual environment etc.). Especially, some complex modifications which require hand-working can be

performed with the system having great potential in medical applications (Brain surgery without error and operations which require great skill etc.). This is only one of the implementations of haptic devices in digital environment.

Aim of this study is to design and manufacture a 7 DOF (degrees of freedom) haptic device which serves the mentioned application areas. All different haptic devices in literature have maximum 6 DOF. The designed 7 DOF haptic device has about 20% extra working space and more flexible working capability compared to the other haptic devices with the similar link lengths and joint limitations.

This study is important in terms of the development of haptic devices in the world as well as spreading of haptic devices and its applications in Turkey.

Keywords: Haptic device, Virtual reality, Force feedback, Haptic modeling

ÖZ

HAPTİK CİHAZ TASARIMI

BAŞER, Özgür

Yüksek Lisans, Makina Mühendisliği Bölümü
Tez Yöneticisi : Yrd. Doç. Dr. E. İlhan KONUKSEVEN
Yardımcı Tez Yöneticisi : Yrd. Doç. Dr. Buğra KOKU

Ocak 2006, 119 sayfa

Haptik cihaz, kullanıcı ile bilgisayar arasında üç boyutlu veri transferi sağlayan bir cihazdır. Bu cihaz kullanıcıya sanal ortamdaki bir nesneyi görmenin yanında, bu sanal nesneye dokunma olanağı da sağlar. Aynı zamanda bu cihaz ile gerçek bir nesneden veriler alınarak bu verilerin sanal ortamda kullanımı da gerçekleştirilebilir.

Günümüzde sanal gerçeklik teknolojisinin gelişimine paralel olarak haptik cihazlarının kullanımı, sanayi, egitim ve tıp alanlarında gittikçe artmakdadır. Bu teknolojinin değişik uygulama alanları, farklı bilim dallarına ait disiplinlerarası çalışmaları gerektirdiğiden, kendi içinde özgün çalışma konularını da

yaratmaktadır (Haptik arayüz tasarımı, serbest modelleme, sanal ortamda ameliyat eğitimi vb.). Medikal uygulamalarda önemli potonsiyele sahip bu teknoloji ile daha önceleri el işçiliği ile yapılmak zorunda kalınan karmaşık modifikasyonlar gerçekleştirilebilmektedir (beyin cerrahisinde hata kabul etmeyen, ustalık ve ameliyat öncesi uzun uğraşlar gerektiren operasyonlar). Bu örnek haptik cihazlar ile dijital ortamda gerçekleştirilebilecek olan uygulamalardan sadece bir tanesidir.

Bu tez kapsamında, bahsedilen uygulama alanlarına yönelik 7 serbestlik dereceli bir haptik cihaz tasarlanıp üretilmiştir. Günümüze kadar tasarlanmış olan bütün haptik cihazlar maksimum altı serbestlik derecesine sahiptirler. Tasarlanan 7 serbestlik dereceli haptik cihaz, bugüne kadar üretilmiş aynı uzuv uzunlukları ve eklem değişkenlerine sahip diğer haptik cihazlar ile karşılaştırıldığında; yaklaşık %20 daha büyük bir çalışma hacmine ve daha esnek bir çalışma kabiliyetine sahiptir.

Bu çalışma; Dünya'daki haptik cihazların geliştirilmesi ve Türkiye'deki haptik cihazların ve uygulama alanlarının yaygınlaşması açısından son derece önemlidir.

Anahtar Sözcükler: Haptik cihaz, Sanal gerçeklik, Kuvvet geribesleme, Haptik modelleme

ACKNOWLEGMENTS

I would like to thank my thesis supervisor Asst. Prof. Dr. E. İlhan Konukseven and co-supervisor Asst. Prof. Dr. Buğra Koku for providing me this research opportunity, guiding me throughout the study.

I would like to express my gratitude to Res. Asst. Orhan Ölçücüoğlu, Mehmet Zahmakıran, Gökhan Bayar, and Ömer Necati Cora for their encouragement, continuous help. METU BILTIR – CAD/CAM and Robotics Center, the staff of the center and especially technician Halit Şahin are gratefully acknowledged.

I am deeply grateful to my father, mother and brother for their support, encouragement, trust.

Lastly, I would like to send my special thanks to my wife for her endless love.

TABLE OF CONTENTS

LIST OF TABLES

TABLE

LIST OF FIGURES

FIGURE

LIST OF SYMBOLS

θ_i	Joint variables of manipulator
d_i	Joint offsets of manipulator
a_i	Effective link lengths of manipulator
α_i	Twist angles of manipulator
$\hat{C}$	Transformation matrix of the tip point
$\vec{r}$	Wrist point location in vector form
$\overline{r}$	Wrist point location in matrix form
$\vec{u}_1, \vec{u}_2, \vec{u}_3$	Unit vectors of Cartesian coordinates
$e^{\tilde{u}_k \theta_k}$	Exponential rotation matrix with k_{th} joint variable around $\vec{u}_k$
x, y, z	Base frame components of the wrist point location
r_1, r_2, r_3	Base frame components of the wrist point location
σ	Uncertainty coefficient
$M_{peak(yaw,pitch)}$	Required peak torque of haptic device around yaw and pitch axis
$M_{peak(roll)}$	Required peak torque of the haptic device around roll axis
$M_{\max(yaw,pitch)}$	Required max. cont. torque of haptic device around yaw, pitch axis

$M_{\max,roll}$	Required max. cont. torque of haptic device around roll axis
M_{Stall}	Stall torque of selected motors
$M_{\max,cont}$	Maximum continuous torque of the selected motors
i	Transmission ratio
η	Efficiency of selected gearheads
$\overline{Q}$	Driving torques of manipulator
$\overline{G}$	Gravity forces and torques of manipulator
$\overline{R}$	Task forces and torques of manipulator in wrist point
$\hat{J}_r$	Jacobean matrix with respect to the wrist point
$\overline{J}_{rk}$, $\overline{J}_{ak}$	Components of the Jacobean matrix
F_{peak}	Required peak forces of the haptic device
$F_{\max cont}$	Required maximum continuous forces of the haptic device
Q_{peak}	Peak driving torque corresponding to peak requirement
$Q_{\max cont}$	Max. cont. driving torque corresponding to max. cont. requirement
$\vec{r}_G$	Mass center of the haptic device in vector form
m_k, l_k	Masses and lengths of the positioning stage
m_c	Mass of the counterweight
R_Y	Rotational resolution around yaw axis
R_p	Rotational resolution around pitch axis
R_R	Rotational resolution around roll axis

q	Joint variables of manipulator in matrix form
$\Delta\overline{r}$	Change of the wrist point corresponding to encoder's counter angle

CHAPTER 1

INTRODUCTION

Haptic devices are manipulators used to provide force or tactile feedback to humans interacting with virtual or remote environments [1]. In literature, they are also called *force displays, master manipulators or hand controllers*. Haptic devices sense motion and force at the end effector and produce force feedback to the user based on the given simulation. Thus, these devices have also been called force-reflecting interfaces. Through the force feedback to the user, these devices can be used to simulate an environment containing objects with mass, friction and spring as well as virtual walls. They can also mimic the mechanical behavior of a tool and the interactions with their environment. With such capabilities, virtual reality applications are widely spreading in the area of engineering, medical operation, teleoperation, welfare and entertainment with the rapid development of computer and robotics technology. Haptic devices with force and tactile feedback to interactive user are indispensable to enhance virtual reality systems which require the feeling of touch in the mentioned application areas [2].

Many researchers have proposed different types of haptic devices such as exoskeleton type or tool type [3]. A parameter of basic concern about haptic device design is the number of degrees of freedom (DOF) of the device. One DOF might be rotation around one axis. Two DOF might be translational motion on a plane. Three DOF could be translational motion on a plane and also orientation within the plane. The progression continues with greater range of motion and

modeling capability. Devices which have high degrees of freedom increase the number of applications areas, but greatly increase design complexity and cost. Earlier generation, haptic devices have only parallel mechanisms or serial mechanisms. Parallel mechanisms have the characteristics of high rigidity, compactness, precise resolution compared with other mechanisms. Existing parallel mechanisms have usually disadvantages such as large inertia, difficult forward kinematics and small workspaces. Therefore, mechanisms of haptic device applications have been focused on serial-parallel mechanism for high stiffness and wide workspace.

1.1 Previous Work

In this section, previous works about haptic device design will be introduced. The most basic design of haptic device is a device with one DOF. The principal aim of such a device is to learn about haptic control and optimization. For instance, Brown and Colgate have learned about the physics and control in implementing a virtual wall using a one DOF device [4]. A schematic of the device is illustrated in Figure 1.1.

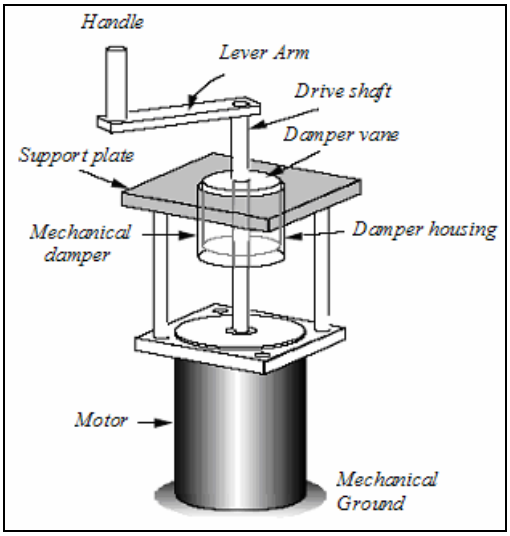

Figure 1.1 Brown and Colgate's One DOF Device

The origin of the haptic devices is actually based on the master-slave arms. Master arms were manipulated by the operator to command the slave arms in the task space and master arms were actuated so that they could create feedback forces to the operator. The computational requirements for master-slave systems were fairly minimal since the control could be accomplished joint to joint. While computers become more powerful, force reflecting hand controller (FRHC) was developed and it had better force resolution than the most master arms [5]. After all these developments, researchers began to realize that this new generation of hand controllers could be used for simulating virtual environments as well as reproducing the forces sensed in a real environment. In this context, FRHC's belong to a class of robotic mechanisms usually referred to haptic devices. By employing new materials and drive components, the current generation of haptic devices has come into existence, which is adequate for many applications. For instance, new components such as force and torque feedback sensors have been used in haptic devices due to the very low mass and its function on easy measurement capability in applications [6]. Recently, different types of haptic devices were developed and there are several haptic devices currently in production. These devices range from being oriented for specific users to being more general. There are three main categories in terms of haptic device configuration;

- Mechanical arm haptic devices
- Cable driven haptic devices
- Magnetic Levitation haptic devices

In the next sections, these different devices will be discussed. It is important to realize that many more devices exist, but these devices are selected in order to give a variety of basic haptic interface designs for these categories.

1.1.1 Mechanical Arm Haptic Devices

First mechanical arm haptic device was developed by MIT in 1993 and produced by Sensable Technology Inc. [7]. This type of haptic device is an electromechanical device that was originally developed to handle both force and motion. Not only this device handle force and motion, but it also interprets the geometry of objects as well as the layout of objects in virtual space. The mechanical arm haptic device is a full duplex device, because it allows the user to manipulate virtual objects as they get feedback from the virtual environment. In addition, this haptic device works in real-time providing precise user-environment feedback. Generally, these devices have 6 degrees of freedom (DOF) which include x, y, z, roll, pitch, and yaw. These types of devices have some advantages and disadvantages.

Advantages of mechanical arm haptic devices;

- Maximum exertable force and torque is very high
- Large workspace
- High stiffness with good configurations
- Low inertia with good configurations
- Low backlash with cable driven transmission system
- Various application areas

Disadvantages of mechanical arm haptic devices;

- High complexity
- High cost

Recently, there are different types of haptic devices which are produced by different companies, some of which are introduced;

The Phantom devices allow users to explore application areas that require force feedback in six degrees of freedom (6DOF). This device is produced by Sensable Technology Inc. [8]

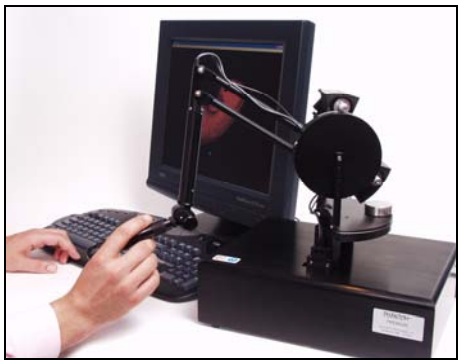

Figure 1.2 Phantom 1.5/6DOF Haptic Device

Figure 1.3 Phantom Desktop and Omni Haptic Devices

The "Freedom 6S" haptic device (a high fidelity force feedback device operating in 6 degrees of freedom) is similar to Phantom haptic device and provides the user with a realistic sense of touch in both virtual and real-world applications. This device was produced by MPB Technology Inc. [9].

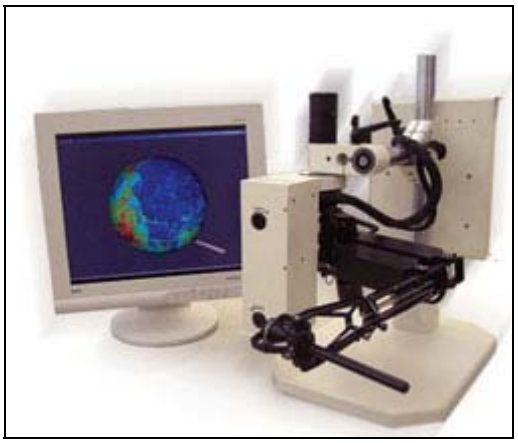

Figure 1.4 Freedom 6S Haptic Device

CyberForce is a force feedback armature that not only conveys realistic grounded forces to the hand and arm but also provides six-degrees-of-freedom positional tracking that accurately measures translation and rotation of the hand in three dimensions. This device was designed by Immersion Technologies Inc. [10].

Figure 1.5 CyberForce Haptic Device

The Delta haptic device is designed as a complete solution for most haptic applications. This device has only parallel mechanism. With its mechanical

design, the Delta 6 DOF is Force Dimension's most flexible and skillful haptic device [11].

Figure 1.6 Delta Haptic Device

The HapticMaster is 3 DOF, force-controlled haptic interface. It provides the user with a crisp haptic sensation and the power to closely simulate the weight and force found in a wide variety of human tasks. This device was designed by FCS Control Systems Inc. [12]

Figure 1.7 HapticMaster

1.1.2 Cable Driven Haptic Devices

Cable driven haptic devices are manipulators wherein the end effector link is supported by n-cables with n-tensioning motors. This haptic device consists of a hand-grip supported by n-cables controlled by n-independent tensioning actuators. Each cable actuator system includes a torque motor, cable, tensioning mechanism and force sensor.

Firstly, two cable driven haptic interfaces have been built and tested, the Texas 9-string [13] and the Spidar [14]. The Texas 9-string device was too bulky, suffered from cable interference, and failed to provide small feedback forces due to large actuator friction. The Spidar system was developed with four strings to give force-reflection to a single operator's finger tip. For six-DOF spatial operation, there must be at least six cables. Since cables can only exert tension on the hand-grip, there must be more than six cables to avoid configurations where the hand-grip can go slack. So, this system was extended to eight strings to include thumb feedback. Figure 1.8 shows eight cables independently controlled by eight actuators mounted to the frame of the device. This scenario represents actuation redundancy but not kinematics redundancy. That is, there are two extra motors which provide infinite choices for applying six-DOF wrench vectors, but the hand-grip has only six DOF. There are some advantages and disadvantages of cable driven haptic devices;

Advantages of this device,

- No backlash
- Low friction
- Low cost
- High stiffness

Disadvantages of this device

- Maximum exertable force is very low
- Vibration handicaps
- Low sensitivity
- Limited rotation

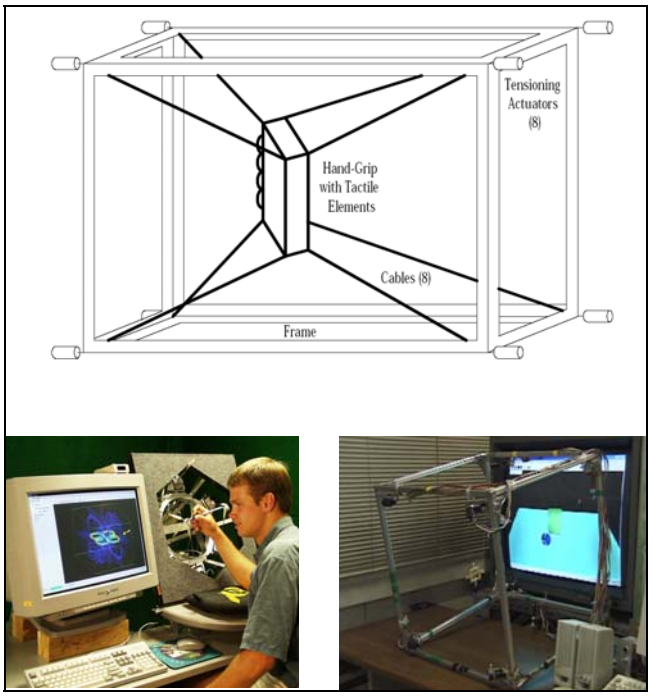

Figure 1.8 Cable Driven Haptic Devices

1.1.3 Magnetic Levitation Haptic Devices

Moving away from the devices mentioned earlier, other types of haptic devices are magnetic levitation haptic devices. Similar to most other haptic devices, the user has a tool that they can utilize with their fingers allowing them to interact with virtual environments. However, these new devices don't require a mechanical arm but are instead based on Lorentz Force Magnetic Levitation Theory. Most of

the work in this area of haptic research is being done at Carnegie Mellon University and is headed by Ralph Hollis [15].

Figure 1.9 Magnetic Levitation Haptic Devices

Magnetic levitation haptic devices consists of two major parts. The first part is the magnetic levitation device cabinet (maglev device). This contains the power supplies, amplifiers, and control processors. The second part sits on top of the "maglev" device and is the hand operation device. A user handle protrudes from a bowl where 6 magnetic coils are located. The handle is located in an ideal location for fingertip manipulation with the user's wrist resting on the rim of the bowl. There are some advantages and disadvantages of this type of device.

Advantages of this device;

- Does not require a mechanical arm
- Maximum peak force and torque is very high (50N & 6 Nm)
- High stiffness (25 N/mm)
- High sensitivity

Disadvantages of this device;

- These devices have small workspaces
- These devices can not take any data from a real object

Characteristics of all types of haptic devices are tabulated in Table 1.1. All comparisons were performed by considering their best designs.

Table 1.1 Characteristics of Different Haptic Devices

	Hybrid Mechanical Arm Haptic Devices	Serial Mechanical Arm Haptic Devices	Parallel Mechanical Arm Haptic Devices	Cable Driven Haptic Devices	Magnetic Levitation Haptic Devices
Workspace	HIGH	HIGH	LOW	LOW	LOW
Maximum Force	HIGH	HIGH	HIGH	LOW	HIGH
Maximum Torque	HIGH	HIGH	HIGH	LOW	HIGH
Backdrive Friction	LOW	HIGH	HIGH	LOW	LOW
Stiffness	HIGH	LOW	HIGH	HIGH	HIGH
Backlash	LOW	LOW	LOW	LOW	LOW
Resolution	HIGH	HIGH	HIGH	LOW	HIGH
Apparent Mass at Tip Point	LOW	HIGH	HIGH	LOW	LOW
Application Areas	HIGH	HIGH	HIGH	LOW	LOW

1.2 Application Areas for Haptic Devices

Haptic devices are increasingly being used in various types of applications to provide an improved dialogue between a computer interface and a user. The use of touch sense creates a new range of application. The scope of haptic applications looks set to grow further, with the release of significantly lower cost haptic devices for individuals or small institutions. There is an increased need to develop guidelines and standards for their use to allow a new group of developers to design effective haptic experiences. This required guideline is dedicated to exploring the relationships between haptic interface devices, human perception and computer applications.

In the virtual reality technology, the virtual reality modeling language (VRML) was developed in order to transmit dynamic virtual space over the internet. This makes communicating over great distances in three dimensional spaces. Possible gestures which carry large amounts of information in three dimensional spaces can be accomplished with the implementation of a haptic interface [16]. There are several ways to implement a haptic interface in a virtual space created with the virtual reality modeling language. Due to this improvement on haptic interfaces, application areas increased more and more. Recently, different haptic application areas have emerged.

1.2.1 Computer Aided Industrial Design

Haptic research has become a significant issue in industrial design recently by offering a revolutionary approach for combining physical and digital modeling. In industrial design, there are broad areas of research into this technology, using different kinds of haptic devices in more complex applications like three dimensional computer aided design modeling for virtual prototyping. With this technique, a user can import solid models directly from design packages, then convert specific regions to clay and rapidly add complex blends. When finished,

users can surface the clay areas within the system or export the model and surface in other surfacing tools. Alternatively, the combined model can be used for Rapid Prototyping or CAM. This mentioned operation can be performed by using virtual reality modeling language developed serve computer aided industrial design. Figure 1.10 shows an example about modifying a hair dryer by haptic device tools in the mentioned above sequence [8].

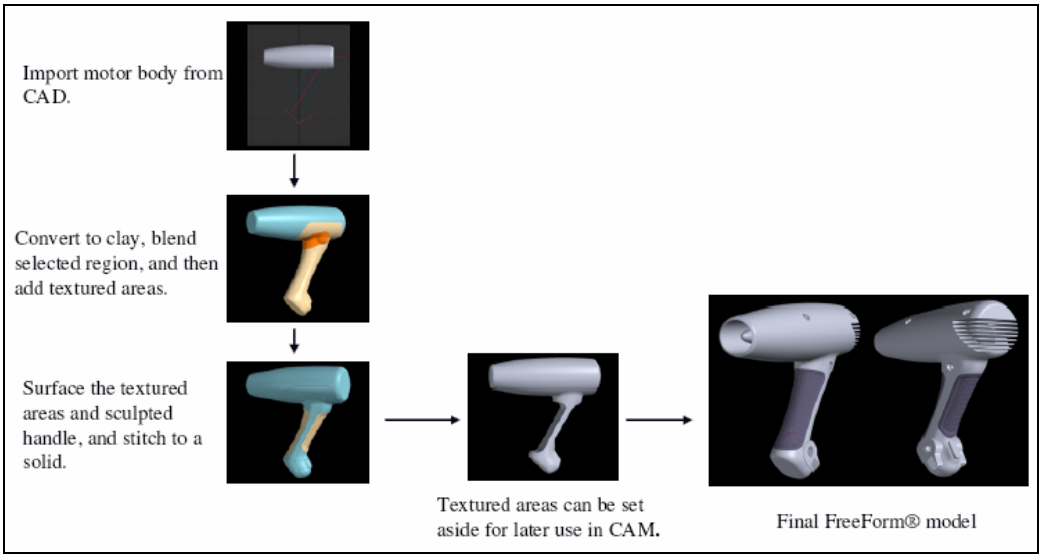

Figure 1.10 Computer Aided Industrial Design Application

1.2.2 Master-Slave Applications

Remote control of a robot (teleoperation) can be achieved by using a haptic device. These types of applications are used for telesurgery, industrial robot remote control, aircraft remote control in aerospace engineering etc. In a teleoperated manipulation system, the operator needs not only a visual representation but also a haptic representation of a system existing in a remote place. Those devices of haptic display, at present, have problems, such as insufficiencies in the display functions and complications in their constitutions.

Typically, there is a master robotic device (haptic device) designed to detect the user's commands by being directly held and manipulated by the user. At the remote location, a slave robot tries to mimic the motions of the master. The communication between master system and slave system is performed by an internet connection. In this way, haptic simulations of this nature have potential not only in virtual reality, but also for augmenting user interfaces in actual telerobotic systems. Typical applications include training tools for medical tasks, such as minimally remote invasive surgery and remote veterinary applications [17]. In the Figure 1.11, a teleoperation system within used any haptic device is shown.

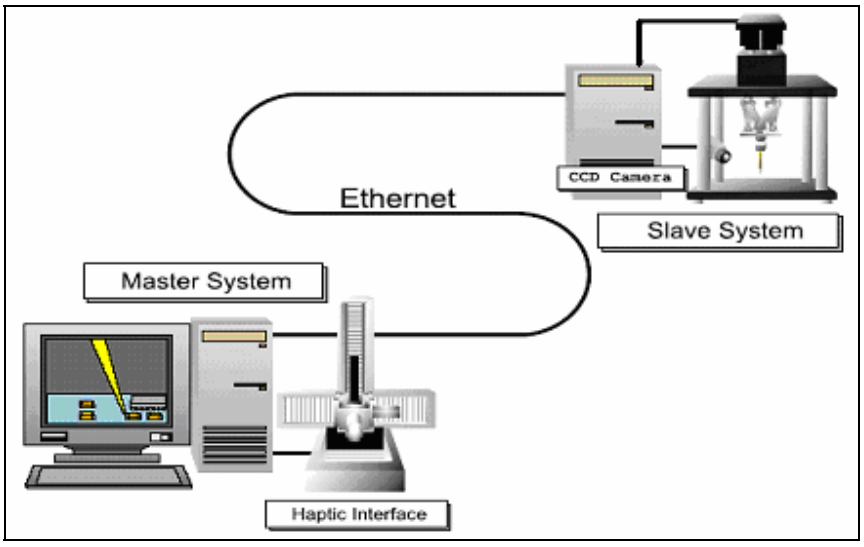

Figure 1.11 Master-Slave Application

1.2.3 Professional Education

In order to contribute to haptic applications, many different haptic tools were developed. For example, as part of the FreeForm® product family, the Free-Form Concept system lets sculptors and painters hand off designs in 3D. This approach reduces the amount of time spent. The FreeForm Concept system also accelerates

the sculpting and painting process by importing and exporting standard 2D and 3D file formats. Same processes can be used for dentist and painter education as well. In Figure 1.12, an example of sculptor education is shown.

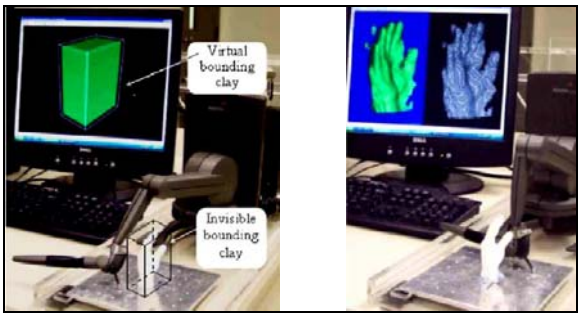

Figure 1.12 Sculptor Education with Haptic Device

1.2.4 Surgical Training

Haptic device technology has great potential for supporting medical training including the teaching of spatial and functional anatomy and the test of surgical procedures (penetrating, cutting and probing). Using a virtual reality training environment will reduce the need for expensive cadaver-based training and reduce the use of live patients in clinical training [18].

Figure 1.13 Surgical Training with Haptic Device

1.2.5 Surgical Assistant

A lot of surgical operations have been performed worldwide using a specially designed robotic apparatus. The robotic surgical tools within used haptic devices give the doctor finer control over delicate movements and more accurate pinpointing of the diseased area. This allows the surgery to be performed without fitting patients with a painful, cumbersome immobilizing frame that is needed for traditional surgical operations [18].

Figure 1.14 Surgical Assistant with Haptic Device

1.2.6 Implant and Tissue Design

Through the haptic device technology, bone or soft tissue prosthesis and implant models can be produced sensitively by using the any CT and MR data of a patient. In the following figure, generating a physical model from the digital model using a 3D printer and creating a mold and filling it with a colored silicone to match the patient's skin tone were shown by using haptic device.

Figure 1.15 Designed Prosthesis Model and Its Producing Steps

Clearly, haptic devices are used to provide force and tactile feedback to humans interacting with virtual or remote environments. They contribute to different types of application areas such as computer aided industrial design, teleoperation, professional education, surgical assistant, implant and tissue design for orthopedic operations. Furthermore, new application areas are explored more and more. High workspace and manipulation capability enable haptic devices to adapt the different application areas. For this purpose, a new haptic device, which has 7 degrees of freedom and large workspace, was designed and produced within the context of this thesis.

The outline of the thesis can be given as follows;

In Chapter 2, design consideration for haptic devices will be introduced. Kinematics design will be given in Chapter 3. Workspace analysis of our design will be given in Chapter 4. In Chapter 5, design procedure that we have followed will be presented. Finally, Chapter 6 touches on the results and conclusions.

CHAPTER 2

DESIGN CONSIDERATIONS

2.1 Overview

Haptic devices include several electronic and mechanical parts in contact with a user in order to create mechanical signals to user's hand and to sense other mechanical signals at same user's hand. Therefore, mechanical design and selecting a suitable configuration is very important in haptic device design. In this chapter, the design issues, design constraints and alternative mechanical configurations will be discussed, and a suitable configuration will be determined in order to satisfy these issues and constraints.

2.2 Design Issues and Constraints

There are different types of haptic devices mentioned in Chapter 1 together with the problems regarding to their performance and functions. These problems can be occurred due to the lack of satisfaction of human or mechanical constraints, which related to all forces, torques, mimics and virtual objects in a desired virtual environment. In order to achieve these constraints, a designer should concentrate on device ergonomics. A haptic device user should be able to use the device easily and reach any point in the desired virtual workspace. Therefore, the best suitable

design for this purpose can be a desktop device. Thus, the device will be in front of the user at chest level and should be able to reach any point in a desired virtual workspace. The other type of constraint for haptic device design is mechanical constraint. Mechanical constraints in a design define the degree of freedom and force capability of the system to meet the requirements of the user. Although there are some haptic devices high degrees of freedom and with good workspace, they do not provide required forces and torques at the endpoint for some applications. Even though some devices can provide required forces and torques, they do not have good workspace [19]. The other mechanical constraints for haptic devices are mass, inertia and back drive friction. In this thesis, we aimed to design a device satisfying the defined constraints with superior performance. So that, the device designed with low apparent mass, low inertia, low friction, high structural stiffness, backdrivability, very low backlash, high force bandwidth, absence of mechanical singularities in workspace, accessibility to the operator, compactness, an even "feel" through the workspace and good transportability.

Table 2.1 Haptic Device Design Criteria

Design Criterion	**Requirement**
Workspace	Maximized (A half sphere with radius 50 cm)
Peak Force	Maximized (10 N)
Peak Torque	Maximized (500 Nmm yaw, pitch, 130 Nmm roll)
Maximum Cont. Force	Maximized (1.5 N)
Maximum Cont. Torque	Maximized (180 Nmm yaw, pitch, 50 Nmm roll)
Stiffness	Maximized (1N/mm)
Backlash	Minimized (zero or very low)
Inertia	Minimized
Apparent mass at tip point	Minimized (150 g)
Backdrive friction	Minimized (0.2 N)

In the literature, there are some studies about haptic device design criteria and requirements [19]. These requirements based on both experimental results and design experiences, which performed by different researchers. The haptic device design criteria and the desired requirements are tabulated in Table 2.1. These criteria and requirements are explained under three main titles: workspace, force and torque at the end point, and dynamic performance.

2.2.1 Workspace

A haptic device should simulate the virtual environment in its workspace. This simulation requires large and useful workspace. So, it is important to obtain the possible largest workspace without sacrificing the performance of haptic device. The workspace can be defined as the useful volume of space in front of the user at chest level. The Phantom Premium 1.5/6 DOF haptic device has a translational workspace in the shape of 260mm (width) x 460mm (high) x 120mm (deep) [7]. This volume is sufficient for any haptic task in the chest level. Furthermore, this workspace volume in haptic devices can be enlarged for any specific tasks. Especially, spread of haptic device on industrial and medical applications requires larger workspace volume. Therefore, while selecting a suitable configuration to design a haptic device, workspace volume of the device should be taken into account. Researcher's experiences show that high degrees of freedom haptic devices are suitable for the applications where it is necessary to reach largest workspace [19]. A designer can reach larger workspace in two ways. The first one is to increase link lengths and the other method is to increase degrees of freedom using same link lengths. Increasing the link lengths in haptic devices causes high inertia, bad dynamic performance and low stiffness. Therefore, we decided to design 7 DOF haptic device without changing the effective link lengths in similar designs. There are certain tasks in haptic applications which require not only to touch one object from front side, but also to touch it from the other sides; top, bottom or back. The end effector should be able to rotate nearly 360 degrees about the pitch, yaw and roll axis of the handle in the desired workspace. Furthermore, it

is possible to reach any point from different positions with the designed 7 DOF haptic device's redundancy.

2.2.2 Force and Torque

The resultant force and torque values in haptic devices depend on several criteria such as motor torque, transmission ratio, inertia of the device and device friction. In order to reach required forces and torques in the desired workspace, these four parameters should be optimized. The transmission ratio for each actuator should be determined during the early stages of a design due to the maximum allowable backdrive friction. In order to avoid high backdrive friction, low transmission ratio should be selected (less than 10). Furthermore, transmission technique is also important in haptic device design. There are two different transmission techniques in practice: Gearhead transmission and Cable drive transmission.

Gearhead transmission is not an appropriate technique to be used in haptic design, since it causes high backlash and high backdrive friction due to the gear gaps and gear friction. Backdrive friction and backlash can be minimized by using cable driven transmission systems. Therefore, we used this type of transmission technique with a low transmission ratio in our design. Inertia and friction are the other parameters which affect the endpoint force and torque. These parameters should be minimized for the effectiveness of a haptic force feedback device. In order to achieve low inertia, moving part's mass should be very low and should be concentrated in the rotating center of each link. In order to achieve low friction, a designer should avoid from unnecessary contact surfaces and use high precision bearings. The last parameter to be decided is the motor torque and size.

Millman [20] performed simple experiments related to human subjects grasping with a 6 axis force sensor and obtained experimental results about forces and torques for most tasks. According to the Millman, 10 lb (44.48 N) force and 1 lb-ft (1.356 Nm) torque are upper limit for most tasks. The Phantom Premium 1.5/6

DOF haptic device has 8.5 N of peak force, 500 Nmm of peak torque about yaw and pitch axis, 130 Nmm of peak torque about roll axis and 1.4 N of maximum continuous translational force, 180 Nmm of maximum continuous torque about yaw and pitch axis, 50 Nmm of maximum continuous torque about roll axis [7]. The motors are selected in minimum size and mass for the minimum value of inertia in order to satisfy the dynamic performance of the haptic device. In this study, performing all necessary kinematics and dynamics design calculations, the motors are selected according to the specified values given in Table 2.1.

2.2.3 Dynamic Performance

Haptic users should easily feel any virtual environment by using a haptic device. The device should not be an awkward and heavy mechanism. Also, the device should simulate the virtual environment accurately. Therefore, two parameters need to be optimized: stiffness and backdrivabilty.

Structural stiffness should be maximized in order to minimize the unwanted deflection at the endpoint due to linkages, joints and backlash. The Phantom Premium 1.5/6 DOF haptic device has 4 N/mm of structural stiffness. This stiffness value can be achieved by considering the certain design facts. In this study, in order to overcome backlash cable driven transmission technique is used. In order to overcome joint deflections, high precision bearings and manufacturing methods are used. Besides, light and strong materials (aluminum, polyamide and composite) are used in order to minimize the deflection due to the stiffness of the linkages.

According to Townsend [21], there are two types of backdrivabilty: acceleration dependent and velocity dependent. Acceleration dependent backdrivabilty can be minimized by decreasing structural inertia and keeping the transmission ratio relatively small. Velocity dependent backdrivabilty can be minimized by decreasing the system friction. For this reason, the transmission ratios are selected

as 5, 8 and 10 in our design (If the motors are numbered from the base, transmission ratios can be listed as; 10 for first motor, 8 for second and third motors, 5 for fourth motor). The design is made of light materials and the mass center of the moving parts is concentrated on the device origin (support center of the device).

2.3 Alternative Configurations

Serial and parallel linkage mechanisms can be used in a manipulator design [22]. The serial manipulators have linkages, which are connected with joints from end to end and the last linkage is the end effector. Puma manipulator is an example of serial manipulator. Parallel manipulators are mechanisms, whose two different links are connected one to another and actuated by another third or fourth link. The simplest parallel manipulator is the four bar linkage. Steaward manipulator can given as an example of complex parallel manipulator.

In general, parallel mechanisms are stiffer than serial mechanisms and display a higher degree of accuracy. Parallel structures are very high stiffness for very small mass and their positioning accuracy is quite high. These characteristics of parallel manipulators make them suitable for machine tool applications. Unlike the serial mechanisms, parallel mechanisms have very simple inverse kinematics but difficult direct kinematics. This situation for serial manipulators is in direct contradiction. Serial manipulators for many applications have large workspace. These two different configurations have some advantages and disadvantages. In order to compare the manipulators easily, the following table can be constructed;

Table 2.2 Characteristics of Serial and Parallel Mechanisms

Characteristics	**Serial**	**Parallel**
Workspace	Large	Small
Forward Kinematics Computability Load	Low	High
Inverse Kinematics Computability Load	High	Low
Stiffness	Low	High

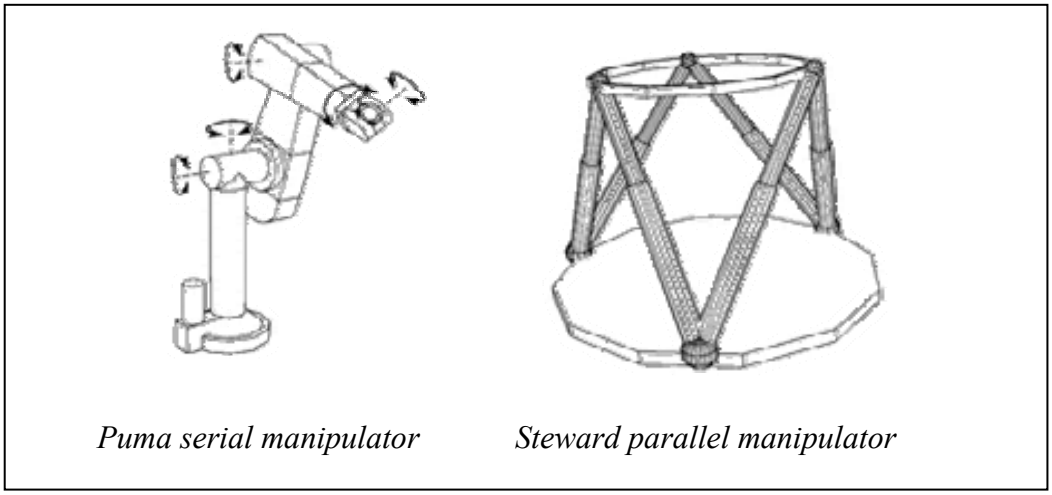

Puma serial manipulator *Steward parallel manipulator*

Figure 2.1 Serial and Parallel Mechanisms

2.3.1 Hybrid Parallel-Serial Configuration

A manipulator may have purely serial or purely parallel mechanisms. The advantages of these two mechanisms can be incorporated in one design. The configurations, which include parallel and serial linkages, are called hybrid configuration [22]. Using the hybrid configuration manipulator, high stiffness can be achieved relative to the manipulator with the similar workspace. In this study the designed 7 DOF haptic device does not include a complex serial manipulator,

nor does it include a complex parallel mechanism. Thus, the forward and inverse kinematics can be formulated explicitly with analytical methods. In our design, we used hybrid configuration. There are two 3 DOF serial manipulator in the design, the first 3 DOF serial link is on the base of the manipulator and other is at the end of the manipulator. These two 3 DOF serial links are incorporated to each other with a parallel mechanism.

2.4 Designed 7 DOF Haptic Device

The haptic device designed in this study has two 3 DOF serial configurations, which are connected to each other in parallel form. The movement of the end effector around yaw, pitch and roll axis is provided by 3 DOF serial configuration, which consists of 3 DC minimotors at the end. These 3 DC minimotors provide torques to the user for the required haptic applications. The movement of the complete arm mechanism is provided by the first 3 DOF serial configuration connected to the base. 3 DOF serial configuration and 1 DOF parallel configuration links are derived using four brushless DC motors. These four brushless DC motors provide forces to the user for the desired haptic applications.

Very light materials, such as aluminum and polyamide are used for the moving parts, while heavy material (steel) is used as a counter and support weight. In order to transmit the movement from DC minimotors to links at the end point, gearheads with very low backlash are used. Cable driven transmission systems are used in order to transmit the other movements from brushless motors to links. The CAD model and real photograph of the 7 DOF haptic device are given in Figure 2.2 and Figure 2.3.

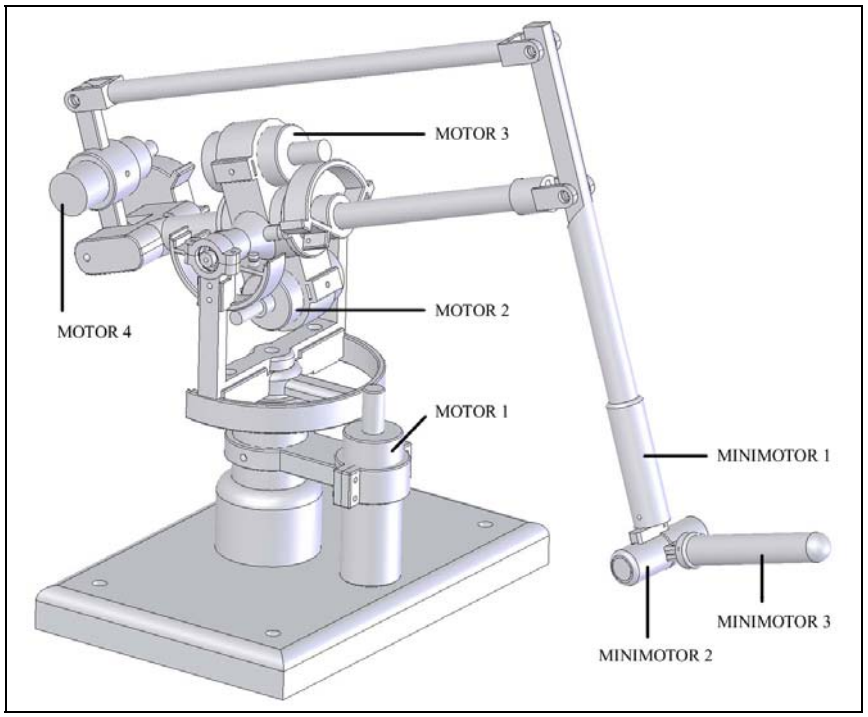

Figure 2.2 CAD Model of the Designed 7 DOF Haptic Device

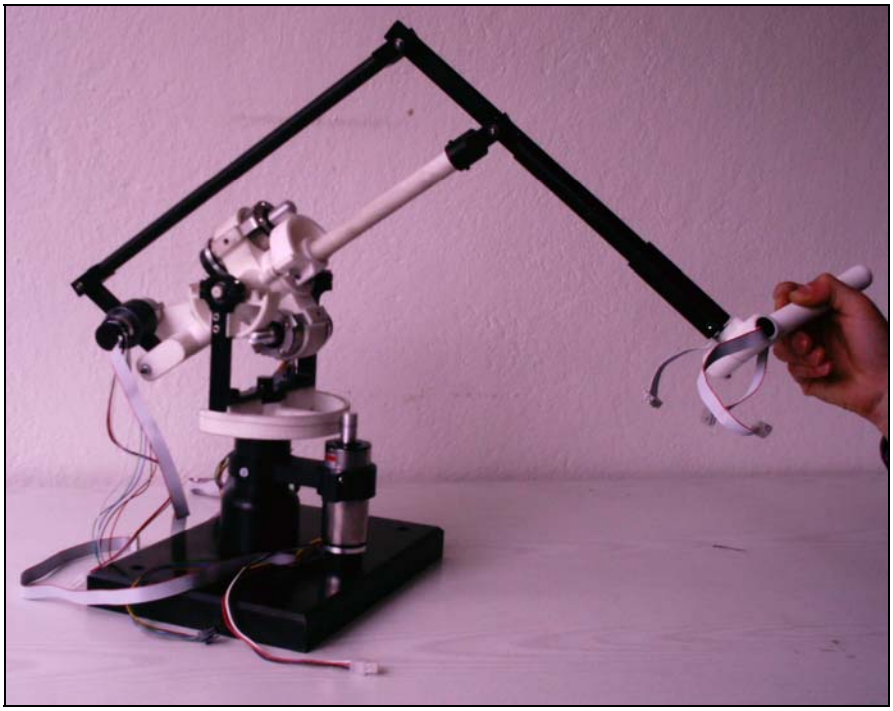

Figure 2.3 Real Photograph of the Designed 7 DOF Haptic Device

The haptic device designed in this study is similar to the human arm. The rotation axes of the first three links of the haptic device intersect at one point. This is similar for the last three rotation axes. Such a configuration reduces the kinematics design to a simpler state and provides larger workspace with the same effective link lengths. As we mentioned before, for the first three links, the motor torques are transmitted through the cable driven transmission system. Such a transmission system, especially for the selected kinematics configuration, requires more complex design procedure. In this design procedure, inertia effects caused from selected motor weights should also be considered. In order to avoid inertia effect caused from motor weights, the first link's motor is located on the base platform; second and third motors are located in opposite direction near to the rotation center for counterweighing the weight of each motor.

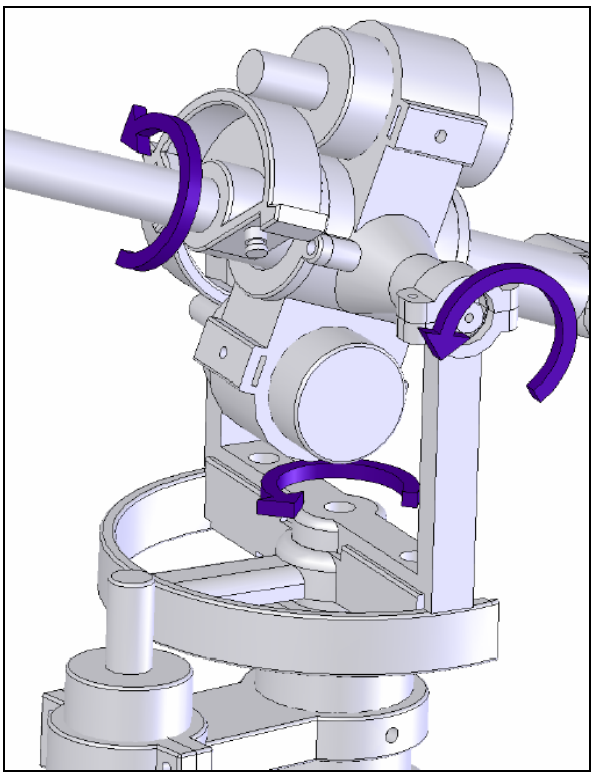

Figure 2.4 First 3 DOF Serial Configuration in the Start Point

Minimotors are used for the last three links similar to the first three links. For the last three links, motor torques are transmitted by the gearheads with very low backlash. Cable driven transmission system can not be used for the last three links because of the limited space. Besides, the backlashes in the last three joints are less important than the first three joints. Any backlash in the first three joints may cause high displacement at the end point of the haptic device.

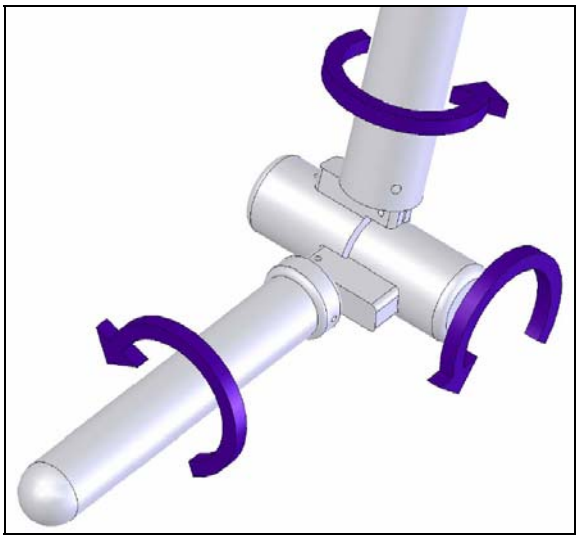

Figure 2.6 Last 3 DOF Serial Configurations in the End Point

High precision manufacturing technologies are used for the manufacturing of the device, all metal parts (aluminum, steel) are manufactured using the CNC machine tools and all polyamide parts are manufactured using rapid prototyping machines. Since polyamide is light, high strength and suitable for rapid prototyping equipment, it is used for the manufacturing of the complex parts. Carbon rods are used inside the long polyamide links in order to increase the stiffness. Using the combination of these two materials, light and high strength complex parts are manufactured.

CHAPTER 3

KINEMATICS DESIGN

3.1 Overview

Kinematics equations describe the position of the endpoint of a device in space through a set of equations in terms of joint variables. Inverse kinematics equations are just the opposite of the kinematics equations or a set of equations that allow us to solve for the joint positions knowing the position and orientation of the endpoint [22]. Also, the kinematics equations can be used to analyze workspace along with providing the equations that are used to track the endpoint position. In this chapter, kinematics model of the designed 7 DOF device will be presented. By using this kinematics model, forward and inverse kinematics equations are derived and throughout this derivation, all singularities are determined.

3.2 Kinematics Model of 7 DOF Haptic Device

As we mentioned before, first three rotation axes and last three rotation axes in the mechanism intersect at one point. Linkages around intersection point are connected to each other in serial form. These two 3 DOF serial configurations are connected to each other using parallel form, which requires more linkages to transmit movements and causes more complexity for obtaining kinematics

equations. Therefore, a suitable mechanism is selected for parallel configuration. In order to avoid unnecessary complexity, a four-bar mechanism is selected, where every link moves together with the same joint variables and parallel to each other (Figure 3.1). As a result, the kinematics of all the mechanism is analyzed easily.

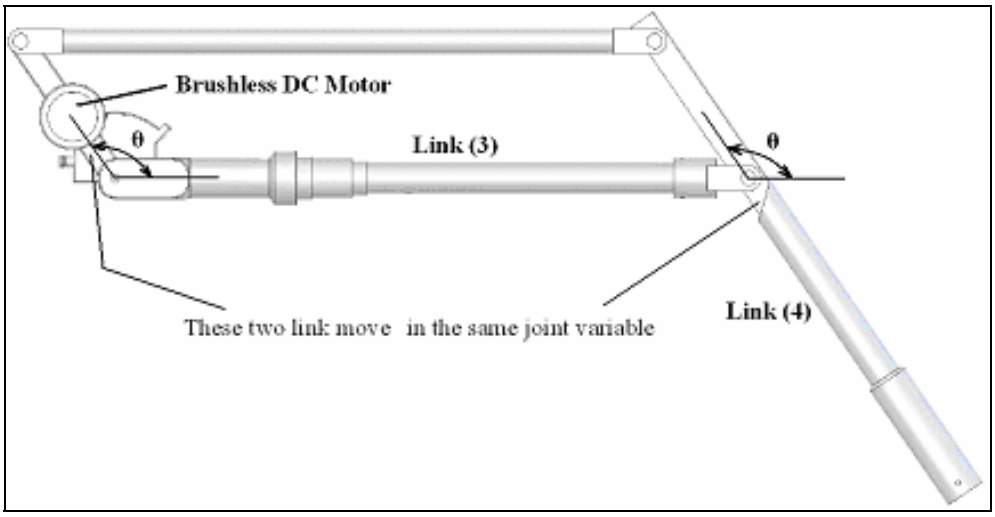

Figure 3.1 Parallel Mechanism in the 7 DOF Haptic Device

The kinematics model of the 7 DOF manipulator can be obtained by using the method of Denavit and Hartenberg. The exponential rotation matrices defined in [23, 24, 25] can be used for kinematics analysis because of their convenience in making the kinematics equations more compact and simple. A more detailed kinematics model of the manipulator is given in Figure 3.2 with existing frame attachments according to the D-H convention, where θ_i, d_i, a_i, α_i represent the joint variables, the joint offsets, the effective link lengths, the twist angles respectively and all parameters were tabulated in Table 3.1

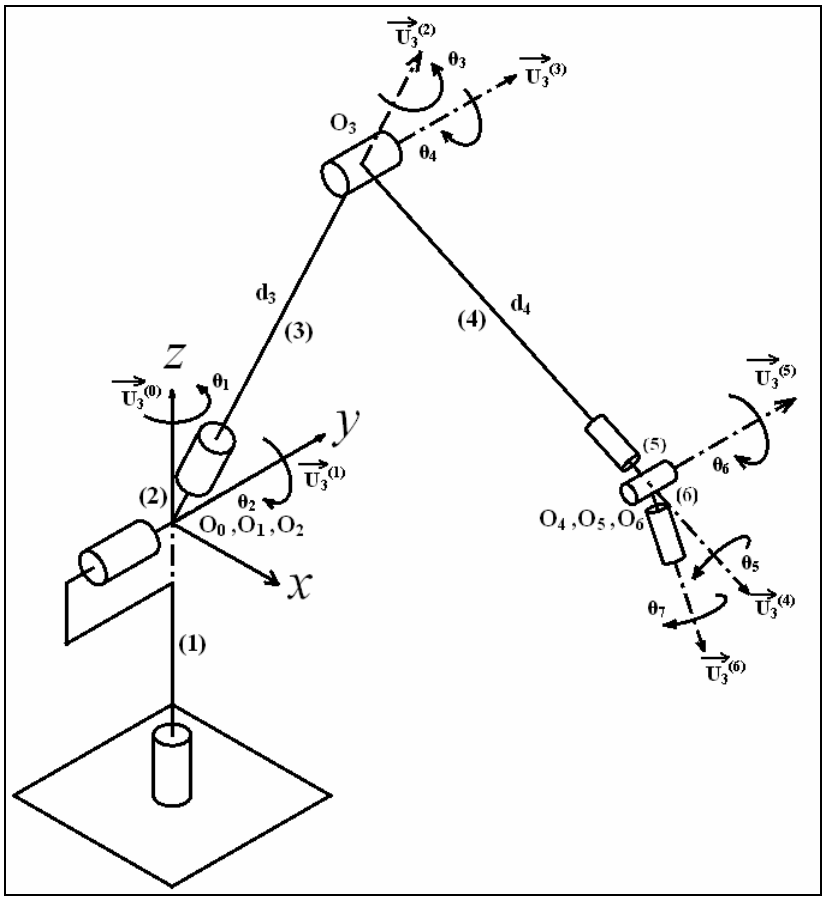

Figure 3.2 Kinematics Model of the 7 DOF Haptic Device

Table 3.1 Kinematics Parameters of the 7 DOF Manipulator

kth Link	a_i	α_i	d_i	θ_i
1	0	-π/2	0	θ_1
2	0	+π/2	0	θ_2
3	0	-π/2	d_3	θ_3
4	0	+π/2	d_4	θ_4
5	0	-π/2	0	θ_5
6	0	+π/2	0	θ_6
7	0	0	0	θ_7

3.3 Forward Kinematics

Our design is a seven-revolute-joint manipulator. Therefore, there are seven link frames and the transformation matrix of the tip point with respect to the base frame can be given as below;

$$\hat{C}^{(0,7)} = \hat{C}^{(0,1)} \quad \hat{C}^{(1,2)} \quad \hat{C}^{(2,3)} \quad \hat{C}^{(3,4)} \quad \hat{C}^{(4,5)} \quad \hat{C}^{(5,6)} \quad \hat{C}^{(6,7)} \tag{3.1}$$

Exponential rotation matrices can be written, by using Eq.(3.2) and given kinematics parameters in Table 3.1;

$$\hat{C}^{(k-1,k)} = e^{\tilde{u}_3\theta_k} e^{\tilde{u}_1\alpha_k} \tag{3.2}$$

$$\hat{C}^{(0,1)} = e^{\tilde{u}_3\theta_1} e^{-\tilde{u}_1\pi/2} \tag{3.3a}$$

$$\hat{C}^{(1,2)} = e^{\tilde{u}_3\theta_2} e^{\tilde{u}_1\pi/2} \tag{3.3b}$$

$$\hat{C}^{(2,3)} = e^{\tilde{u}_3\theta_3} e^{-\tilde{u}_1\pi/2} \tag{3.3c}$$

$$\hat{C}^{(3,4)} = e^{\tilde{u}_3\theta_4} e^{\tilde{u}_1\pi/2} \tag{3.3d}$$

$$\hat{C}^{(4,5)} = e^{\tilde{u}_3\theta_5} e^{-\tilde{u}_1\pi/2} \tag{3.3e}$$

$$\hat{C}^{(5,6)} = e^{\tilde{u}_3\theta_6} e^{\tilde{u}_1\pi/2} \tag{3.3f}$$

$$\hat{C}^{(6,7)} = e^{\tilde{u}_3\theta_7} e^{\tilde{u}_1 0} \tag{3.3g}$$

In order to obtain the orientation matrix of the tip point, the above expressions can be combined as given below;

$$\hat{C}^{(0,2)} = e^{\tilde{u}_3\theta_1} e^{-\tilde{u}_1\pi/2} e^{\tilde{u}_3\theta_2} e^{\tilde{u}_1\pi/2} = e^{\tilde{u}_3\theta_1} e^{\tilde{u}_2\theta_2} \tag{3.4a}$$

$$\hat{C}^{(0,3)} = e^{\tilde{u}_3\theta_1} e^{\tilde{u}_2\theta_2} e^{\tilde{u}_3\theta_3} e^{-\tilde{u}_1\pi/2} \tag{3.4b}$$

$$\hat{C}^{(0,4)} = e^{\tilde{u}_3\theta_1} e^{\tilde{u}_2\theta_2} e^{\tilde{u}_3\theta_3} e^{-\tilde{u}_1\pi/2} e^{\tilde{u}_3\theta_4} e^{\tilde{u}_1\pi/2} = e^{\tilde{u}_3\theta_1} e^{\tilde{u}_2\theta_2} e^{\tilde{u}_3\theta_3} e^{\tilde{u}_2\theta_4} \tag{3.4c}$$

$$\hat{C}^{(0,5)} = e^{\tilde{u}_3\theta_1} e^{\tilde{u}_2\theta_2} e^{\tilde{u}_3\theta_3} e^{\tilde{u}_2\theta_4} e^{\tilde{u}_3\theta_5} e^{-\tilde{u}_1\pi/2} \tag{3.4d}$$

$$\hat{C}^{(0,6)} = e^{\tilde{u}_3\theta_1} e^{\tilde{u}_2\theta_2} e^{\tilde{u}_3\theta_3} e^{\tilde{u}_2\theta_4} e^{\tilde{u}_3\theta_5} e^{-\tilde{u}_1\pi/2} e^{\tilde{u}_3\theta_6} e^{\tilde{u}_1\pi/2} = e^{\tilde{u}_3\theta_1} e^{\tilde{u}_2\theta_2} e^{\tilde{u}_3\theta_3} e^{\tilde{u}_2\theta_4} e^{\tilde{u}_3\theta_5} e^{\tilde{u}_2\theta_6} \tag{3.4e}$$

$$\hat{C}^{(0,7)} = e^{\tilde{u}_3\theta_1} e^{\tilde{u}_2\theta_2} e^{\tilde{u}_3\theta_3} e^{\tilde{u}_2\theta_4} e^{\tilde{u}_3\theta_5} e^{\tilde{u}_2\theta_6} e^{\tilde{u}_3\theta_7} e^{\tilde{u}_1 0} \tag{3.4f}$$

For simplicity, the last term can be canceled;

$$\hat{C}^{(0,7)} = e^{\tilde{u}_3\theta_1} e^{\tilde{u}_2\theta_2} e^{\tilde{u}_3\theta_3} e^{\tilde{u}_2\theta_4} e^{\tilde{u}_3\theta_5} e^{\tilde{u}_2\theta_6} e^{\tilde{u}_3\theta_7} \tag{3.5}$$

The wrist point of the manipulator can be expressed in terms of joint variables;

$$\vec{r} = d_3 \vec{u}_3^{(2)} + d_4 \vec{u}_3^{(4)} \tag{3.6}$$

Using the column representation of the vectors defined in the base coordinate system, this equation becomes;

$$\overline{r} = d_3 \overline{u}_3^{(2/0)} + d_4 \overline{u}_3^{(4/0)} = d_3 \hat{C}^{(0,2)} \overline{u}_3 + d_4 \hat{C}^{(0,4)} \overline{u}_3 \tag{3.7}$$

The transformation matrices can be replaced in this equation;

$$\overline{r} = d_3 e^{\tilde{u}_3\theta_1} e^{\tilde{u}_2\theta_2} \overline{u}_3 + d_4 e^{\tilde{u}_3\theta_1} e^{\tilde{u}_2\theta_2} e^{\tilde{u}_3\theta_3} e^{\tilde{u}_2\theta_4} \overline{u}_3 \tag{3.8}$$

When Eq.(3.8) is simplified, the position and orientation of the end point of the haptic device with respect to the base coordinate frame can be given as;

$$\overline{r} = e^{\tilde{u}_3\theta_1} e^{\tilde{u}_2\theta_2} (d_3 \overline{u}_3 + d_4 e^{\tilde{u}_3\theta_3} e^{\tilde{u}_2\theta_4} \overline{u}_3) \tag{3.9}$$

The exponential rotation matrices for k^{th} joint variables around $\vec{u}_1, \vec{u}_2, \vec{u}_3$ vectors are defined as;

$$e^{\tilde{u}_1\theta_k} = \begin{bmatrix} 1 & 0 & 0 \\ 0 & \cos(\theta_k) & -\sin(\theta_k) \\ 0 & \sin(\theta_k) & \cos(\theta_k) \end{bmatrix}$$

$$e^{\tilde{u}_2\theta_k} = \begin{bmatrix} \cos(\theta_k) & 0 & \sin(\theta_k) \\ 0 & 1 & 0 \\ -\sin(\theta_k) & 0 & \cos(\theta_k) \end{bmatrix}$$

$$e^{\tilde{u}_3\theta_k} = \begin{bmatrix} \cos(\theta_k) & -\sin(\theta_k) & 0 \\ \sin(\theta_k) & \cos(\theta_k) & 0 \\ 0 & 0 & 1 \end{bmatrix}$$

where;

$$\bar{u}_1 = \begin{bmatrix} 1 \\ 0 \\ 0 \end{bmatrix}, \quad \bar{u}_2 = \begin{bmatrix} 0 \\ 1 \\ 0 \end{bmatrix}, \quad \bar{u}_3 = \begin{bmatrix} 0 \\ 0 \\ 1 \end{bmatrix}$$

Wrist point location can be obtained in matrix form by using exponential rotation matrices and unit vectors. In cartesian coordinates, the base frame components of the wrist point location matrix can also be written as;

$$x = r_1 = c\theta_1 s\theta_2 d_3 + (c\theta_1 c\theta_2 c\theta_3 s\theta_4 - s\theta_1 s\theta_3 s\theta_4 + c\theta_1 s\theta_2 c\theta_4) d_4 \tag{3.10}$$

$$y = r_2 = s\theta_1 s\theta_2 d_3 + (s\theta_1 c\theta_2 c\theta_3 s\theta_4 + c\theta_1 s\theta_3 s\theta_4 + s\theta_1 s\theta_2 c\theta_4) d_4 \tag{3.11}$$

$$z = r_3 = c\theta_2 d_3 + (-s\theta_2 c\theta_3 s\theta_4 + c\theta_2 c\theta_4) d_4 \tag{3.12}$$

3.4 Inverse Kinematics and Singularity Analysis

The end-effector position, where the tool or gripper is attached, is one of the primarily subjects of interest in robotics applications. Normally, we know the positions of the end-effector in terms of the base cartesian coordinate system to specify a location in a working volume. But it is necessary to define these position values in terms of joint coordinates to reach the goal position. In other words, we need to know how much to rotate (or translate) each joint in order to

obtain the required end-effector position given in terms of the base coordinate system. In robotics, this analysis is called the *Inverse Kinematics*. If the endpoint location and transformation matrix are known, it is relatively simple to find the analytical inverse kinematics solution for any 6 DOF manipulators. Our design is a 7 DOF redundant manipulator. The inverse kinematics of a redundant kinematic chain has infinitely many solutions. In order to solve inverse kinematics for redundant manipulators, one of the joint variables can be defined and the other remaining joint variables can be solved in terms of the defined variable. However, for certain required end-effector positions it may not be possible to find a unique solution in terms of joint coordinates, which is called singularity. In practice, the designed haptic device may not be exactly in a configuration that results in a singularity; however, these points should be defined during the design stage in order to describe how one can avoid them.

Eq.(3.9) can be used in order to derive inverse kinematics equations;

$$\bar{r} = e^{\tilde{u}_3\theta_1} e^{\tilde{u}_2\theta_2} (d_3\bar{u}_3 + d_4 e^{\tilde{u}_3\theta_3} e^{\tilde{u}_2\theta_4} \bar{u}_3)$$

$$e^{-\tilde{u}_2\theta_2} e^{-\tilde{u}_3\theta_1} \bar{r} = (d_3\bar{u}_3 + d_4 e^{\tilde{u}_3\theta_3} e^{\tilde{u}_2\theta_4} \bar{u}_3) \tag{3.13}$$

$$e^{-\tilde{u}_2\theta_2} e^{-\tilde{u}_3\theta_1} \bar{r} = [d_3\bar{u}_3 + d_4(c\theta_4\bar{u}_3 + c\theta_3 s\theta_4\bar{u}_1 + s\theta_3 s\theta_4\bar{u}_2)] \tag{3.14}$$

$$e^{-\tilde{u}_2\theta_2} e^{-\tilde{u}_3\theta_1} \bar{r} = [(c\theta_3 s\theta_4 d_4)\bar{u}_1 + (s\theta_3 s\theta_4 d_4)\bar{u}_2 + (d_3 + c\theta_4 d_4)\bar{u}_3)] \tag{3.15}$$

Premultiplying these equations by $\bar{u}_1^{\,t}$, $\bar{u}_2^{\,t}$, $\bar{u}_3^{\,t}$ will yield three scalar equations;

$$c\theta_2 c\theta_1 r_1 + c\theta_2 s\theta_1 r_2 - s\theta_2 r_3 = c\theta_3 s\theta_4 d_4 \tag{3.16}$$

$$-s\theta_1 r_1 + c\theta_1 r_2 = s\theta_3 s\theta_4 d_4 \tag{3.17}$$

$$s\theta_2 c\theta_1 r_1 + s\theta_2 s\theta_1 r_2 + c\theta_2 r_3 = d_3 + c\theta_4 d_4 \tag{3.18}$$

In the above three equations, r_1, r_2, r_3, d_3, d_4 are known and θ_1, θ_2, θ_3, θ_4 are unknown.

Using the three equations (3.16, 3.17 and 3.18), θ_4 can be obtained. We can simply square both sides;

$$c^2\theta_1 c^2\theta_2 r_1^2 + 2c\theta_1 s\theta_1 c^2\theta_2 r_1 r_2 + c^2\theta_2 s^2\theta_1 r_2^2 - 2(c\theta_1 c\theta_2 r_1 + c\theta_2 s\theta_1 r_2) s\theta_2 r_3 + s^2\theta_2 r_3^2 = c^2\theta_3 s^2\theta_4 d_4^2 \quad (3.19)$$

$$s^2\theta_2 r_1^2 - 2s\theta_1 c\theta_1 r_1 r_2 + c^2\theta_1 r_2^2 = s^2\theta_3 s^2\theta_4 d_4^2 \quad (3.20)$$

$$s^2\theta_2 c^2\theta_1 r_1^2 + 2c\theta_1 s\theta_1 s^2\theta_2 r_1 r_2 + s^2\theta_2 s^2\theta_1 r_2^2 + 2(s\theta_2 c\theta_1 r_1 + s\theta_2 s\theta_1 r_2) c\theta_2 r_3 + c^2\theta_2 r_3^2 = (d_3 + c\theta_4 d_4)^2 \quad (3.21)$$

and we may sum both sides of the equations side by side

$$r_1^2 + r_2^2 + r_3^2 = d_3^2 + d_4^2 + 2d_3 d_4 c\theta_4 \quad (3.22)$$

$$\cos\theta_4 = \frac{r_1^2 + r_2^2 + r_3^2 - d_3^2 - d_4^2}{2d_3 d_4} \quad (3.23)$$

$$\theta_4 = \sigma\cos^{-1}\left(\frac{r_1^2 + r_2^2 + r_3^2 - d_3^2 - d_4^2}{2d_3 d_4}\right) \qquad \sigma = \pm 1 \quad (3.24)$$

θ_1, θ_2 and θ_3 joint variables can not be found separately using the equations Eq.(3.16), Eq.(3.17) and Eq.(3.18). These equations can be solved by choosing one of θ_1, θ_2, θ_3 joint variables as desired, and then all alternative solutions based on chosen variable can be found;

Inverse kinematics solution based on parameterized joint variable θ_1;

In order to find θ_3, Eq.(3.17) can be used;

$$-s\theta_1 r_1 + c\theta_1 r_2 = s\theta_3 s\theta_4 d_4$$

$$\sin\theta_3 = \frac{-\sin\theta_1 r_1 + \cos\theta_1 r_2}{\sin\theta_4 d_4} \quad (3.25)$$

If $\sin\theta_3$ is not equal to zero, θ_3 can be found as;

$$\theta_3=\sigma\sin^{-1}\left[\frac{-\sin\theta_1 r_1+\cos\theta_1 r_2}{\sin\theta_4 d_4}\right] \qquad \sigma=\pm 1 \tag{3.26}$$

If $\sin\theta_4$ is equal to zero ($\sin\theta_4=0 \Rightarrow \theta_4=0,\pm\pi$), first singularity occurs. In this singularity, θ_3 and θ_5 can not be found separately.

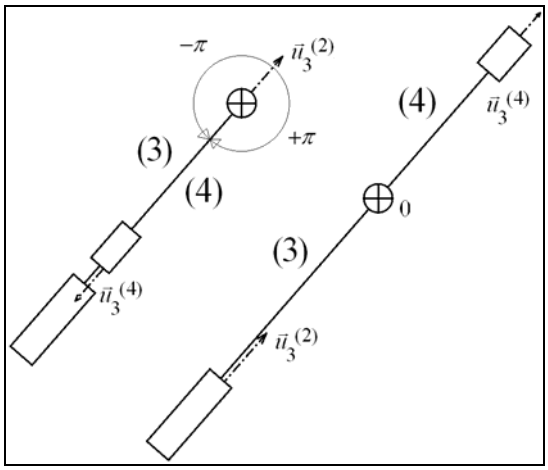

Figure 3.3 First Singularity Illustration

If Eq.(3.16) and Eq.(3.18) can be arranged in order to find θ_2

$$(c\theta_1 r_1+s\theta_1 r_2)c\theta_2-r_3 s\theta_2 = c\theta_3 s\theta_4 d_4 \tag{3.27}$$

$$(c\theta_1 r_1+s\theta_1 r_2)s\theta_2+r_3 c\theta_2 = d_3+d_4 c\theta_4 \tag{3.28}$$

If Eq.(3.27) and Eq.(3.28) can be written in matrix form;

$$\begin{bmatrix}(c\theta_1 r_1+s\theta_1 r_2) & -r_3\\ r_3 & (c\theta_1 r_1+s\theta_1 r_2)\end{bmatrix}\begin{bmatrix}c\theta_2\\ s\theta_2\end{bmatrix}=\begin{bmatrix}c\theta_3 s\theta_4 d_4\\ d_3+d_4 c\theta_4\end{bmatrix} \tag{3.29}$$

$$\det(\hat{A})=\left(r_1 c\theta_1+r_2 s\theta_1\right)^2+r_3^2=r_1^2 c^2\theta_1+r_2^2 s^2\theta_1+2r_1 r_2 s\theta_1 c\theta_1+r_3^2=\Delta \tag{3.30}$$

If $\det(\hat{A}) \neq 0$ then $\hat{X}=\hat{A}^{-1}\hat{B}$

$$\begin{bmatrix} c\theta_2 \\ s\theta_2 \end{bmatrix} = \frac{1}{\Delta}\begin{bmatrix} (c\theta_1 r_1 + s\theta_1 r_2) & r_3 \\ -r_3 & (c\theta_1 r_1 + s\theta_1 r_2) \end{bmatrix} \begin{bmatrix} c\theta_3 s\theta_4 d_4 \\ d_3 + d_4 c\theta_4 \end{bmatrix} \tag{3.31}$$

$$\sin\theta_2 = \frac{-r_3\cos\theta_3\sin\theta_4 d_4 + (\cos\theta_1 r_1 + \sin\theta_1 r_2)(d_3 + d_4\cos\theta_4)}{\Delta} = \eta_2 \tag{3.32}$$

$$\cos\theta_2 = \frac{(\cos\theta_1 r_1 + \sin\theta_1 r_2)\cos\theta_3\sin\theta_4 d_4 + r_3(d_3 + d_4\cos\theta_4)}{\Delta} = \xi_2 \tag{3.33}$$

$$\theta_2 = \text{atan}_2[\eta_2, \xi_2] \tag{3.34}$$

If $\det(\hat{A})=0$, second singularity occurs, where wrist point collides with the origin of the device as illustrated in Figure 3.4.

$$r_1^2 c^2\theta_1 + r_2^2 s^2\theta_1 + 2r_1 r_2 s\theta_1 c\theta_1 + r_3^2 = 0 \Leftrightarrow r_1 = r_2 = r_3 = 0$$

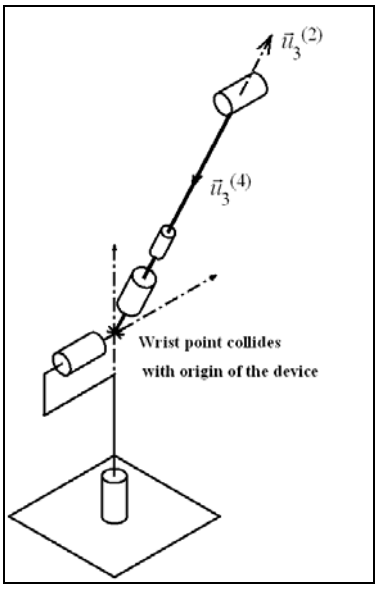

Figure 3.4 Second Singularity Illustration

Inverse kinematics solution based on parameterized joint variable θ_2;

θ_1 can be found by rearranging Eq.(3.18) using tan (θ/2);

$$t_1=\tan(\theta/2) \Rightarrow \sin\theta_1=\frac{2t_1}{1+t_1^2} \Rightarrow \cos\theta_1=\frac{1-t_1^2}{1+t_1^2}$$

$$s\theta_2 r_1 \frac{1-t_1^2}{1+t_1^2}+s\theta_2 r_2 \frac{2t_1}{1+t_1^2}-(d_3+c\theta_4 d_4-c\theta_2 r_3)=0 \qquad (3.35)$$

$$s\theta_2 r_1-s\theta_2 r_1 t_1^2+2s\theta_2 r_2 t_1-(d_3+c\theta_4 d_4-c\theta_2 r_3)-(d_3+c\theta_4 d_4-c\theta_2 r_3)t_1^2=0 \qquad (3.36)$$

$$(s\theta_2 r_1+d_3+c\theta_4 d_4-c\theta_2 r_3)t_1^2-(2s\theta_2 r_2)t_1+(d_3+c\theta_4 d_4-c\theta_2 r_3-s\theta_2 r_1)=0 \qquad (3.37)$$

If Eq.(3.37) (second degree of polynomial) is solved, θ_1 can be found and t_1 can be obtained from the same second degree of polynomial;

$$t_1=\frac{s\theta_2 r_2+\sigma\sqrt{s^2\theta_2(r_1^2+r_2^2)-(d_3+c\theta_4 d_4-c\theta_2 r_3)^2}}{s\theta_2 r_1+d_3+c\theta_4 d_4-c\theta_2 r_3} \qquad \sigma=\pm 1 \qquad (3.38)$$

where

$$\theta_1=\text{atan}[2t_1;1-t_1^2] \qquad (3.39)$$

If $r_1=r_2=0$ or $\sin\theta_2=0$, Eq.(3.37) can not be solved. First singularity occurs for the following values and this singularity was illustrated in Figure 3.5

$$r_1=r_2=0 \quad \text{or} \quad \sin\theta_2=0 \Rightarrow \theta_2=0,\ \pm\pi$$

When $\theta_2=0, \pm\pi$, θ_1 and θ_3 can not be found separately and if $r_1=r_2=0$, θ_1 can be any value. That is, changing the value of θ_1 don't effect on wrist point location. In addition, if the term in the square roots for Eq.(3.38) is less than zero, this

equation will be unsolvable. Therefore, this term should be more than zero and equal to zero. This expression can be called as workspace limitation;

$$s^2\theta_2(r_1^2+r_2^2)-(d_3+c\theta_4 d_4-c\theta_2 r_3)^2 \geq 0 \Rightarrow s^2\theta_2(r_1^2+r_2^2) \geq (d_3+c\theta_4 d_4-c\theta_2 r_3)^2 \qquad (3.40)$$

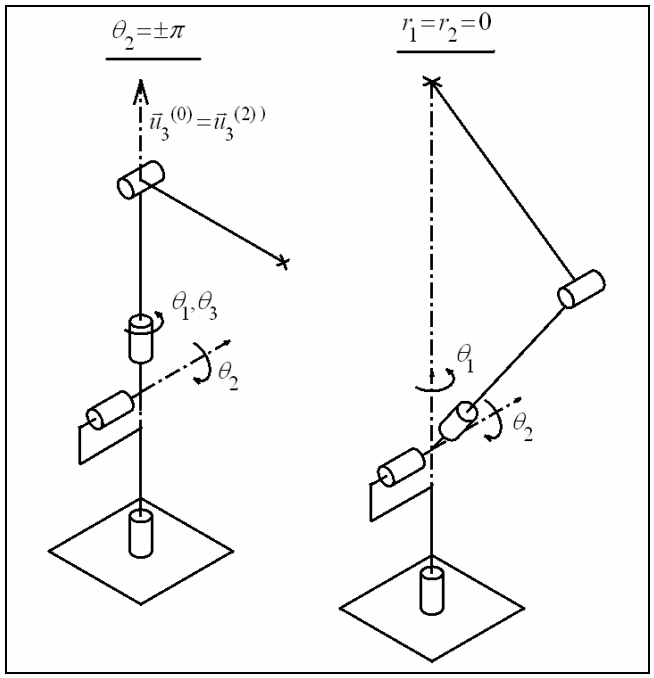

Figure 3.5 Third Singularity Illustration

In order to find θ_3, Eq.(3.16) and Eq.(3.17) can be used;

$$c\theta_2 c\theta_1 r_1+c\theta_2 s\theta_1 r_2-s\theta_2 r_3 = c\theta_3 s\theta_4 d_4$$
$$-s\theta_1 r_1+c\theta_1 r_2 = s\theta_3 s\theta_4 d_4$$

$$\sin\theta_3 = \frac{-\sin\theta_1 r_1+\cos\theta_1 r_2}{\sin\theta_4 d_4} = \eta_3 \qquad (3.41)$$

$$\cos\theta_3 = \frac{\cos\theta_2\cos\theta_1 r_1+\cos\theta_2\sin\theta_1 r_2-\sin\theta_2 r_3}{\sin\theta_4 d_4} = \xi_3 \qquad (3.42)$$

If $\sin\theta_4$ is not equal to zero;

$$\theta_3 = \text{atan}_2[\eta_3;\xi_3] \tag{3.43}$$

If $\sin\theta_4$ is equal to zero, second singularity occurs, illustration of this singularity is given in Figure 3.3

$$\sin\theta_4 = 0 \Rightarrow \theta_4 = 0,\ \pm\pi$$

Inverse kinematics solution based on parameterized joint variable θ_3;

In order to find θ_1, Eq.(3.17) can be rearranged by using tan (θ/2) ;

$$t_1 = \tan(\theta/2) \Rightarrow \sin\theta_1 = \frac{2t_1}{1+t_1^2} \Rightarrow \cos\theta_1 = \frac{1-t_1^2}{1+t_1^2}$$

$$-\frac{2t_1r_1}{1+t_1^2} + \frac{(1-t_1^2)r_2}{1+t_1^2} = s\theta_3 s\theta_4 d_4 \tag{3.44}$$

$$-2t_1r_1 + r_2 - r_2t_1^2 - s\theta_3 s\theta_4 d_4 - s\theta_3 s\theta_4 d_4 t_1^2 = 0 \tag{3.45}$$

$$(s\theta_3 s\theta_4 d_4 + r_2)t_1^2 + 2r_1t_1 + (s\theta_3 s\theta_4 d_4 - r_2) = 0 \tag{3.46}$$

If Eq.(3.45) (second degree of polynomial) is solved, θ_1 can be found and t_1 can be obtained from the same second degree of polynomial;

$$t_1 = \frac{r_1 + \sigma\sqrt{r_1^2 + r_2^2 - (s\theta_3 s\theta_4 d_4)^2}}{(s\theta_3 s\theta_4 d_4 + r_2)} \qquad \sigma = \pm 1 \tag{3.47}$$

where,

$$\theta_1 = \text{atan}_2[2t_1;1-t_1^2] \tag{3.48}$$

If $r_1=r_2=0$, Eq.(3.45) can not be solved. Therefore, first singularity occurs for the points where $r_1=r_2=0$. Illustration of this singularity is given Figure 3.5.

In addition, the term in the square root should not be negative (Workspace limitation);

$$r_1^2+r_2^2-(s\theta_3 s\theta_4 d_4)^2 \geq 0 \Rightarrow r_1^2+r_2^2 \geq (s\theta_3 s\theta_4 d_4)^2 \tag{3.49}$$

Eq.(3.16) and Eq.(3.18) can be arranged in order to find θ_2;

$$(c\theta_1 r_1+s\theta_1 r_2)c\theta_2-r_3 s\theta_2 = c\theta_3 s\theta_4 d_4 \tag{3.50}$$

$$(c\theta_1 r_1+s\theta_1 r_2)s\theta_2+r_3 c\theta_2 = d_3+d_4 c\theta_4 \tag{3.51}$$

Eq.(3.27) and Eq.(3.28) can be written in matrix form;

$$\begin{bmatrix} (c\theta_1 r_1+s\theta_1 r_2) & -r_3 \\ r_3 & (c\theta_1 r_1+s\theta_1 r_2) \end{bmatrix} \begin{bmatrix} c\theta_2 \\ s\theta_2 \end{bmatrix} = \begin{bmatrix} c\theta_3 s\theta_4 d_4 \\ d_3+d_4 c\theta_4 \end{bmatrix} \tag{3.52}$$

$$\det(\hat{A}) = \left(r_1 c\theta_1+r_2 s\theta_1\right)^2+r_3^2 = r_1^2 c^2\theta_1+r_2^2 s^2\theta_1+2r_1 r_2 s\theta_1 c\theta_1+r_3^2 = \Delta \tag{3.53}$$

If $\det(\hat{A}) \neq 0$ then $\hat{X}=\hat{A}^{-1}\hat{B}$

$$\begin{bmatrix} c\theta_2 \\ s\theta_2 \end{bmatrix} = \frac{1}{\Delta} \begin{bmatrix} (c\theta_1 r_1+s\theta_1 r_2) & r_3 \\ -r_3 & (c\theta_1 r_1+s\theta_1 r_2) \end{bmatrix} \begin{bmatrix} c\theta_3 s\theta_4 d_4 \\ d_3+c\theta_4 d_4 \end{bmatrix} \tag{3.54}$$

$$\sin\theta_2 = \frac{-r_3\cos\theta_3\sin\theta_4 d_4+(\cos\theta_1 r_1+\sin\theta_1 r_2)(d_3+d_4\cos\theta_4)}{\Delta} = \eta_2 \tag{3.55}$$

$$\cos\theta_2 = \frac{(\cos\theta_1 r_1+\sin\theta_1 r_2)\cos\theta_3\sin\theta_4 d_4+r_3(d_3+d_4\cos\theta_4)}{\Delta} = \xi_2 \tag{3.56}$$

$$\theta_2 = \text{atan}_2\left[\eta_2;\xi_2\right] \tag{3.57}$$

If $\det(\hat{A})=0$, second singularity occurs;

$$r_1^2c^2\theta_1+r_2^2s^2\theta_1+2r_1r_2s\theta_1c\theta_1+r_3^2 = 0 \;\Leftrightarrow\; r_1 = r_2 = r_3 = 0$$

(Wrist point collides with the origin of the device) Illustration of this singularity is given in Figure 3.4.

The remaining joint variables to be determined are the last three joint variables. Since the first four joint variables (θ_1, θ_2, θ_3, θ_4) were determined above, the exponential rotation matrices of those variables and transformation matrix of the tip point are also known. Therefore, if the known elements are collected on the right side of the Eq.(3.5), left side of the equation which represent to hand orientation will be in the form of a 3-2-3 rotation sequence as follows;

$$e^{\tilde{u}_3\theta_5}e^{\tilde{u}_2\theta_6}e^{\tilde{u}_3\theta_7} = e^{-\tilde{u}_2\theta_4}e^{-\tilde{u}_3\theta_3}e^{-\tilde{u}_2\theta_2}e^{-\tilde{u}_3\theta_1} = \hat{C} \quad \text{(known)} \tag{3.58}$$

Pre-multiply by $\bar{u}_3^{\,t}$ and pos-multiply by $\bar{u}_3$;

$$\bar{u}_3^{\,t}e^{\tilde{u}_3\theta_5}e^{\tilde{u}_2\theta_6}e^{\tilde{u}_3\theta_7}\bar{u}_3 = c_{33} \tag{3.59}$$

$$\bar{u}_3^{\,t}(\bar{u}_3\cos\theta_6+\bar{u}_1\sin\theta_6) = c_{33} \tag{3.60}$$

$$\cos\theta_6 = c_{33} \tag{3.61}$$

$$\sin\theta_6 = \sigma\sqrt{1-c_{33}^{\,2}} \qquad \sigma=\pm1 \tag{3.62}$$

$$\theta_6 = \text{atan}_2\left[c_{33};\sigma\sqrt{1-c_{33}^{\,2}}\right] \tag{3.63}$$

Pre-multiply by $\bar{u}_1^{\,t}$ and pos-multiply by $\bar{u}_3$

$$\bar{u}_1^{\,t}e^{\tilde{u}_3\theta_5}e^{\tilde{u}_2\theta_6}e^{\tilde{u}_3\theta_7}\bar{u}_3 = c_{13} \tag{3.64}$$

$$(\bar{u}_1{}^t\cos\theta_5 - \bar{u}_2{}^t\sin\theta_5)(\bar{u}_3\cos\theta_6 + \bar{u}_1\sin\theta_6) = c_{13} \tag{3.65}$$

$$\cos\theta_5\sin\theta_6 = c_{13} \tag{3.66}$$

$$\cos\theta_5 = \frac{c_{13}}{\sin\theta_6} \tag{3.67}$$

Pre-multiply by $\bar{u}_2{}^t$ and pos-multiply by $\bar{u}_3$;

$$\bar{u}_2{}^t e^{\tilde{u}_3\theta_5} e^{\tilde{u}_2\theta_6} e^{\tilde{u}_3\theta_7} \bar{u}_3 = c_{23} \tag{3.68}$$

$$(\bar{u}_2{}^t\cos\theta_5 + \bar{u}_1{}^t\sin\theta_5)(\bar{u}_3\cos\theta_6 + \bar{u}_1{}^t\sin\theta_6) = c_{23} \tag{3.69}$$

$$\sin\theta_5\sin\theta_6 = c_{23} \tag{3.70}$$

$$\sin\theta_5 = \frac{c_{23}}{\sin\theta_6} \tag{3.71}$$

If $\sin\theta_6$ is not equal to zero $(\sin\theta_6 = 0 \Rightarrow \theta_6 = 0, \pm\pi)$, first singularity occurs. In this singularity, θ_5 and θ_7 can not be found separately.

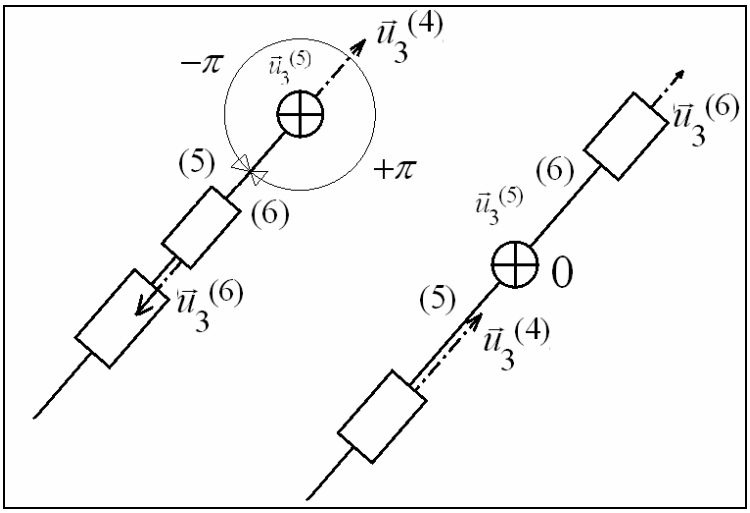

Figure 3.6 Fourth Singularity Illustrations

If $\sin\theta_6$ is not equal to zero;

$$\theta_5 = \text{atan}_2[c_{23};c_{13}] \tag{3.72}$$

Pre-multiply by $\bar{u}_3^t$ and pos-multiply by $\bar{u}_1$;

$$\bar{u}_3^t e^{\tilde{u}_3\theta_5} e^{\tilde{u}_2\theta_6} e^{\tilde{u}_3\theta_7} \bar{u}_1 = c_{31} \tag{3.73}$$

$$(\bar{u}_3^t \cos\theta_6 - \bar{u}_1^t \sin\theta_6)(\bar{u}_1 \cos\theta_7 + \bar{u}_2 \sin\theta_6) = c_{31} \tag{3.74}$$

$$-\sin\theta_6 \cos\theta_7 = c_{31} \tag{3.75}$$

$$\cos\theta_7 = \frac{-c_{31}}{\sin\theta_6} \tag{3.76}$$

Pre-multiply by $\bar{u}_3^t$ and pos-multiply by $\bar{u}_2$;

$$\bar{u}_3^t e^{\tilde{u}_3\theta_5} e^{\tilde{u}_2\theta_6} e^{\tilde{u}_3\theta_7} \bar{u}_2 = c_{32} \tag{3.77}$$

$$(\bar{u}_3^t \cos\theta_6 - \bar{u}_1^t \sin\theta_6)(\bar{u}_2 \cos\theta_7 - \bar{u}_1^t \sin\theta_7) = c_{32} \tag{3.78}$$

$$\sin\theta_6 \sin\theta_7 = c_{32} \tag{3.79}$$

$$\sin\theta_7 = \frac{c_{32}}{\sin\theta_6} \tag{3.80}$$

If $\sin\theta_6$ is not equal to zero;

$$\theta_7 = \text{atan}_2[c_{32};-c_{31}] \tag{3.81}$$

If $\sin\theta_6$ is equal to zero $(\sin\theta_6 = 0 \Rightarrow \theta_6 = 0,\pm\pi)$, singularity occurs.

A graphical study has been performed to verify the forward and inverse kinematics equations in MATLAB software program. Wrist point coordinates of the device can be found easily by using the forward kinematics equations and first

four joint variables (θ_1, θ_2, θ_3, θ_4), in contrast, the first four joint variables can be found by using the inverse kinematic equations and wrist point coordinates. However, because of the redundancy, one of the first three joint variables (θ_1, θ_2, θ_3) should be selected as desired value in each set. In the context of the graphical study, this guiding principle was followed. Firstly, three different joint variable graphs were formed in which one of the first three joint variables (θ_1, θ_2, θ_3) was selected as desired while the others were increased regularly and these three different graphs were applied to obtain the wrist point graphs in the forward kinematics equations. Next, the initial joint variable graphs were produced again by applying the last obtained wrist point graphs in the inverse kinematics equations (Figure 3.7, 3.8 and 3.9 show MATLAB results). In this way, we returned to the joint variable graphs formed in the beginning, by using the forward and inverse kinematics equations, so these equations can be used safely for any application.

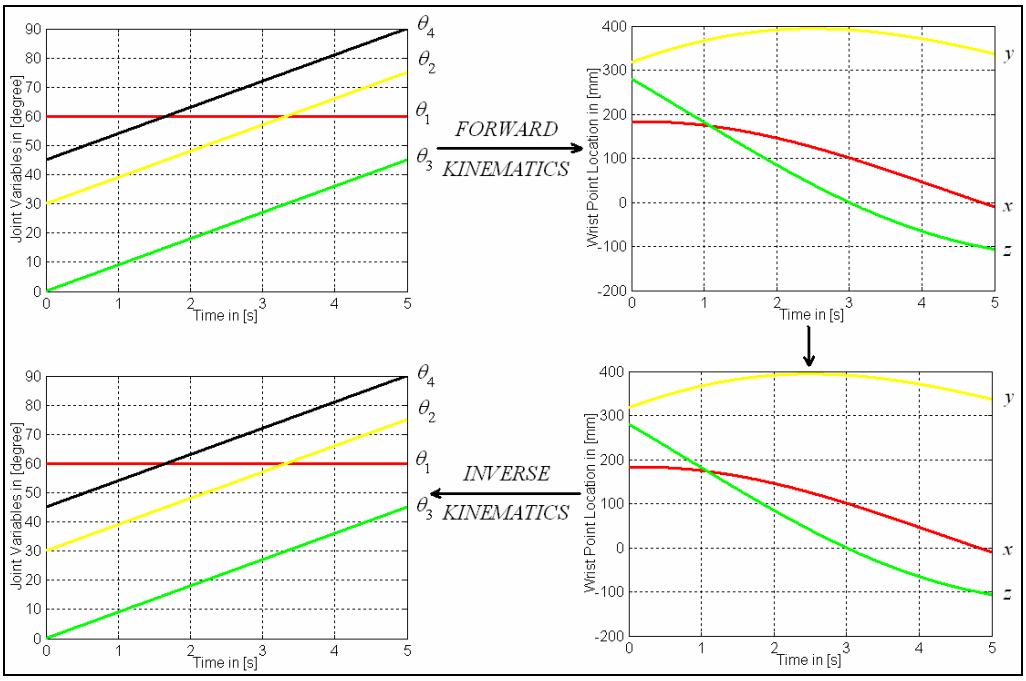

Figure 3.7 Forward and Inverse Kinematics Verification Based on θ_1

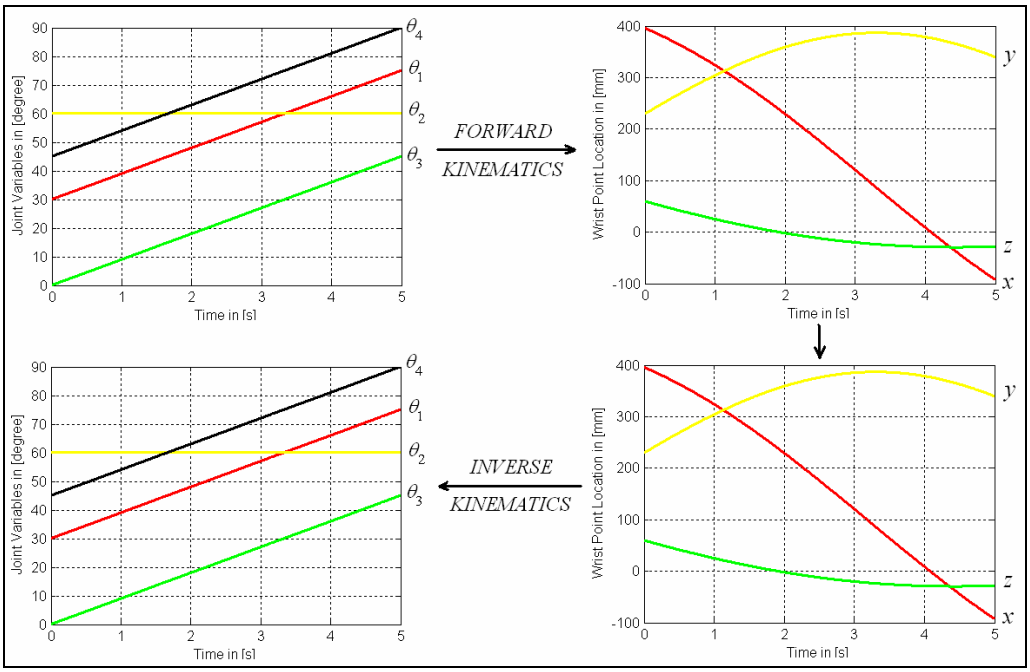

Figure 3.8 Forward and Inverse Kinematics Verification Based on θ_2

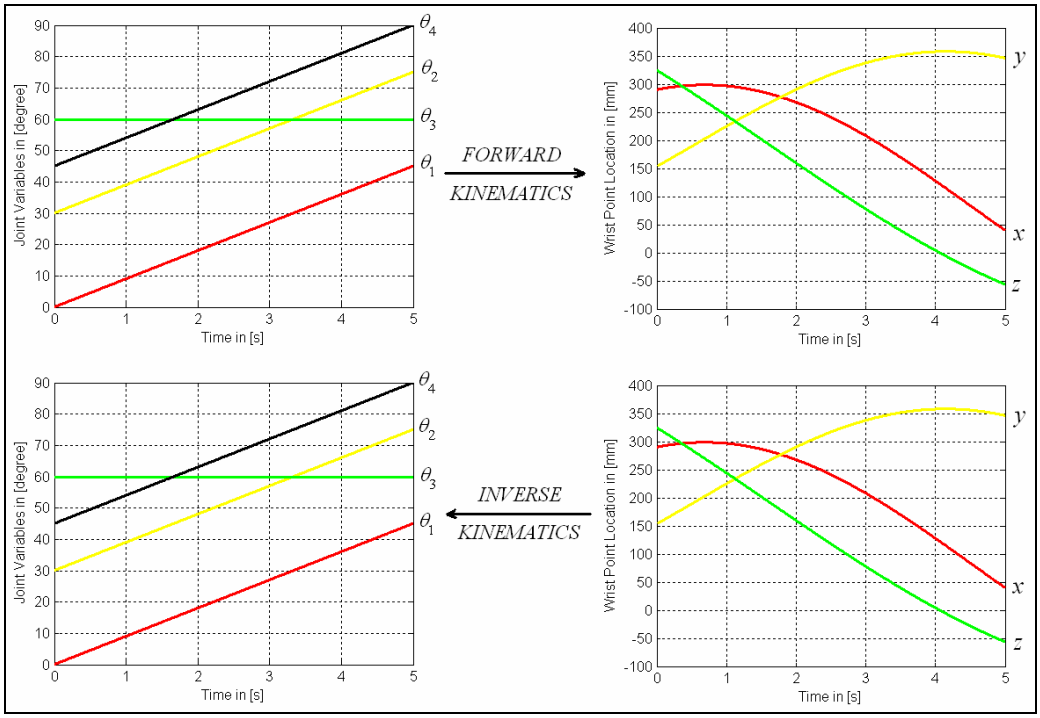

Figure 3.9 Forward and Inverse Kinematics Verification Based on θ_3

CHAPTER 4

WORKSPACE ANALYSIS

The limitation of the workspace is the most important constraint in haptic device design. Haptic devices with large workspace can be adapted to different applications. So, it is important to obtain the possible largest workspace without sacrificing the other constraints such as high stiffness and low inertia, to make it possible, the limitation of the workspace should be considered together with the other constraints. In the haptic devices, there are two types of workspace; translational and rotational workspace. The translational workspace can be defined as the workspace in which the translation of user's hand is sensed but in the case of the rotational workspace, the rotation of user's hand is sensed. At the beginning of the design, it was aimed to reach a half sphere translational workspace with 50 cm radius and the rotational workspaces with 360 degree around yaw, pitch, roll axes of the haptic pen. For this purpose, there are two alternative methods; the first method is to increase link lengths and the other is to increase the degrees of freedom. The increase in link lengths effects badly inertia and stiffness, for this reason, the second method was followed in which a 7 DOF haptic device was designed with the same link lengths in the similar designs. Besides increasing the working volume, 7 DOF haptic device, enables us to reach a point from different positions due to the redundancy. In our design, the first four joint variables (θ_1, θ_2, θ_3, θ_4) serve as the translational workspace and the last three joint variables (θ_5, θ_6, θ_7) serve as the rotational workspace.

Since the device can not be controlled easily in the singularity points, at the beginning, some mechanical joint limitations were attached to the design to avoid the detected singularity points. The joint limitations were determined according to the device kinematics and singularity points which are listed in Table 4.1. The effective link lengths were selected as 250 mm ($d_3 = d_4 = 250$ mm) in order to reach the desired workspace. All of the singularity points detected during the derivation of the inverse kinematics equations can be listed as below;

First singularity $\rightarrow \theta_2 = 0, +\pi, -\pi$
Second singularity $\rightarrow \theta_4 = 0, +\pi, -\pi$
Third singularity $\rightarrow x = y = 0$
Fourth singularity $\rightarrow \theta_6 = 0, +\pi, -\pi$

Table 4.1 Joint variable limits of the 7 DOF Manipulator

Joint variables (θ_k)	**Upper Limit (degree)**	**Lower Limit (degree)**
θ_1	-90	90
θ_2	30	120
θ_3	-60	60
θ_4	-45	45
θ_5	0	360
θ_6	0	360
θ_7	0	360

The kinematics and CAD models, and the reference positions of the first joint variables of the 7 DOF haptic device are given Figure 4.1 and 4.2 respectively, so one can visualize the joint limitations, wrist point locations and axes of the 7 DOF haptic device.

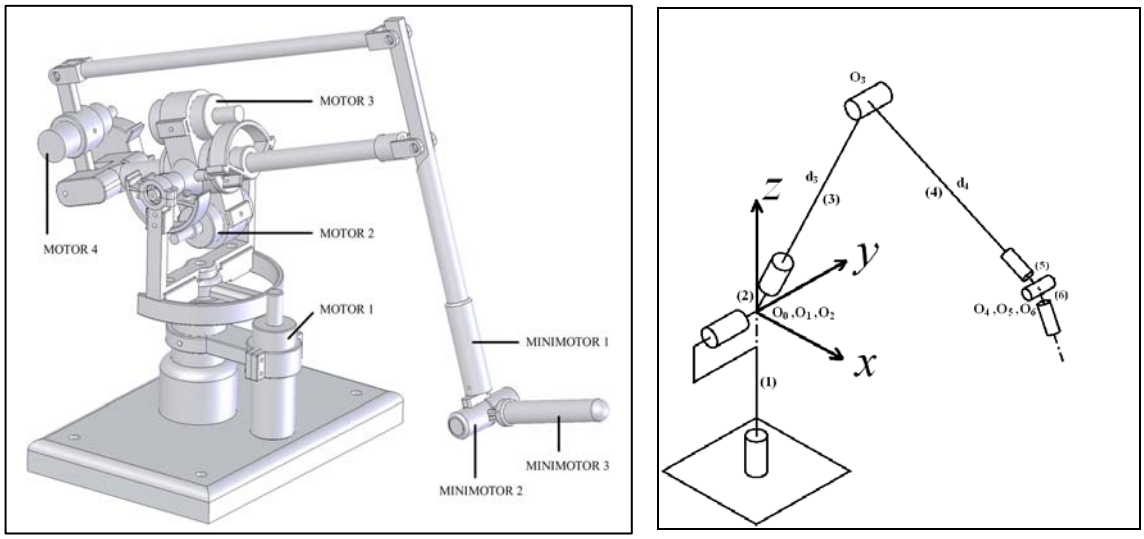

(a) (b)

Figure 4.1 CAD Model and Kinematics Model of the 7 DOF Haptic Device

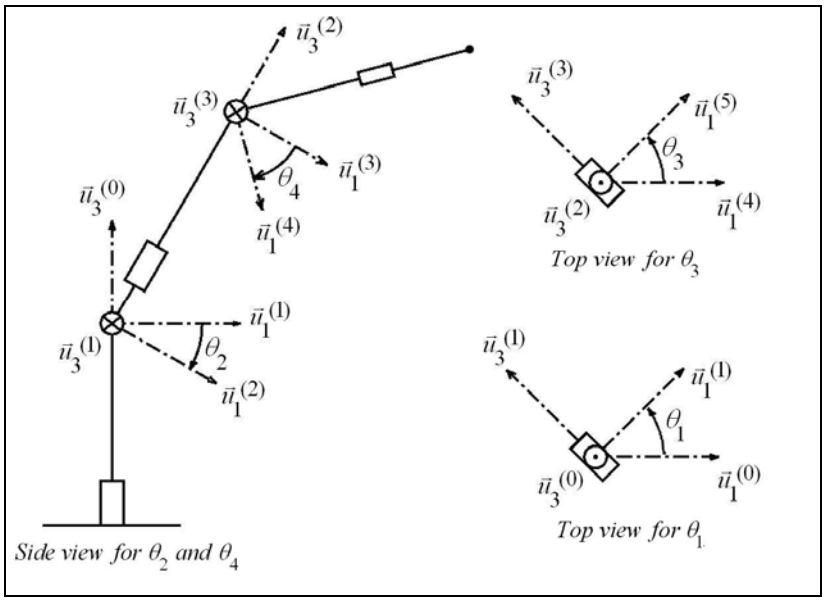

Figure 4.2 Reference Positions of the First Four Joint Variables

The translational workspace of the 7 DOF haptic device can be obtained by tracking all possible wrist point paths on the graph. In order to do that, the forward kinematics equations listed below are used;

$$x = c\theta_1 s\theta_2 d_3 + (c\theta_1 c\theta_2 c\theta_3 s\theta_4 - s\theta_1 s\theta_3 s\theta_4 + c\theta_1 s\theta_2 c\theta_4) d_4 \quad (4.1)$$

$$y = s\theta_1 s\theta_2 d_3 + (s\theta_1 c\theta_2 c\theta_3 s\theta_4 + c\theta_1 s\theta_3 s\theta_4 + s\theta_1 s\theta_2 c\theta_4) d_4 \quad (4.2)$$

$$z = c\theta_2 d_3 + (-s\theta_2 c\theta_3 s\theta_4 + c\theta_2 c\theta_4) d_4 \quad (4.3)$$

The translational workspace of the 7 DOF haptic device, figured out by using the forward kinematics equations in MATLAB, is given in Figure 4.3. All possible wrist point paths were created by changing one of the first four joint variables alternately between upper and lower limits, and plotted on one graph to obtain the translational workspace. The formed translational workspace is similar to the desired workspace (a half sphere with radius 50cm) and the desired rotational workspace is achieved by the last 3 DOF serial configuration (nearly 360 degree around yaw, pitch and roll axis).

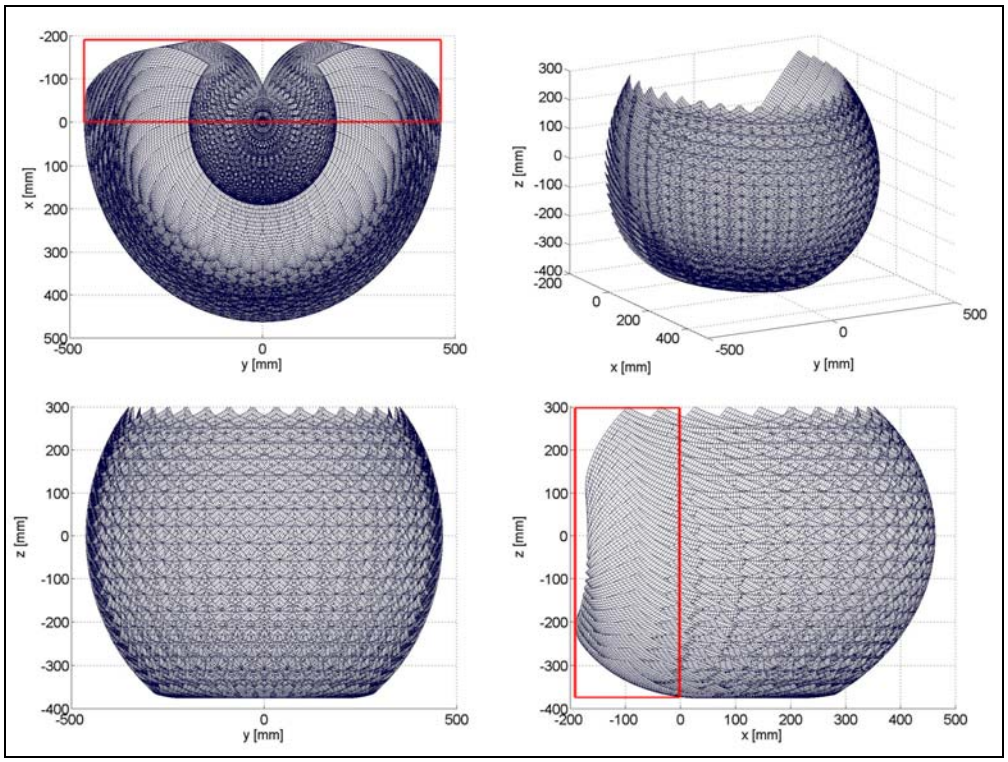

Figure 4.3 Translational Workspace of the 7 DOF Haptic Device

The evaluation of the translational workspace of the 7 DOF haptic device was performed by comparing it with Phantom haptic device. Phantom haptic device is simply defined as 6 DOF desktop haptic device, has largest translational workspace in literature [7] and it does not include only θ_3 joint variable as compared with the 7 DOF haptic device. Figure 4.4 shows translational workspace of the Phantom haptic device, created with same link lengths and same joint variable limits.

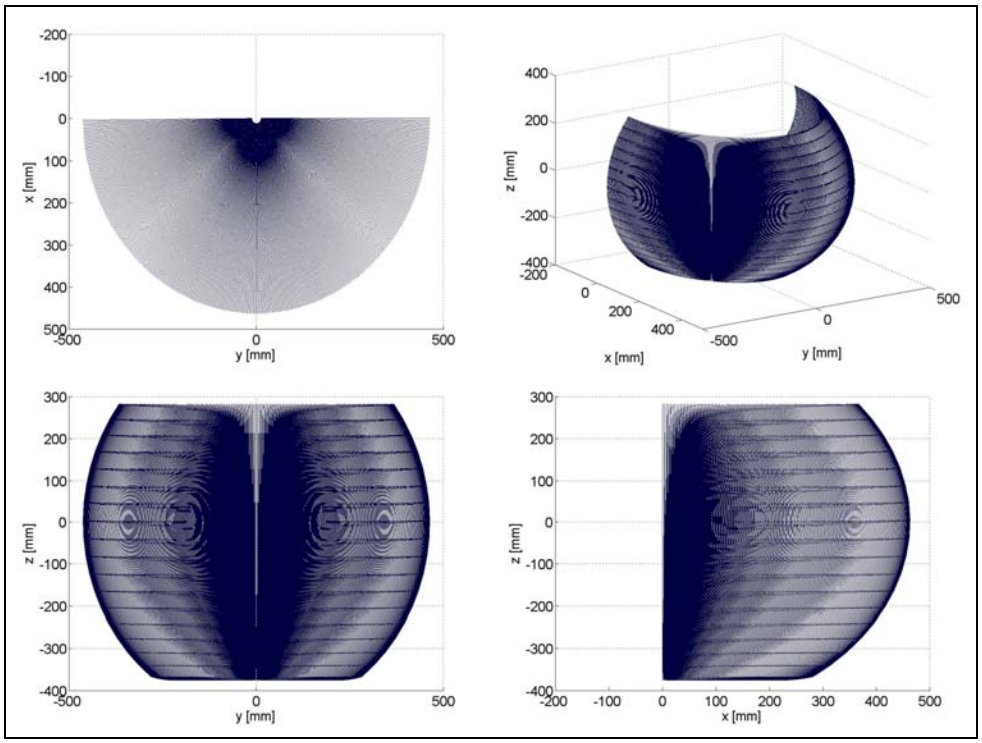

Figure 4.4 Translational Workspace of the 6 DOF Phantom Haptic Device

One can conclude that the 7 DOF haptic device has larger workspace than that of 6 DOF Phantom haptic device with the same link lengths and joint variable limits by comparing Figure 4.3 and Figure 4.4. The extended workspace was marked with red frames in Figure 4.3. Moreover, the extended workspace was calculated by SolidWorks CAD program and approximately found to be 20 % extra volume for the 7 DOF haptic device.

CHAPTER 5

DESIGN PROCEDURES

5.1 Motor Selection

The part of a robot that actually does real work is the actuator. Whether electric, hydraulic or pneumatic, this is the device that provides motion and torque to the system [26]. There are different types of motors in terms of their design concepts and function. One of them, the AC induction motor is the most common used motor in general use. This motor essentially can work at a constant speed but is rarely used in servo applications. It can be used in industrial applications due to its high power, light weight and reliable. On the other hand, an AC motor is more difficult to control than a DC motor. Therefore, brush DC motors are commonly used in servo applications which require feedback control. In addition, brushless DC motors are suitable for most servo applications because of the fact that it gives higher power in smaller size. Lastly, stepper motors are used for only position control applications, which don't require torque control.

One of the most important problems on a motion system design is the motor size. A designer should find best motors, which are suitable for the required tasks and engineering design including moment of inertia and friction characteristics of the design structure.

Figure 5.1 shows the torque-speed curves along with a corresponding current-torque curve. It can be seen that as the torque increases, speed must decrease and as the speed decreases, the current must increase. This curve gives important information about motor characteristics such that it tells us the speed and the torque are directly related to the voltage, and the current respectively. The torque-speed graph also gives the information about no-load speed (where the torque is zero) and the stall torque (where the speed is zero). Once the torque requirement is known the speed can be inferred from the graph and the power requirement calculated from P=ST for power P, speed S and torque T [26].

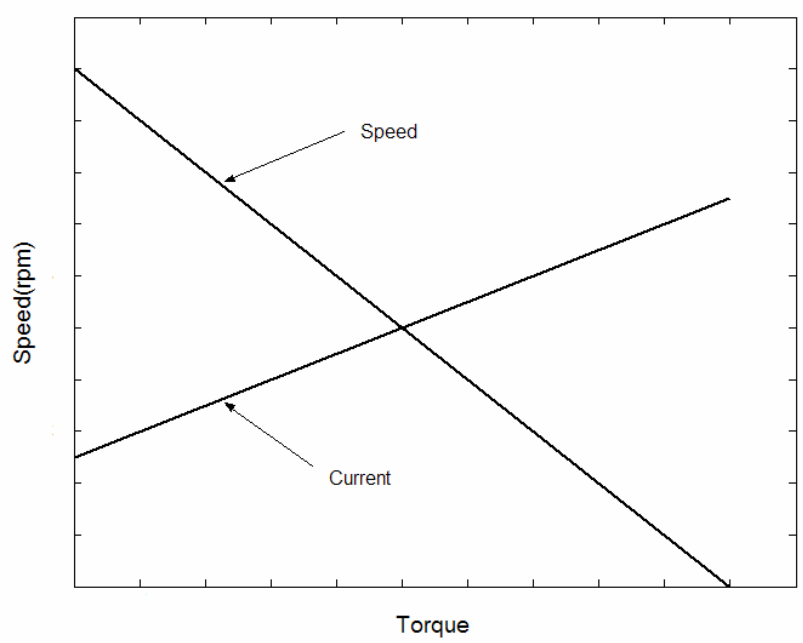

Figure 5.1 Torque-Speed Graph of Motors Corresponding Current-Torque Curve

5.1.1 AC Motors

AC induction motors are the most common motors used in industrial motion control systems. The main advantages of AC induction motors are simple design, low cost, low maintenance and direct connection to an AC power source. Although AC induction motors are easier to design than DC motors, the speed and the torque control in various types of AC induction motors require a greater understanding of the design and the characteristics of these motors [27].

5.1.2 DC Motors

DC motors can be controlled to rotate in two direction or their drives are relatively simple in analog or digital control signals by this way speed (voltage) or torque (current) can be controlled to drive DC motors. These properties make DC motors are most preferred actuators for most different servo feedback systems. They also come in a lot of different sizes from the minimotors for medical applications to the large motors for industrial robots.

5.1.3 Brushless DC Motors

Brushless Direct Current (BLDC) motors do not include brushes for commutation; instead, they are electronically commutated. BLDC motors have different types of application areas such as automotive, aerospace, consumer, medical, industrial automation equipment and instrumentation. BLDC motors have many advantages over AC induction motors and brushed DC motors which are summarized in Table 5.1 and Table 5.2.

Table 5.1 Comparison between Brushless DC and AC Induction Motor [28]

Feature	BLDC Motor	AC induction motor
Speed/Torque Characteristics	Enables operation at all speeds with rated load.	Lower torque at lower speeds.
Output power/ Frame Size	Since it has permanent magnets on the rotor, smaller size can be achieved for a given output power.	Since both stator and rotor have windings, the output power to size is lower than BLDC.
Rotor Inertia	Better dynamic characteristics.	Poor dynamic characteristics.
Starting Current	No special starter circuit required.	Starter circuit rating should be carefully selected.
Control Requirements	A controller is always required to keep the motor running. The same controller can be used for variable speed control.	No controller is required for fixed speed; a controller is required only if variable speed is desired
Slip	No slip is experienced between stator and rotor frequencies.	The rotor runs at a lower frequency than stator by slip frequency and slip increases with load on the motor.

Table 5.2 Comparison between Brushless DC and Brushed DC Motor [28]

Feature	BLDC Motor	Brushed DC motor
Commutation	Electronic commutation based on hall position sensors.	Brushed commutation.
Maintenance	Less maintenance required due to absence of brushes.	Periodic maintenance is required.
Life	Longer.	Shorter.
Speed/Torque Characteristics	Enables operation at all speeds with rated load.	At higher speeds, brush friction increases, thus reducing useful torque.
Efficiency	No voltage drop across brushes.	Moderate.
Output Power/Frame Size	Reduced size due to superior thermal characteristics. Because BLDC has the windings on the stator, which is connected to the case, the heat dissipation is better.	The heat produced by the armature is dissipated in the air gap, thus increasing the temperature in the air gap and limiting specs on the output power/frame size.
Rotor Inertia	It has permanent magnets on the rotor. This improves the dynamic response.	Higher rotor inertia which limits the dynamic characteristics.
Speed Range	No mechanical limitation imposed by brushes/commutator.	Mechanical limitations by the brushes.
Electric Noise Generation	Low.	Arcs in the brushes will generate noise causing EMI in the equipment nearby.
Cost of Build	Since it has permanent magnets, building costs are higher.	Low.
Control	Complex and expensive.	Simple and inexpensive.
Control Requirements	A controller is always required to keep the motor running. The same controller can be used for variable speed control.	No controller is required for fixed speed; a controller is required only if variable speed is desired.

5.1.4 Stepper Motors

Stepper motors are good solution for the open loop problem. There are many applications which require point to point movement of a small load in a known time. If the velocity and torque are not critical, stepper motors can be an excellent solution because of their simplicity. Additionally, they can be accurate, inexpensive and handle small light loads effectively.

When we consider all different types of motors, BLDC motors have more advantages than the others. Especially, high output power/frame size, high efficiency and low rotor inertia of the BLDC motors are excellent advantages to design a mechanical arm haptic device. This type of design requires high torque, high efficiency, low inertia at small sizes and weights. Therefore, four BLDC motors were preferred to create the required force at wrist point in our design. Then, three DC minimotors were used to create the required torques around yaw, pitch and roll axes of the haptic pen.

5.1.4 Motor Selection Calculations

Due to the fact that haptic pen of the device is actuated by user's hand, therefore, haptic devices work under very low velocity. While performing haptic applications, encoders sense the position and orientation of the haptic pen and all motors provide required forces and torques to user's hand at specified points. As mentioned in Chapter 2, maximum required forces and torques can be listed as below;

- 10 N peak force on every direction at wrist point
- 1.5 N continuous force on every direction at wrist point
- 500 Nmm yaw, pitch axis peak torque and 130 Nmm roll axis peak torque,
- 180 Nmm yaw, pitch axis continuous torque, 50 Nmm roll axis continuous torque

All peak forces and peak torques should be provided by stall torques of selected motors. Since these all specified values correspond to very low speed motions or start and stop operations.

Minimotor selection for the specified torques;

The specified peak torques given for the frames of haptic tool were used as reference to select the last three DC minimotors directly. In the selection of DC minimotors, some criteria such as minimum size (less than 20mm diameter), backdrive friction and required torques were taken into consideration. When Maxon DC minimotors are examined, it can be concluded that the required torques can not be produced without using gearheads. Therefore, gearheads with small gear ratio should be used in order to create the required torques in minimum backdrive friction. In order to satisfy these conditions, the gear ratio of the selected gearheads of the yaw and pitch axes for minimotor 1 and 2 are 19:1, the gear ratio of the gearhead of the roll axis for minimotor 3 is 5.4:1 and These commercially available gearheads have 90 % efficiency. The minimum stall torques required in our case were determined by using the corresponding values of peak torque, gear ratios and efficiency;

Minimum stall torques for minimotor 1 and 2;

$$M_{Stall} = \frac{M_{peak\ (yaw,\ pitch)}}{i.\eta} = \frac{500}{(19/1).(0.9)} = 28.72\ \text{Nmm}$$

Minimum stall torque for minimotor 3;

$$M_{Stall} = \frac{M_{peak(roll)}}{i.\eta} = \frac{130}{(5.4/1).(0.9)} = 26.75\ \text{Nmm}$$

Three Maxon minimotors with 28.8 Nmm stall torque (118730 series Moxon Minimotor with 16 mm diameter) were selected to provide the minimum stall

torque values. Additionally, the maximum continuous torques of the 7 DOF haptic device were calculated by using corresponding values of continuous torque, gear ratios and efficiency of the selected minimotors;

Yaw and pitch axis maximum continuous torque of 7 DOF haptic device;

$$M_{max,yaw} = M_{max,pitch} = M_{max,cont}.i.\eta = (4.98).(19/1).(0.9) = 86.2 \text{ Nmm}$$

Roll axis maximum continuous torque of 7 DOF haptic device;

$$M_{max,roll} = M_{max,cont}.i.\eta = (4.98).(5.4/1).(0.9) = 24.2 \text{ Nmm}$$

These obtained results may not provide prerequisite torques' values for some specific applications. In such cases, BLDC minimotors with higher output torques in small sizes can be used to overcome this problem.

Motor selection for the specified forces;

The virtual work method in the static force analysis can be used in order to determine the motors to be used for specified forces due to the very low velocity on the basis of a single general equation given in the literature [29]. As shown in the formula, all driving torques depend on the wrist forces and torques. The gravity forces and torques and a Jacobean transformation matrix can be given as;

$$\bar{Q} = \bar{G} - \hat{J}_r^T.\bar{R} \qquad (5.1)$$

In our design, all moving parts were balanced and their mass center was concentrated on the intersection point of first three rotation axes (support center). The detailed information about the static balance will be discussed in the next section. The gravity forces and torques in Eq. (5.1) can be omitted due to this

performed static balance. So, Eq (5.2) can be written to find out required motor torques;

$$\bar{Q} = -\hat{J}_r^{\,T}.\bar{R} \tag{5.2}$$

The parameters $\hat{J}_r^{\,T}$, $\hat{J}$, $\bar{Q}$, $\bar{R}$ in Eq. (5.2) represent a transformation matrix that converts the wrist space into the joint space, Jacobean matrix, the driving torques, and the task forces and torques at wrist point, respectively. The Jacobean matrix for 7 DOF haptic device includes 7 column and 6 row;

$$\hat{J} = \begin{bmatrix} \bar{J}_{r1} & \bar{J}_{r2} & \bar{J}_{r3} & \bar{J}_{r4} & \bar{J}_{r5} & \bar{J}_{r6} & \bar{J}_{r7} \\ \bar{J}_{a1} & \bar{J}_{a2} & \bar{J}_{a3} & \bar{J}_{a4} & \bar{J}_{a5} & \bar{J}_{a6} & \bar{J}_{a7} \end{bmatrix} \tag{5.3}$$

The Jacobean matrix components $\bar{J}_{rk}$ and $\bar{J}_{ak}$ can be represented as below;

$$\bar{J}_{rk} = \frac{\partial \bar{r}}{\partial \theta_k} \tag{5.4}$$

$$\bar{J}_{ak} = \mathrm{col}\left[\left(\frac{\partial \hat{C}}{\partial q_k}\right).\hat{C}^T\right] \tag{5.5}$$

The Jacobean matrix components can be derived by using Eq. (5.4), Eq (5.5);

$$\bar{J}_{r1} = e^{\tilde{u}_3\theta_1}\tilde{u}_3 e^{\tilde{u}_2\theta_2}\left[d_3\bar{u}_3 + d_4 e^{\tilde{u}_3\theta_3} e^{\tilde{u}_2\theta_4}\bar{u}_3\right] \tag{5.6}$$

$$\bar{J}_{r2} = e^{\tilde{u}_3\theta_1} e^{\tilde{u}_2\theta_2}\tilde{u}_2\left[d_3\bar{u}_3 + d_4 e^{\tilde{u}_3\theta_3} e^{\tilde{u}_2\theta_4}\bar{u}_3\right] \tag{5.7}$$

$$\bar{J}_{r3} = e^{\tilde{u}_3\theta_1} e^{\tilde{u}_2\theta_2} d_4 e^{\tilde{u}_3\theta_3}\tilde{u}_3 e^{\tilde{u}_2\theta_2}\bar{u}_3 \tag{5.8}$$

$$\bar{J}_{r4} = e^{\tilde{u}_3\theta_1} e^{\tilde{u}_2\theta_2} d_4 e^{\tilde{u}_3\theta_3} e^{\tilde{u}_2\theta_2}\tilde{u}_2\bar{u}_3 \tag{5.9}$$

$$\bar{J}_{r5} = \bar{J}_{r6} = \bar{J}_{r7} = 0 \tag{5.10}$$

$$\overline{J}_{a1} = \overline{u}_3 \tag{5.11}$$

$$\overline{J}_{a2} = e^{\tilde{u}_3\theta_1}\overline{u}_2 \tag{5.12}$$

$$\overline{J}_{a3} = e^{\tilde{u}_3\theta_1}e^{\tilde{u}_2\theta_2}\overline{u}_3 \tag{5.13}$$

$$\overline{J}_{a4} = e^{\tilde{u}_3\theta_1}e^{\tilde{u}_2\theta_2}e^{\tilde{u}_3\theta_3}\overline{u}_2 \tag{5.14}$$

$$\overline{J}_{a5} = e^{\tilde{u}_3\theta_1}e^{\tilde{u}_2\theta_2}e^{\tilde{u}_3\theta_3}e^{\tilde{u}_2\theta_4}\overline{u}_3 \tag{5.15}$$

$$\overline{J}_{a6} = e^{\tilde{u}_3\theta_1}e^{\tilde{u}_2\theta_2}e^{\tilde{u}_3\theta_3}e^{\tilde{u}_2\theta_4}e^{\tilde{u}_3\theta_5}\overline{u}_2 \tag{5.16}$$

$$\overline{J}_{a7} = e^{\tilde{u}_3\theta_1}e^{\tilde{u}_2\theta_2}e^{\tilde{u}_3\theta_3}e^{\tilde{u}_2\theta_4}e^{\tilde{u}_3\theta_5}e^{\tilde{u}_2\theta_6}\overline{u}_3 \tag{5.17}$$

All of the static analyses in the selection of the motors should be performed in most extended form of the device, matching to the most critical positions. For this reason, all critical positions were determined at the beginning. Figure 5.2 shows the possible critical positions of the 7 DOF haptic device within the joint limitations.

The motor torques for the 7 DOF haptic device were calculated by an iterative algorithm including the combination of Eq.(5.2) and its sub-equations using MATLAB software program. This iterative algorithm enables us to find out all driving torques in the known positions (θ_1, θ_2, θ_3, θ_4, θ_5, θ_6, θ_7), task forces and torques. The motor torque values for the given three positions in Figure 5.2 were obtained by considering the specified peak force/torque and maximum continuous force/torque on the basis of different (x, y, z)-coordinates. The results were obtained by using this specified method considering of the different conditions including; three critical positions given in Figure 5.2, (x, y, z) directed forces and all possible specified torques.

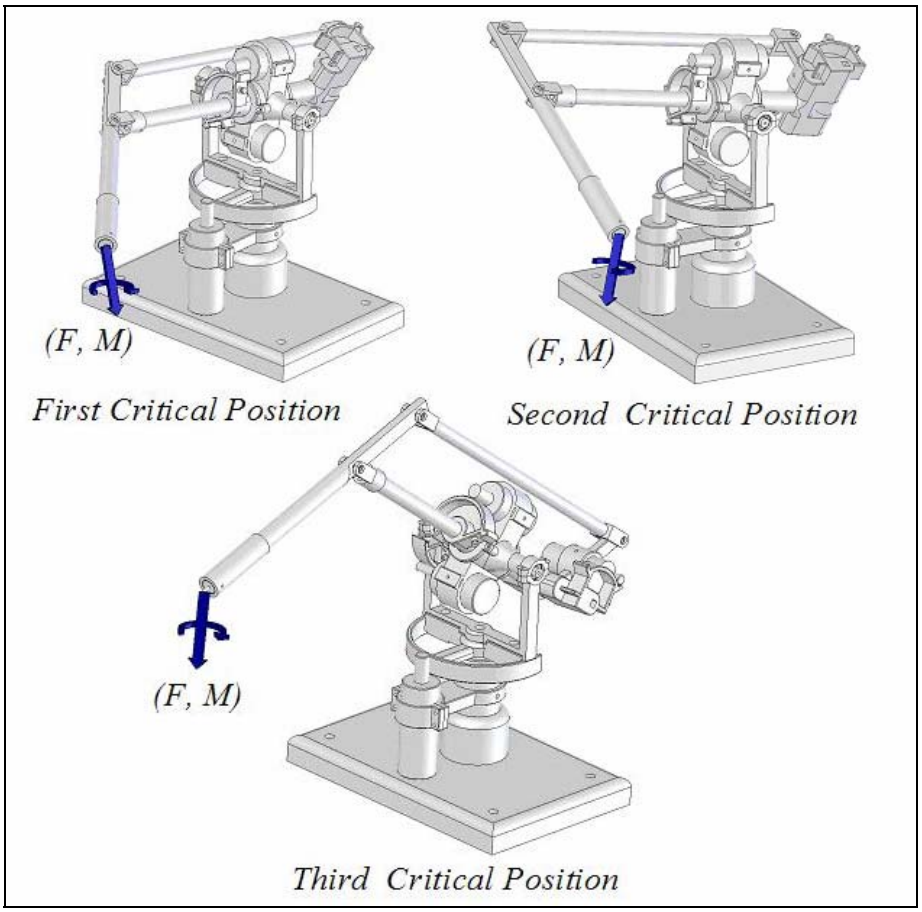

Figure 5.2 Critical Positions of the 7 DOF Haptic Device for Motor Selection

The possible driving torque results corresponding to the first critical position

(θ_1=0, θ_2=90, θ_3=60, θ_4= 45 θ_5=90, θ_6=90, θ_7=90)

$$Fx_{peak} = \begin{bmatrix} 10 \\ 0 \\ 0 \end{bmatrix} N \quad , \quad M_{peak} = \begin{bmatrix} 0.5 \\ 0.5 \\ 0.5 \end{bmatrix} Nm \quad \Rightarrow \quad Q_{peak} = \begin{bmatrix} 0.848 \\ 0.401 \\ 0.224 \\ 0.935 \end{bmatrix} Nm$$

$$Fy_{peak} = \begin{bmatrix} 0 \\ 10 \\ 0 \end{bmatrix} N \quad , \quad M_{peak} = \begin{bmatrix} 0.5 \\ 0.5 \\ 0.5 \end{bmatrix} Nm \quad \Rightarrow \quad Q_{peak} = \begin{bmatrix} 4.951 \\ 0.483 \\ 1.108 \\ 2.364 \end{bmatrix} Nm$$

$$Fz_{peak}=\begin{bmatrix}0\\0\\10\end{bmatrix}N \quad , \quad M_{peak}=\begin{bmatrix}0.5\\0.5\\0.5\end{bmatrix}Nm \quad \Rightarrow \quad Q_{peak}=\begin{bmatrix}0.683\\3.785\\1.755\\0.051\end{bmatrix}Nm$$

$$Fx_{maxcont}=\begin{bmatrix}1.5\\0\\0\end{bmatrix}N \quad , \quad M_{maxcont}=\begin{bmatrix}0.18\\0.18\\0.18\end{bmatrix}Nm \quad \Rightarrow \quad Q_{maxcont}=\begin{bmatrix}0.016\\0.041\\0.081\\0.035\end{bmatrix}Nm$$

$$Fy_{maxcont}=\begin{bmatrix}0\\1.5\\0\end{bmatrix}N \quad , \quad M_{maxcont}=\begin{bmatrix}0.18\\0.18\\0.18\end{bmatrix}Nm \quad \Rightarrow \quad Q_{maxcont}=\begin{bmatrix}0.886\\0.174\\0.213\\0.510\end{bmatrix}Nm$$

$$Fz_{maxcont}=\begin{bmatrix}0\\0\\1.5\end{bmatrix}N \quad , \quad M_{maxcont}=\begin{bmatrix}0.18\\0.18\\0.18\end{bmatrix}Nm \quad \Rightarrow \quad Q_{maxcont}=\begin{bmatrix}0.246\\0.466\\0.310\\0.167\end{bmatrix}Nm$$

The possible driving torque results corresponding to the second critical position (θ_1=0, θ_2=90, θ_3=60, θ_4= 90 θ_5=90, θ_6=90, θ_7=90)

$$Fx_{peak}=\begin{bmatrix}10\\0\\0\end{bmatrix}N \quad , \quad M_{peak}=\begin{bmatrix}0.5\\0.5\\0.5\end{bmatrix}Nm \quad \Rightarrow \quad Q_{peak}=\begin{bmatrix}1.482\\1.067\\0.5\\1.817\end{bmatrix}Nm$$

$$Fy_{peak}=\begin{bmatrix}0\\10\\0\end{bmatrix}N \quad , \quad M_{peak}=\begin{bmatrix}0.5\\0.5\\0.5\end{bmatrix}Nm \quad \Rightarrow \quad Q_{peak}=\begin{bmatrix}3.183\\0.183\\1.750\\0.683\end{bmatrix}Nm$$

$$Fz_{peak}=\begin{bmatrix}0\\0\\10\end{bmatrix}N \quad , \quad M_{peak}=\begin{bmatrix}0.5\\0.5\\0.5\end{bmatrix}Nm \quad \Rightarrow \quad Q_{peak}=\begin{bmatrix}0.683\\2.317\\2.665\\0.683\end{bmatrix}Nm$$

$$Fx_{maxcont}=\begin{bmatrix}1.5\\0\\0\end{bmatrix}N \quad , \quad M_{maxcont}=\begin{bmatrix}0.18\\0.18\\0.18\end{bmatrix}Nm \quad \Rightarrow \quad Q_{maxcont}=\begin{bmatrix}0.079\\0.122\\0.180\\0.129\end{bmatrix}Nm$$

$$Fy_{maxcont}=\begin{bmatrix}0\\1.5\\0\end{bmatrix}N \quad , \quad M_{maxcont}=\begin{bmatrix}0.18\\0.18\\0.18\end{bmatrix}Nm \quad \Rightarrow \quad Q_{maxcont}=\begin{bmatrix}0.621\\0.066\\0.368\\0.246\end{bmatrix}Nm$$

$$Fz_{maxcont}=\begin{bmatrix}0\\0\\1.5\end{bmatrix}N \quad , \quad M_{maxcont}=\begin{bmatrix}0.18\\0.18\\0.18\end{bmatrix}Nm \quad \Rightarrow \quad Q_{maxcont}=\begin{bmatrix}0.246\\0.309\\0.400\\0.246\end{bmatrix}Nm$$

The possible driving torque results corresponding to the third critical position

(θ_1=0, θ_2=60, θ_3=0, θ_4= 45 θ_5=90, θ_6=90, θ_7=90)

$$Fx_{peak}=\begin{bmatrix}10\\0\\0\end{bmatrix}N \quad , \quad M_{peak}=\begin{bmatrix}0.5\\0.5\\0.5\end{bmatrix}Nm \quad \Rightarrow \quad Q_{peak}=\begin{bmatrix}0.500\\0.957\\0.780\\0.293\end{bmatrix}Nm$$

$$Fy_{peak}=\begin{bmatrix}0\\10\\0\end{bmatrix}N \quad , \quad M_{peak}=\begin{bmatrix}0.5\\0.5\\0.5\end{bmatrix}Nm \quad \Rightarrow \quad Q_{peak}=\begin{bmatrix}5.080\\0.354\\2.548\\0.354\end{bmatrix}Nm$$

$$Fz_{peak}=\begin{bmatrix}0\\0\\10\end{bmatrix}N \quad , \quad M_{peak}=\begin{bmatrix}0.5\\0.5\\0.5\end{bmatrix}Nm \quad \Rightarrow \quad Q_{peak}=\begin{bmatrix}0.500\\4.226\\0.780\\2.061\end{bmatrix}Nm$$

$$Fx_{maxcont}=\begin{bmatrix}1.5\\0\\0\end{bmatrix}N \quad , \quad M_{maxcont}=\begin{bmatrix}0.18\\0.18\\0.18\end{bmatrix}Nm \quad \Rightarrow \quad Q_{maxcont}=\begin{bmatrix}0.180\\0.218\\0.281\\0.030\end{bmatrix}Nm$$

$$Fy_{maxcont} = \begin{bmatrix} 0 \\ 1.5 \\ 0 \end{bmatrix} N \quad , \quad M_{maxcont} = \begin{bmatrix} 0.18 \\ 0.18 \\ 0.18 \end{bmatrix} Nm \quad \Rightarrow \quad Q_{maxcont} = \begin{bmatrix} 0.867 \\ 0.127 \\ 0.446 \\ 0.127 \end{bmatrix} Nm$$

$$Fz_{maxcont} = \begin{bmatrix} 0 \\ 0 \\ 1.5 \end{bmatrix} N \quad , \quad M_{maxcont} = \begin{bmatrix} 0.18 \\ 0.18 \\ 0.18 \end{bmatrix} Nm \quad \Rightarrow \quad Q_{maxcont} = \begin{bmatrix} 0.180 \\ 0.560 \\ 0.281 \\ 0.235 \end{bmatrix} Nm$$

Next, all of these given driving torque results were examined to select the most suitable motors by considering the maximum values of the peak driving torques and maximum continuous torques separately. Finally, these maximum values and selected gear ratios were used to specify stall torques and maximum continuous torques of every motor;

Motor 1 $\Rightarrow$ $Q1_{peak}$=5.080Nm, $Q1_{maxcont}$=0.867Nmm, i=10:1

$$M1_{stall} = \frac{Q1_{peak}}{i} = \frac{5.080}{10} = 0.508Nm, \qquad M1_{maxcont} = \frac{Q1_{maxcont}}{i} = \frac{0.867}{10} = 0.087Nm$$

Motor 2 $\Rightarrow$ $Q2_{peak}$=4.226Nm, $Q2_{maxcont}$=0.550Nmm, i=8:1

$$M2_{stall} = \frac{Q2_{peak}}{i} = \frac{4.226}{8} = 0.528Nm, \qquad M2_{maxcont} = \frac{Q2_{maxcont}}{i} = \frac{0.550}{8} = 0.069Nm$$

Motor 3 $\Rightarrow$ $Q3_{peak}$=2.665Nm, $Q3_{maxcont}$=0.446Nmm, i=5:1

$$M3_{stall} = \frac{Q3_{peak}}{i} = \frac{2.665}{5} = 0.530Nm, \qquad M3_{maxcont} = \frac{Q3_{maxcont}}{i} = \frac{0.446}{5} = 0.089Nm$$

Motor 4 $\Rightarrow$ $Q4_{peak}$=2.364Nm, $Q3_{maxcont}$=0.510Nmm, i=8:1

$$M4_{stall} = \frac{Q4_{peak}}{i} = \frac{2.364}{8} = 0.295\text{Nm}, \qquad M3_{maxcont} = \frac{Q3_{maxcont}}{i} = \frac{0.510}{8} = 0.063\text{Nm}$$

The first four motors of the 7 DOF haptic device were selected depending on the calculated values of stall torques and maximum continuous torques from Maxon catalogue;

Motor 1 : 283873 Maxon BLDC (2.19 Nm stall and 0.186 Nm max. cont. Trq)
Motor 2 : 283869 Maxon BLDC (0.64 Nm stall and 0.0849 Nm max. cont. Trq)
Motor 3 : 283869 Maxon BLDC (0.64 Nm stall and 0.0849 Nm max. cont. Trq)
Motor 4 : 283763 Maxon BLDC (0.447 Nm stall and 0.0608 Nm max. cont. Trq)

The last three minimotors combinations were determined before;

Minimotor 1 and 2: 1118730 Maxon DC minimotor - 110322 Gearhead (28.8Nmm stall and 4.98 Nmm max.cont. Torque-19/1 gear ratio)
Minimotor 3: 1118730 Maxon DC Minimotor - 110321 Gearhead (28.8Nmm stall and 4.98Nmm max. cont. Torque - 5.4/1 gear ratio)

5.2 Balance of the Positioning Stages

The part of the 7 DOF haptic device locating its tool in the workspace is called as positioning stage. It consists of two major parts; counterbalanced parallelogram and motor-shaft combination. These two counterbalanced systems achieve the static balance of the 7 DOF haptic device as well as minimum inertia. A simple line drawing of the positioning stage is given in Figure 5.3.

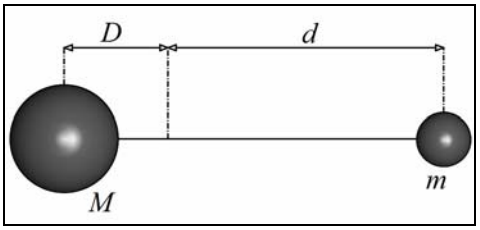

Figure 5.3 Simple Line Drawing of the Positioning Stage

Figure 5.3 refers to the mass of a cantilevered structure set at distance d from a pivot point. Parameters m and d are given by geometrical and structural requirements. M and D should be found such that the system is balanced under gravity and the inertia is minimized. Static balancing yields md = MD. M should be found such that $I = MD^2 + md^2 = md^2 (m / M + 1)$ is minimum [30]. This expression is minimum, when M is maximum which means that the best design has the heaviest counter-weight. The mass is assumed to be concentrated at the motors, so we will use them as counter-weights. The first requirement is to place the motors so that the mass center of the system coincides with its support center and the second is to keep this property invariant under any motion of the device. For this purpose, a counterbalanced parallelogram was designed, which is given in Figure 5.4. In this way, mass center of the positioning stage was concentrated on the support center, so that it is near to the support center.

In Figure 5.4, all of the link masses, the lumped mass of wrist assembly and the counter weight are shown together with its locations, on the skeleton view of the

positioning stage. Since first and third links are in the same direction of $\vec{u}_3^{(2)}$, similarly second and fourth links are in the same direction of $\vec{u}_1^{(4)}$ in the kinematics model of the device, the general mass center equation can be applied around these two vector in order to balance the positioning stage. As a result of this procedure, two simple equations were derived using the general mass center equation. The weight of the haptic pen is not included in the derivations, since it is in the user's hand during the haptic operations.

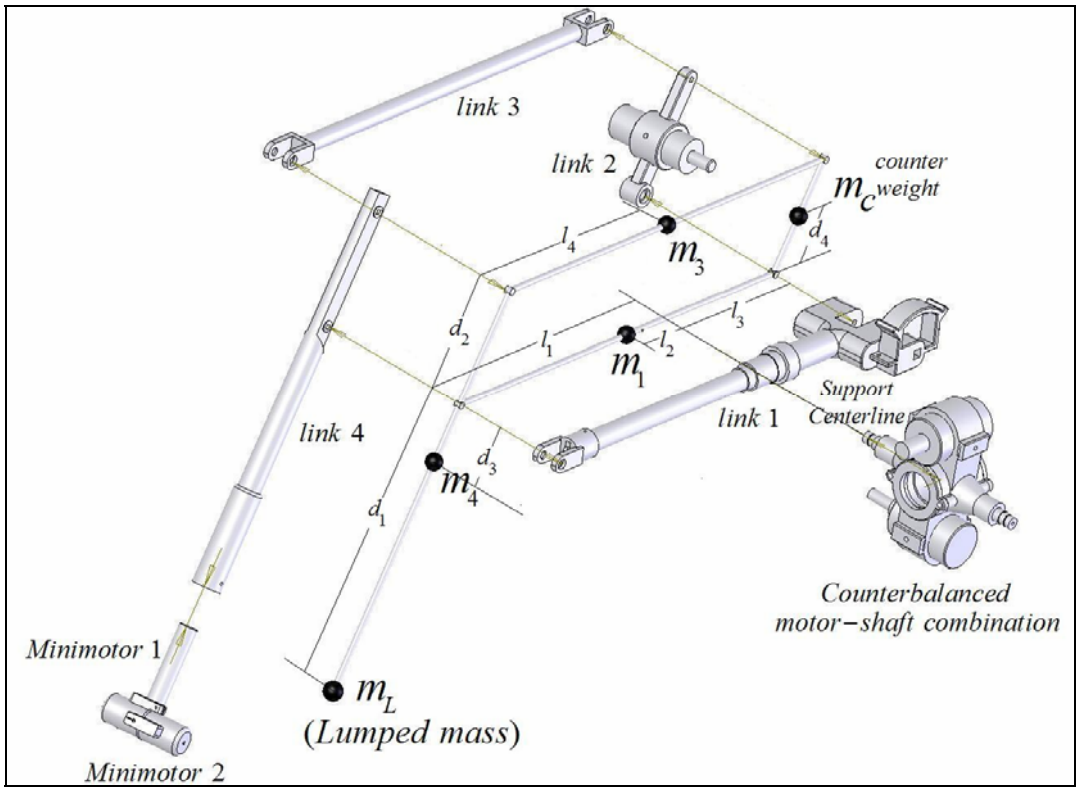

Figure 5.4 Exploded View of the Counterbalanced Parallelogram

Mass center of the system;

$$\vec{r}_G = \frac{\sum m_i \vec{r}_i}{\sum m_i} \tag{5.18}$$

The center of mass of the system can be concentrated on the support center provided that the numerator of the Eq.(5.18) is equal to zero;

$$\sum \vec{m}_i \vec{r}_i = 0 \tag{5.19}$$

If Eq.(5.19) is extended;

$$m_1\vec{r}_1 + m_3\vec{r}_3 + m_4\vec{r}_4 + m_L\vec{r}_L + m_c\vec{r}_c = 0 \tag{5.20}$$

$$\begin{aligned} &m_1 l_2 \vec{u}_3^{(2)} + m_3(l_1 - l_4)\vec{u}_3^{(2)} - m_3 d_2 \vec{u}_1^{(4)} + m_4 l_1 \vec{u}_3^{(2)} + \\ &m_4 d_3 \vec{u}_1^{(4)} + m_L l_1 \vec{u}_3^{(2)} + m_L d_1 \vec{u}_1^{(4)} - m_c l_3 \vec{u}_3^{(2)} - m_c d_4 \vec{u}_1^{(4)} = 0 \end{aligned} \tag{5.21}$$

$$\begin{aligned} &[m_1 l_2 + m_3(l_1 - l_4) + m_4 l_1 + m_L l_1 - m_c l_3]\vec{u}_3^{(2)} + \\ &[-m_3 d_2 + m_4 d_3 + m_L d_1 - m_c d_4]\vec{u}_1^{(4)} = 0 \end{aligned} \tag{5.22}$$

All terms of the Eq.(5.22) can be represented in the matrix form by transforming to the second reference frame ($\vec{u}_k^{(2)}$);

$$\begin{bmatrix} [-m_3 d_2 + m_4 d_3 + m_L d_1 - m_c d_4]\cos\theta_3 \cos\theta_4 \\ [-m_3 d_2 + m_4 d_3 + m_L d_1 - m_c d_4]\sin\theta_3 \cos\theta_4 \\ [m_1 l_2 + m_3(l_1 - l_4) + m_4 l_1 + m_L l_1 - m_c l_3] - [-m_3 d_2 + m_4 d_3 + m_L d_1 - m_c d_4]\sin\theta_4 \end{bmatrix} = \begin{bmatrix} 0 \\ 0 \\ 0 \end{bmatrix} \tag{5.23}$$

In order to achieve Eq.(5.23) and to keep the center of mass location invariant under any motion, the following two simple equations should be satisfied;

$$[m_1 l_2 + m_3(l_1 - l_4) + m_4 l_1 + m_L l_1 - m_c l_3] = 0 \tag{5.24}$$

$$[-m_3 d_2 + m_4 d_3 + m_L d_1 - m_c d_4] = 0 \tag{5.25}$$

In order to achieve the static balance, the link parameters (m_1, m_3, m_4, m_4, l_1, l_2, l_4, d_1, d_2, d_3) given in these two equations can be selected and the counterweight

parameters (mc, l_3, d_4) can be determined before satisfying the other design criteria. Using all defined optimizations, the links and weight parameters can be found;

m_1=210g, m_3=160g, m_4=170g, m_L=120g, m_c=570g, d_1=250mm, d_2=100mm,

l_1=250mm, l_2=-45mm, l_3=130mm, l_4=190mm, d_3=65mm, d_4=45mm

The counterweight consist of two major masses, the first is the motor weight itself (270g) and other is the weight of link 2 (300g), which was made of steel.

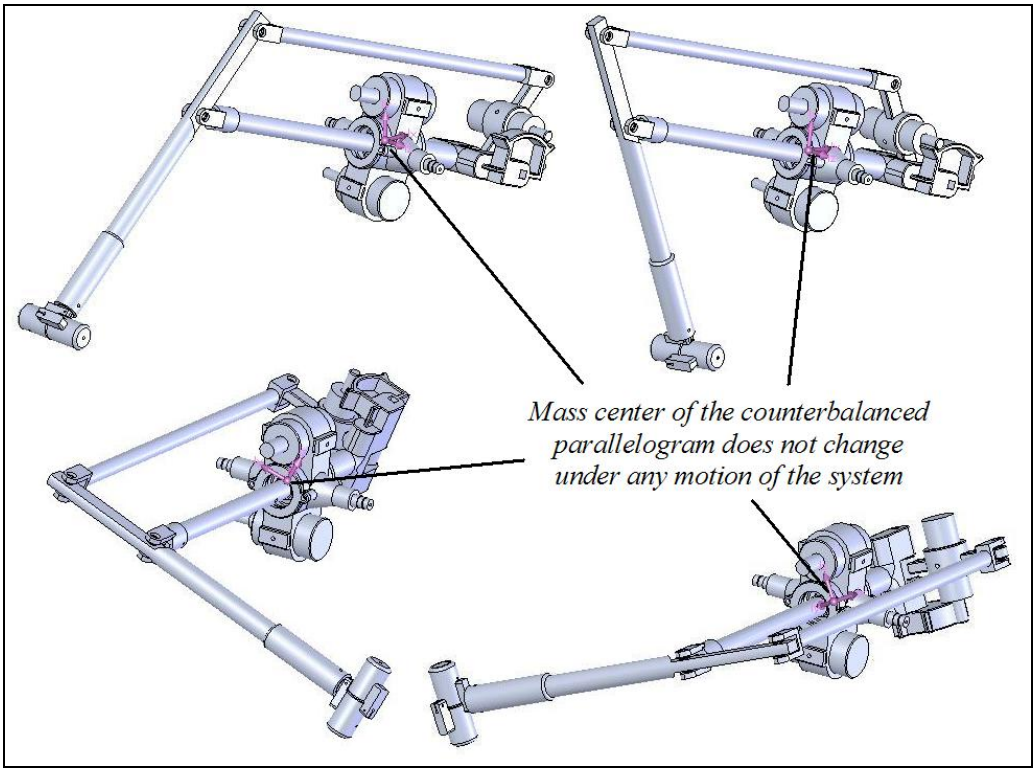

Figure 5.5 Center of Mass of the Counterbalanced Parallelogram

Center of mass location of the haptic device is important to achieve minimum inertia and the desired apparent mass at the tip point. Apparent mass at the tip point is an unwanted mass, which affects the user's hand during operation. This mass was minimized by performing the static balance calculations in our design. The weight of haptic pen was not considered in these calculations due to the fact that it is in the user's hand during the haptic operations.

The specified apparent mass at the tip point, which is about 150 grams, includes the mass of haptic pen and the unbalanced mass of the all moving parts. For the performance evaluation of the 7 DOF haptic device, this value was measured at different positions by using a sensitive weighting machine. The measured average value is approximately 150 grams. This value satisfies our objective. Figure 5.6 shows the apparent mass at tip point measured in different positions.

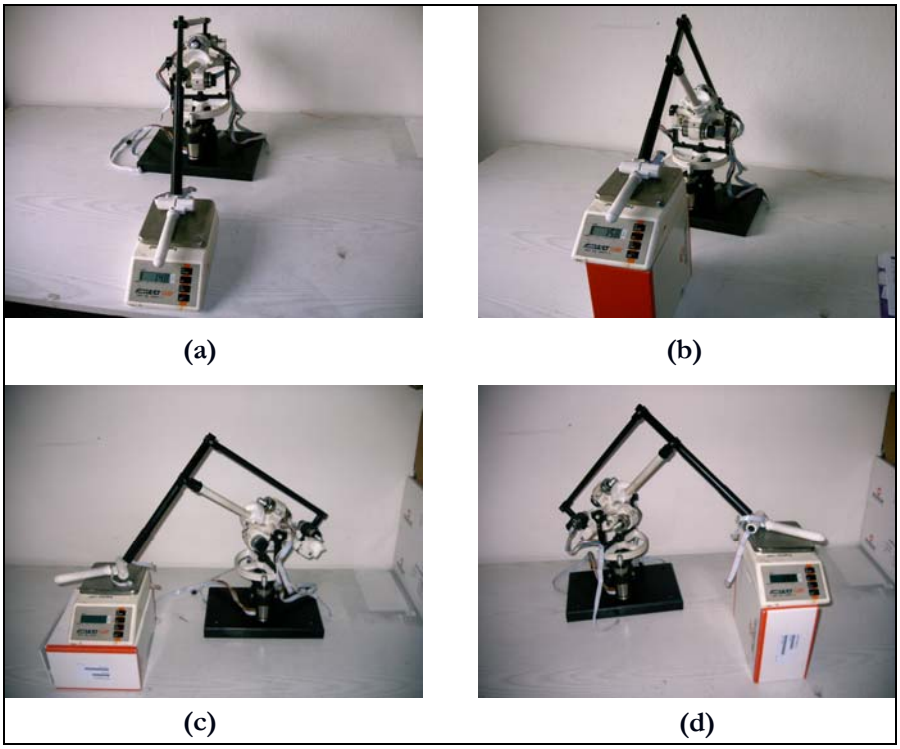

Figure 5.6 Measurements of Apparent Mass for the 7 DOF Haptic Device

5.3 Stiffness Analysis

One of the most desired characteristics of haptic devices is high stiffness, which provides accurate positioning, realistic simulation and high payload capability. Stiffness is a mechanical characteristic, which describes the behavior of a structure under static force in terms of elastic deflection. It can be evaluated for robotic manipulators by means of specific formulation and experimental tests in agreement with the general coded rules [31].

In the haptic device design, stiffness depends on two major characteristics; structure and backlash. These two characteristics should be taken into consideration in order to achieve the desired stiffness.

In order to obtain high stiffness, the structure should have low inertia which can be achieved by low mass. For this reason, aluminum and polyamide materials were preferred due to their lightweight and mechanical properties. However, steel material was selected where we need to create counterweight. In order to strengthen the link made of polyamide material the carbon rod was used. Figure 5.7 shows how the polyamide and carbon rod was combined for the intermediate link.

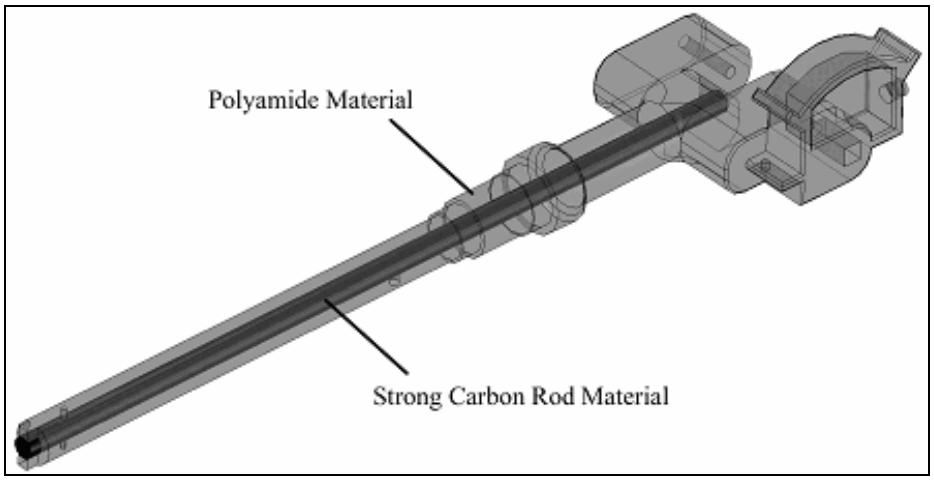

Figure 5.7 Strengthened Composite Link

The actual stiffness of a manipulator can be derived from the deflections of the links forming the arm. The use of parallel linkage configuration gives a better result comparing to the serial linkage configuration in terms of stiffness. Therefore, a parallel linkage has been added to the design (Figure 5.8). As a second precaution, the cable driven transmission mechanism was preferred in order to minimize the unwanted deflections of the tip point due to the transmission backlash. These two precautions; the parallel mechanism and the cable driven mechanism, which are used in the design are shown in Figure 5.8 and Figure 5.9.

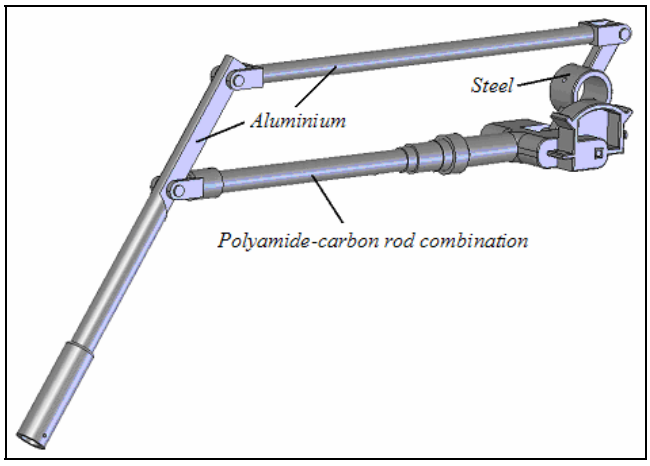

.

Figure 5.8 Parallel Mechanism for High Stiffness in the 7 DOF Haptic Device

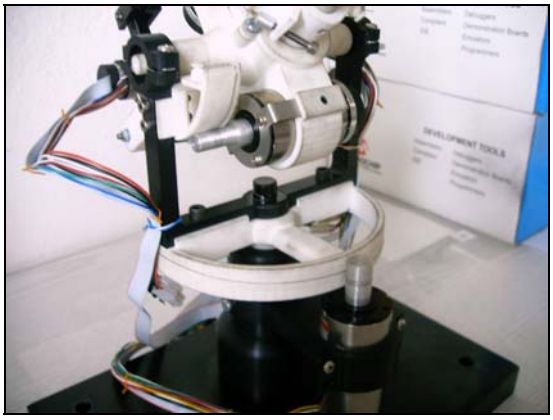

Figure 5.9 Cable Driven Transmission Mechanism in the 7 DOF Haptic Device

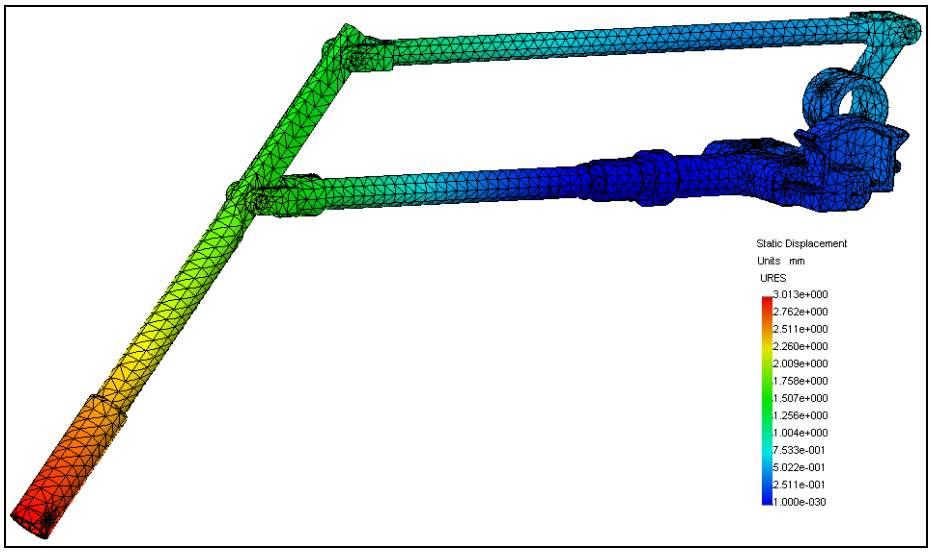

Figure 5.10 Displacement of Parallel Mechanism without Carbon Rod

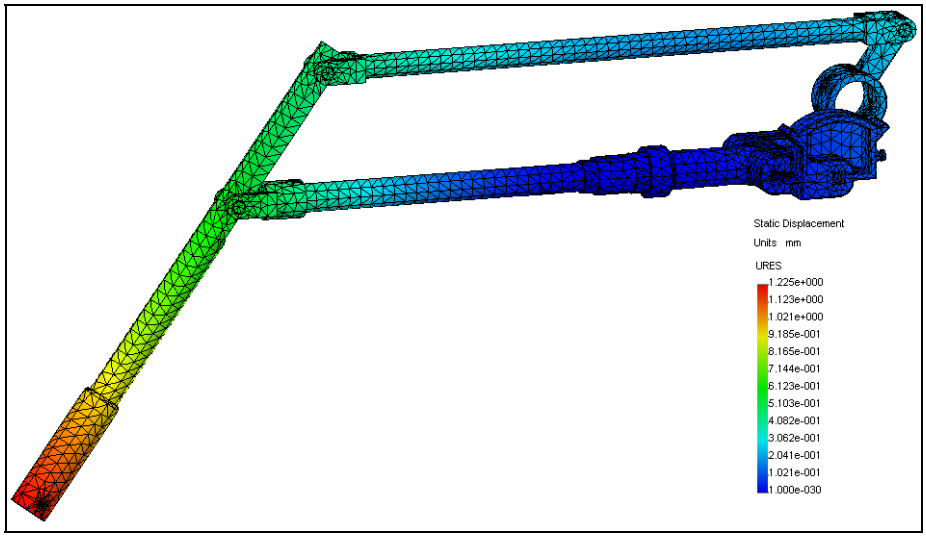

Figure 5.11 Displacement of Parallel Mechanism with Carbon Rod

A finite element analysis has been performed by using COSMOS/Works FEA software package in order to evaluate the stiffness of the designed structure. The result, when 10 N force is applied at the tip point, is given in Figure 5.10 and 5.11. When these two figures are compared, it can be concluded that using a carbon rod

material in the design decreases tip point displacement from 3 mm to 1 mm. The performed analysis does not show overall stiffness, however, it gives only an idea for the stiffness of the device and the obtained theoretical results satisfies our design criteria in order to continue to the detailed design.

The stiffness of the designed 7 DOF haptic device arises from the material deflections, the bearing gaps, the cable tensions and the backlash. In the evaluation of the stiffness, the theoretical representation of 7 DOF haptic device is cumbersome. The exact solution can not be found easily with analytical methods. In order to gain overall stiffness, the 7 DOF haptic device can be tested by experimental methods. To illustrate, the stiffness of the 7 DOF haptic device was measured by using a CMM (Coordinate Measuring Machine). In this procedure, two types of measurements have been performed; the first one is the measurement of the tip point of the device without any load in the most extended form and the other one is the measurement of the tip point with loads in (x, y, z) directions. The loads were directed by using a hanging up mechanism with a mass of 640 grams. Finally, approximately 1N/mm overall stiffness value was measured for the designed 7 DOF haptic device. The measurement of the overall stiffness of the 7 DOF haptic device is shown in Figure 5.12. Figure 5.12 (a) shows the coordinate measurement without any load applied to the haptic device, Figure 5.12 (b) shows the deflection measurement under a specified load along x direction (3.3mm), Figure 5.12 (c) shows the deflection measurement under the same load along y direction (7.1mm), Figure 5.12 (d) shows the deflection measurement under the same load along z direction (5.1mm).

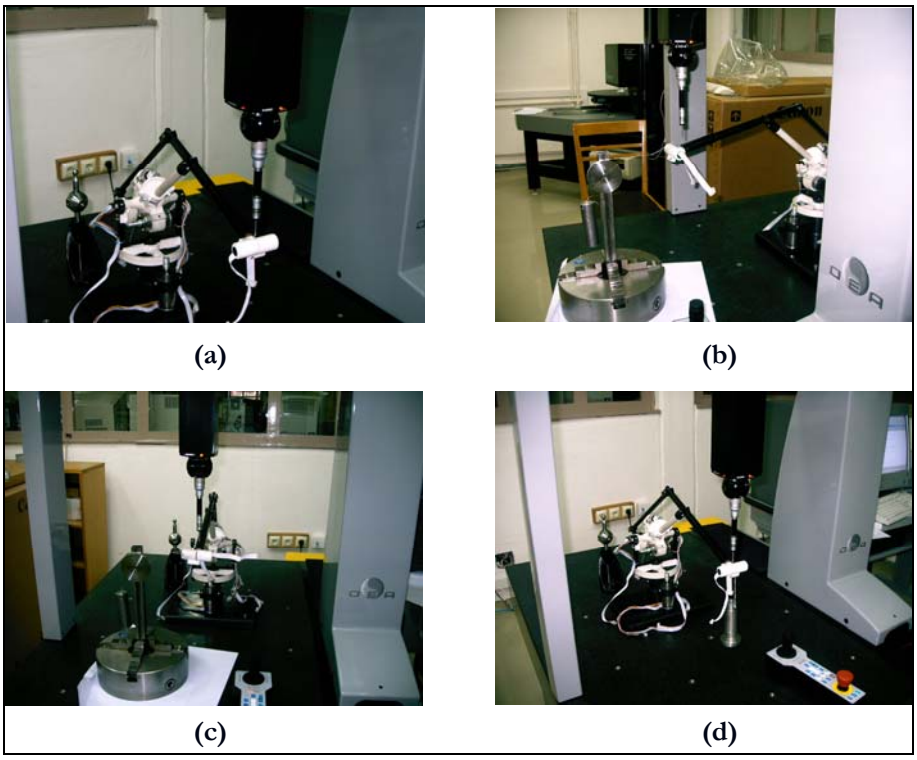

Figure 5.12 Overall Stiffness Measurements for the 7 DOF Haptic Device

5.4 Resolution Analysis

The resolution of the haptic devices is important in order to sense very small motion of the haptic tool in the applications. The best simulation and high accuracy in the haptic applications can be achieved by the help of high resolution haptic devices. Therefore, the resolution of a haptic device should be increased as much as possible in a design. The resolution of haptic devices can be observed in two ways; translational and rotational resolution. The translational resolution is the maximum translational movement of the haptic tool to be sensed and rotational resolution is the maximum rotation of it to be sensed. Commercially available high resolution incremental encoders, suitable for the selected motors, were used to increase the resolution of the 7 DOF haptic device. In order to find out the resolution of the 7 DOF haptic device, some approximate calculations

have been performed by using the forward kinematics equations, gear ratios and the encoder's pulses.

The selected encoders in the design are given below;

- Selected encoders for first four BLDC motors: 225787 Maxon digital MR encoder with 1024 pulses per revolution.
- Selected encoders for last three DC minimotors: 2MCH Hollow shaft encoder with 5000 pulses per revolution.

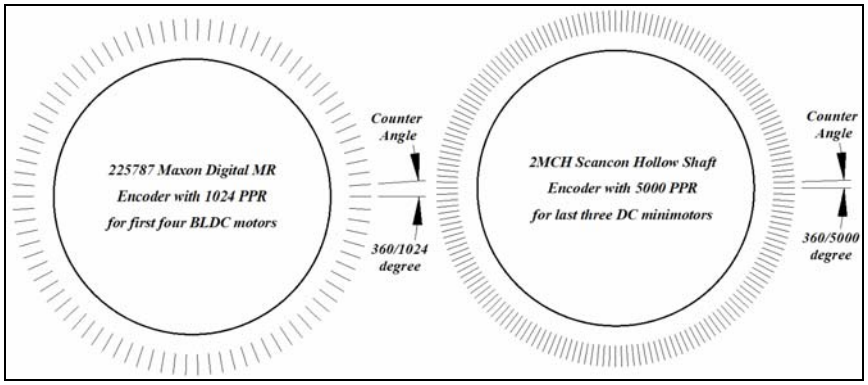

Figure 5.13 Selected Incremental Encoders for the 7 DOF Haptic Device

Rotational resolution;

The rotational resolution around yaw, pitch, roll axes of the haptic pen can be calculated by taking into account the selected encoder's pulses per revolution and gear ratio directly;

Rotational resolution around yaw axis;

$$R_Y = \frac{\text{Complete angle for one revolution}}{\text{(Pulses per rev.)(Gear ratio)}} = \frac{360 \text{ deg.}}{(5000)(19/1)} \cong 0.004 \,\text{deg}.$$

Rotational resolution around pitch axis;

$$R_p = \frac{\text{Complete angle for one revolution}}{(\text{Pulses per rev.})(\text{Gear ratio})} = \frac{360 \text{ deg.}}{(5000)(19/1)} \cong 0.004\,\text{deg}.$$

Rotational resolution around roll axis;

$$R_R = \frac{\text{Complete angle for one revolution}}{(\text{Pulses per rev.})(\text{Gear ratio})} = \frac{360 \text{ deg.}}{(5000)(5.4/1)} \cong 0.013\,\text{deg}.$$

Translational resolution*;*

The translational resolution of the 7 DOF haptic device can be calculated by applying the selected encoder's counter angles and transmission ratios in the forward kinematics equations. As a result of these calculations, one encoder pulse increment, which corresponds to a maximum displacement of the wrist point, gives the translational resolution of the haptic device. The maximum displacement of the wrist point occurs in the most extended form of the device; therefore, all of the calculations should be performed in this case. For this purpose, all possible calculations have been performed with the wrist points (r) regarding the joint variables (q) in the forward kinematics for each encoder separately;

Translational resolution for the first encoder corresponding to the first joint variable in the most extended form of the device;

$$q = \begin{bmatrix} 0 \\ 60 \\ 0 \\ 45 \end{bmatrix} \Rightarrow r = \begin{bmatrix} 457.9878 \\ 0 \\ 60.2952 \end{bmatrix} \xrightarrow[\left(\frac{\text{counter angle}}{\text{gear ratio}}\right)]{\text{increase } \theta_1} q = \begin{bmatrix} 0.0352 \\ 60 \\ 0 \\ 45 \end{bmatrix} \Rightarrow r = \begin{bmatrix} 457.9877 \\ 0.2824 \\ 60.2953 \end{bmatrix}$$

$\Delta\bar{r}$=0.2825mm $\Leftrightarrow$ Translational resolution for θ_1

Translational resolution for the second encoder corresponding to the second joint variable in the most extended form of the device;

$$q=\begin{bmatrix}0\\60\\0\\45\end{bmatrix} \Rightarrow r=\begin{bmatrix}457.9878\\0\\60.2952\end{bmatrix} \xrightarrow[\left(\frac{\text{counter angle}}{\text{gear ratio}}\right)]{\text{increase } \theta_2} q=\begin{bmatrix}0\\60.0439\\0\\45\end{bmatrix} \Rightarrow r=\begin{bmatrix}458.0339\\0\\59.9443\end{bmatrix}$$

$\Delta\bar{r}$=0.3439mm $\Leftrightarrow$ Translational resolution for θ_2

Translational resolution for the third encoder corresponding to the third joint variable in the most extended form of the device;

$$q=\begin{bmatrix}0\\60\\0\\90\end{bmatrix} \Rightarrow r=\begin{bmatrix}341.5064\\0\\-91.5064\end{bmatrix} \xrightarrow[\left(\frac{\text{counter angle}}{\text{gear ratio}}\right)]{\text{increase } \theta_3} q=\begin{bmatrix}0\\60\\0.0703\\90\end{bmatrix} \Rightarrow r=\begin{bmatrix}341.5063\\0.3067\\-91.5062\end{bmatrix}$$

$\Delta\bar{r}$=0.3067mm $\Leftrightarrow$ Translational resolution for θ_3

Translational resolution for the forth encoder corresponding to the fourth joint variable in the most extended form of the device;

$$q=\begin{bmatrix}0\\60\\0\\90\end{bmatrix} \Rightarrow r=\begin{bmatrix}341.5064\\0\\-91.5064\end{bmatrix} \xrightarrow[\left(\frac{\text{counter angle}}{\text{gear ratio}}\right)]{\text{increase } \theta_4} q=\begin{bmatrix}0\\60\\0\\90.0439\end{bmatrix} \Rightarrow r=\begin{bmatrix}341.3404\\0\\-91.6021\end{bmatrix}$$

$\Delta\bar{r}$=0.1916mm $\Leftrightarrow$ Translational resolution for θ_4

When the results are examined, the translational and rotational resolution of the 7 DOF haptic device can be given as;

Translational resolution: 0.35 mm
Rotational resolution around yaw axis: 0.004 degree
Rotational resolution around pitch axis: 0.004 degree
Rotational resolution around roll axis: 0.013 degree

The affects such as deflection and backlash are not considered in the calculation of these values. The effective resolution of the device can be tested when the control system is completed.

CHAPTER 6

RESULTS AND CONCLUSIONS

6.1 Results

At the end of this study, a 7 DOF haptic device is designed and manufactured. One of the major objectives of this study was to obtain a larger workspace compared to other similar haptic devices. Therefore, a 7 DOF hybrid mechanism is preferred. Obtained results are provided in Table 6.1.

Along with increased workspace, in order to increase the usability of a haptic device, one has to consider the backdrive friction and the stiffness of the system in order to decrease the apparent mass at the tool tip. Backdrive friction consideration has implications on motor and transmission mechanism selections. In order to reach desired peak forces/toques and maximum continuous forces/torques, transmission ratios cannot be selected more than 10 due to high backdrive friction. As a result, high torque motors have to be selected. However, high torque motors are heavy, and in order to lower the apparent mass at the tip point, some motors are used as counterweight. Backlash is very important consideration in haptic device design. Motion from the motors should be transmitted to haptic pen without any gaps. Any possible gaps in haptic devices may cause errors in simulation. In our design, cable driven transmission systems are used to minimize all possible backlash. Stiffness is another design consideration in order to achieve a realistic and robust simulation by using a

haptic device. To increase stiffness in this system, a hybrid mechanism is preferred and light weight strong materials are preferred such as aluminum, polyamide and carbon rods.

Table 6.1 Design Criterion Results of the 7 DOF Haptic Device

Design Criterion	**Results**
Workspace	More than a half sphere with radius 50 cm
Peak Force	10 N
Peak Torque	500 Nmm yaw, pitch and 130 Nmm roll
Maximum Continuous Force	1.5 N
Maximum Continuous Torque	85 Nmm yaw, pitch and 25 Nmm roll
Stiffness	1N/mm
Backlash	Very low with cable driven transmission system
Apparent mass at tip point	150 gram
Translational resolution	0.35 mm
Rotational resolution	0.004 deg. around yaw and pitch axis 0.013 deg. around roll axis

As a result, all design criteria are satisfied except maximum continuous torque. This is related to the last three mini-motor torques and gear ratios. High gear ratios cannot be selected due to increased backdrive friction. Due to size restrictions and desired low apparent mass at the tool tip, motor sizes cannot be increased. Available mini-motors couldn't reach torque values that are higher than the values presented in Table 6.1. In order to increase these torques values, special brushless DC mini-motors can be used in the future work. Due to the limited

budget, these motors could not be included in this study. With increased budget, another recommended improvement on this system will be to increase the resolution of motors. Resolution values given in Table 6.1 are calculated values and they should be tested after completing control of the device. Backdrive friction is not presented at Table 6.1, because it can be measured after completing control of device by using a force feedback sensor.

6.2 Conclusions

Virtual reality technology is developing in parallel with the computer and robotics technology. This development in virtual reality technology requires new haptic devices that serve very different application areas. Most effective factor in haptic device adaptation for different applications is the workspace and working capability of haptic devices. In literature, all designed haptic devices have maximum 6 degrees of freedom. In order to increase workspace of these devices, their link lengths should be increased, however, increasing link lengths have a negative effect on inertia and stiffness. In this thesis, a new 7 degrees of freedom haptic device is designed. As desired, by increasing the degrees of freedom, this design increased the workspace of the haptic device without altering the link lengths. In this design, 4 brushless DC motors and 3 DC mini-motors are used. Starting from the base of the device, first four links are actuated with brushless DC motors. They provide required forces at the tip point and they are also used to balance all moving parts as counter weights. Last three links are actuated by using 3 minimotors that provide the required torques at this point. Kinematics model of 7 DOF haptic device looks like a human arm mechanism. As a conclusion, our design has 20 % extra workspace with these effective link lengths and more flexible working capability due to 7 degrees of freedom as compared with the other haptic devices.

This thesis concentrated only on mechanical design of the device. In the future, control of this device will be performed. Additional hardware such as motor

amplifiers, data acquisition cards and force feedback device will be integrated in to this system for control purposes. Since this 7 DOF haptic device is a redundant manipulator, its control requires optimization. First goal in the control of the device is to sense any created virtual object in the virtual environment. Secondly, it will be adapted to different applications. For this purpose, different optimization techniques will be selected according to effective workspaces and various application areas.

REFERENCES

[1] Webster M. Webster's 9th new collegiate dictionary. Spring field, MA: Merriam-Webster; (1985).

[2] Burdea GC., "Force and touch feedback for virtual reality." John Wiley; (1996).

[3] Jungwon Yoon and Jeha Ryu, "Design and Analysis of a New Haptic Device Using a Parallel Mechanisim." Proceedings of the 2000 IEEE/RSJ International Conference on Intellegent Robots and Systems, (2000).

[4] Colgate, J.E., "Issues in the Haptic Display of Tool Use." Proceeedings of the 1995 IEEE/RSJ International Conference on Intellegent Robots and Systems, Pittsburgh, PA, pp. 140-145, (1995).

[5] Bejczy, A. and Salisbury, J.K., "Controlling remote manipulators through kinesthetic coupling." Computers in Mechanical Engineering, 2(1):281-290 (1983).

[6] Craig R. Carignan, Kevin R. Cleary, "Closed-Loop Force Control for Haptic Simulation of Virtual Environments." Haptic-e, Volume.1, Number 2, pp. 1-12, (1999).

[7] Salisbury, J.K. and Mandayam A. Srinivasan, "PHANTOM-Based Haptic Interaction with Virtual Objects." IEEE Computer Graphics and Applications; Volume 17, Number 5, pp. 6-10; September-October (1997).

[8] http://www.sensable.com/products/phantom_ghost/phantompremium.asp, 10.01.2005.

[9] http://www.mpb-technologies.ca/mpbt/haptics/hand_controllers/freedom/ freedom. html, 10.01.2005.

[10] http://www.immersion.com/3d/products/cyber_force.php**,** 10.01.2005.

[11] http://www.forcedimension.com/fd/avs/home/products/6-dof_delta, 10.01.2005.

[12] http://www.fcs-cs.com/robotics/products/hapticmaster, 10.01.2005.

[13] R. Lindemann and D. Tesar, "Construction and Demonstration of a 9-String 6-DOF Force Reflecting Joystick for Telerobotics." NASA International Conference on Space Telerobotics, (4): 55-63 (1989).

[14] M. Ishii and M. Sato, "A 3D Spatial Interface Device Using Tensed Strings." Presence-Teleoperators and Virtual Environments, MIT Press, Cambridge, MA, 3(1): 81-86 (1994).

[15] P. J. Berkelman, R. L. Hollis, and S. E. Salcudean, "Interacting with Virtual Environments using a Magnetic Levitation Haptic Interface." International Conference on Intelligent Robots and Systems, IROS '95, Pittsburgh, August, (1995).

[16] http://www.utoronto.ca/atrc/rd/vrml/haptics.html**,** 10.01.2005.

[17] http://www.eca.ac.uk/tacitus/haptic.htm**,** 10.01.2005.

[18] A. Fisch, C. Mavroidis, Y. Bar-Cohen, and J. Melli-Huber, “Haptic Devices for Virtual Reality, Telepresence and Human Assistive Robotics.” Haptic and Telepresence Robotics, Chapter 4, ibid, pp. 73-101.

[19] R. E. Ellis, O. M. Ismaeil, M. G. Lispett, “Design and Evaluation of a High Performance Haptic Interface.” Robotica 14: 321-327, (1996).

[20] Millman, P., Colgate, J.E. “Design of a four degree of freedom force reflecting manipulandum with a specified force/torque workspace.” IEEE International Conference an Robotics and Automation, Sacremento, CA, pp. 1488-1493 (April 1991).

[21] Townsend, W., “The effect of transmission design on force-controlled manipulator performance.” Ph. D. Thesis, Massachusetts Institute of Technology, (April 1988).

[22] David T. Burns, “Design of A Six Degree of Freedom Haptic Device.” MS. Thesis, Northwestern University, (Agust 1996).

[23] Özgören, M.K., “Application of Exponential Rotation Matrices to the Kinematic Analysis of Manipulators.” in: Proceedings, Seventh World Congress on the Theory of Machines and Mechanisms, Seville, Spain, (1987).

[24] Özgören, M.K., “Topological analysis of 6-joint serial manipulators and their inverse kinematics solutions.” Mechanism and Machine Theory 37 (2002) 511-547.

[25] Özgören, M.K., “Position and Velocity Related SingularityAnalysis of Manipulators.” in Proceedings, Nineth World Congress on the Theory of Machines and Mechanisms, Milan, Italy, (1995).

[26] http://www.manufacturingcenter.com/dfx/archives/0499/499motut.asp, 01.10.2005.

[27] R. Parekh, “Microchip AN887 AC Induction Motor Fundamentals.” Microchip Techmology. Inc. (2003).

[28] P. Yedamele, “Microchip AN885 Brushless DC (BLDC) Motor Fundamentals.” Microchip Techmology. Inc. (2003).

[29] Özgören, M.K., ME 522 “Principle of Robotic” Lecture Notes, METU, Ankara, Turkey, (2004).

[30] V. Hayward, P.Gregorio, O. Greenish, M. Doyon, “Freedom-7: A High Fidelity Seven With Application To Surgical Training”, Preprints of ISER’97, Barcelona Spain (June 15-18 1997).

[31] Marco Ceccarelli, Giuseppe Carbone “A stiffness analysis for CaPaMan (CassinoParallel Manipulator)”, Mechanism and Machine Theory 37 (2002) 427–439, Received 3 January 2001; accepted 10 December 2001.

APPENDIX A

SELECTED MOTOR AND PROPERTIES

A.1 FIRST SELECTED MOTOR

MAXON EC-max 40 Brushless DC Motor – 120 WATT

(Serial number: 283830)

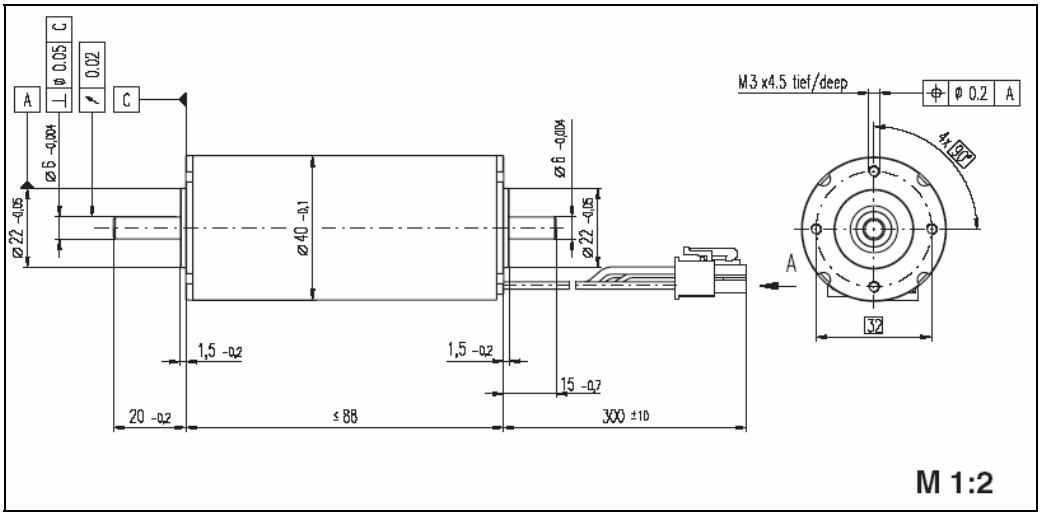

Motor Data (provisional)			
1	Assigned power rating	W	120
2	Nominal voltage	Volt	48.0
3	No load speed [1]	rpm	10000
4	Stall torque [1]	mNm	2190
5	Speed / torque gradient [1]	rpm / mNm	4.61
6	No load current [1]	mA	306
7	Terminal resistance phase to phase	Ohm	0.999
8	Max. permissible speed	rpm	12000
9	Max. continuous current at 5000 rpm [1]	A	4.8
10	Max. continuous torque at 5000 rpm	mNm	186
11	Max. efficiency[1]	%	85
12	Torque constant	mNm / A	45.5
13	Speed constant	rpm / V	210
14	Mechanical time constant	ms	4.9
15	Rotor inertia	gcm²	101
16	Terminal inductance phase to phase	mH	0.196
17	Thermal resistance housing-ambient	K / W	3.5
18	Thermal resistance winding-housing	K / W	0.29
19	Thermal time constant windings	s	3.8
20	Thermal time constant stator	s	952

A.2 SECOND AND THIRD SELECTED MOTORS

MAXON EC-max 40 Brushless DC Motor – 70 WATT

(Serial number: 283869)

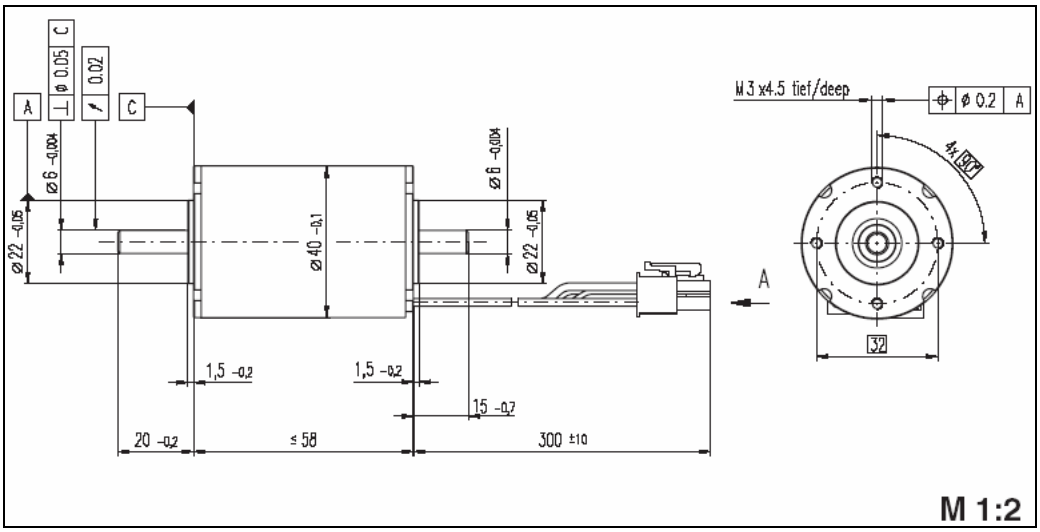

Motor Data (provisional)			
1	Assigned power rating	W	70
2	Nominal voltage	Volt	48.0
3	No load speed [1]	rpm	9080
4	Stall torque [1]	mNm	640
5	Speed / torque gradient [1]	rpm / mNm	14.3
6	No load current [1]	mA	124
7	Terminal resistance phase to phase	Ohm	3.75
8	Max. permissible speed	rpm	12000
9	Max. continuous current at 5000 rpm [1]	A	1.92
10	Max. continuous torque at 5000 rpm	mNm	84.9
11	Max. efficiency[1]	%	82
12	Torque constant	mNm / A	50
13	Speed constant	rpm / V	191
14	Mechanical time constant	ms	7.7
15	Rotor inertia	gcm²	51
16	Terminal inductance phase to phase	mH	0.468
17	Thermal resistance housing-ambient	K / W	4.6
18	Thermal resistance winding-housing	K / W	0.54
19	Thermal time constant windings	s	4.1
20	Thermal time constant stator	s	917

A.3 FOURTH SELECTED MOTOR

MAXON EC-max 30 Brushless DC Motor – 60 WATT

(Serial number: 272763)

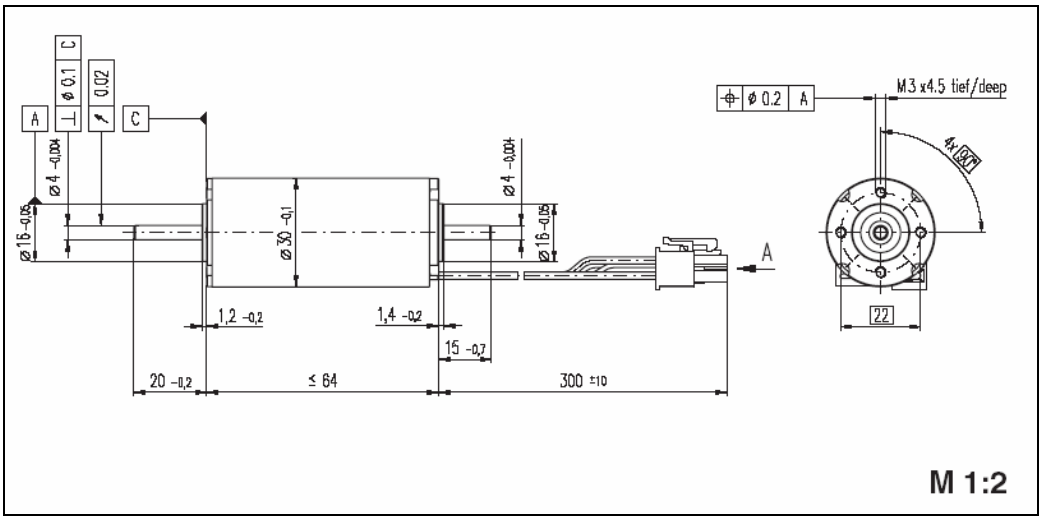

Motor Data (provisional)			
1	Assigned power rating	W	60
2	Nominal voltage	Volt	24.0
3	No load speed [1]	rpm	9740
4	Stall torque [1]	mNm	447
5	Speed / torque gradient [1]	rpm / mNm	22.1
6	No load current [1]	mA	210
7	Terminal resistance phase to phase	Ohm	1.25
8	Max. permissible speed	rpm	15000
9	Max. continuous current at 5000 rpm [1]	A	2.98
10	Max. continuous torque at 5000 rpm	mNm	60.8
11	Max. efficiency[1]	%	80
12	Torque constant	mNm / A	23.3
13	Speed constant	rpm / V	410
14	Mechanical time constant	ms	5.1
15	Rotor inertia	gcm²	21.9
16	Terminal inductance phase to phase	mH	0.124
17	Thermal resistance housing-ambient	K / W	5.9
18	Thermal resistance winding-housing	K / W	0.55
19	Thermal time constant windings	s	2.8
20	Thermal time constant stator	s	669

A.4 SELECTED THREE MINIMOTORS

MAXON RE-16 Brushes DC Motor – 4.5 WATT

(Serial number: 118730)

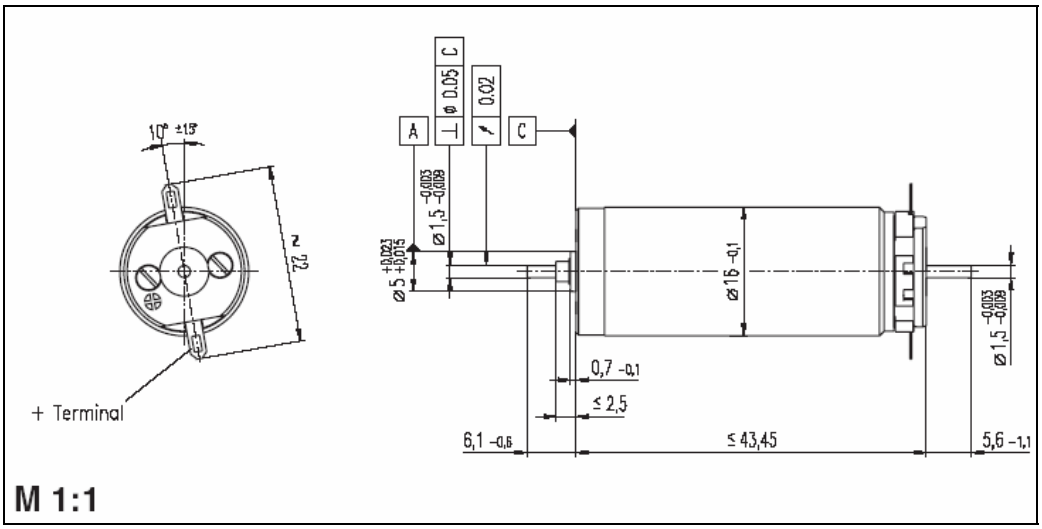

Motor Data			
1	Assigned power rating	W	4.5
2	Nominal voltage	Volt	12.0
3	No load speed	rpm	13900
4	Stall torque	mNm	28.8
5	Speed / torque gradient	rpm / mNm	490
6	No load current	mA	46
7	Starting current	mA	3550
8	Terminal resistance	Ohm	3.38
9	Max. permissible speed	rpm	16000
10	Max. continuous current	mA	614
11	Max. continuous torque	mNm	4.98
12	Max. power output at nominal voltage	mW	10200
13	Max. efficiency	%	78
14	Torque constant	mNm / A	8.11
15	Speed constant	rpm / V	1180
16	Mechanical time constant	ms	7
17	Rotor inertia	gcm²	1.27
18	Terminal inductance	mH	0.11
19	Thermal resistance housing-ambient	K / W	30
20	Thermal resistance rotor-housing	K / W	8.5
21	Thermal time constant winding	s	10

APPENDIX B

SELECTED GEARHEADS AND PROPERTIES

B.1 SELECTED GEARHEADS FOR THREE MINIMOTORS

MAXON PLENATARY GEARHEAD GP 16 A

(Serial number: 110321-110322)

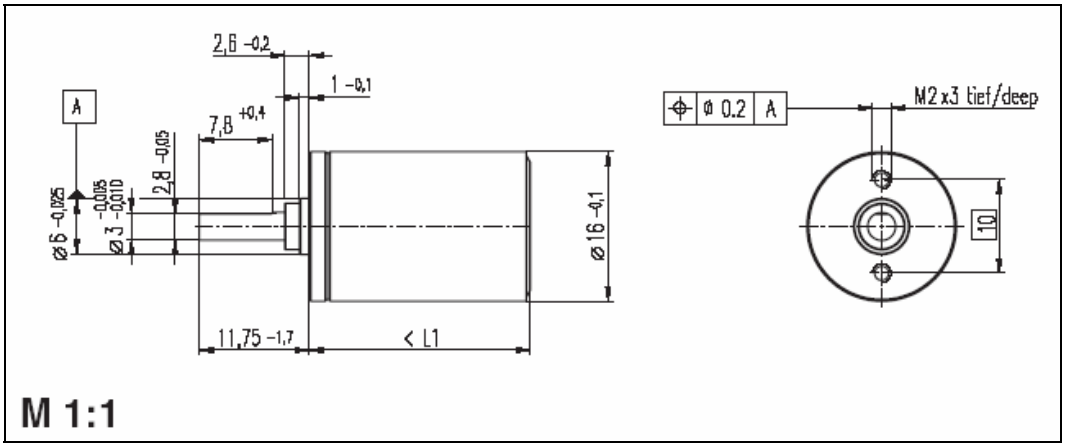

			110321	110322
Gearhead Data				
1	Reduction		5.4 : 1	19 : 1
2	Reduction absolute		$^{27}/_{5}$	$^{3249}/_{169}$
3	Max. motor shaft diameter	mm	1.5	2
4	Number of stages		1	2
5	Max. continuous torque	Nm	0.10	0.15
6	Intermittently permissible torque	Nm	0.150	0.225
7	Max. efficiency	%	90	81
8	Weight	g	20	23
9	Average backlash no load	°	0.7	0.8
10	Mass inertia	gcm²	0.08	0.05
11	Gearhead length L1	mm	15.5	19.1

APPENDIX C

SELECTED ENCODERS AND PROPERTIES

C.1 SELECTED ENCODERS FOR FIRST FOUR BRUSHLESS MOTORS

MAXON DIGITAL MR ENCODER

(Serial number: 225787)

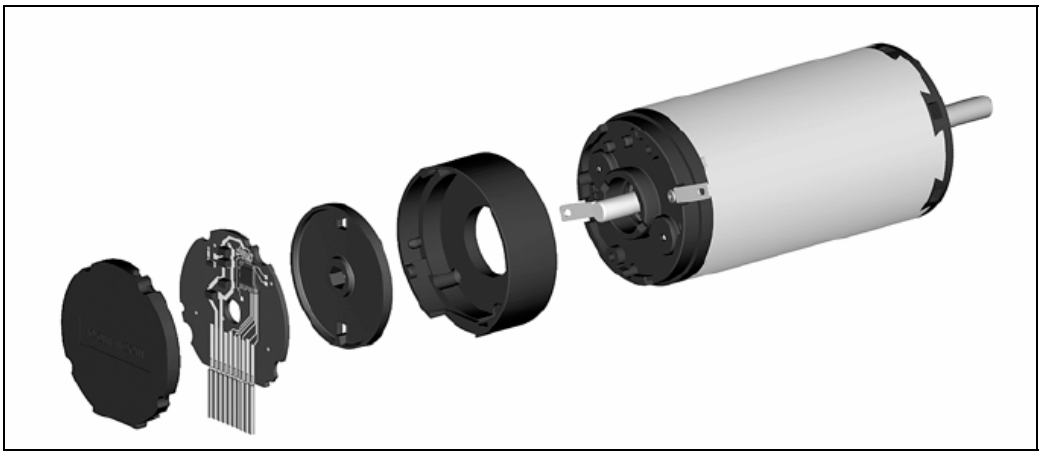

	225787
Type	
Counts per turn	1024
Number of channels	3
Max. operating frequency (kHz)	320

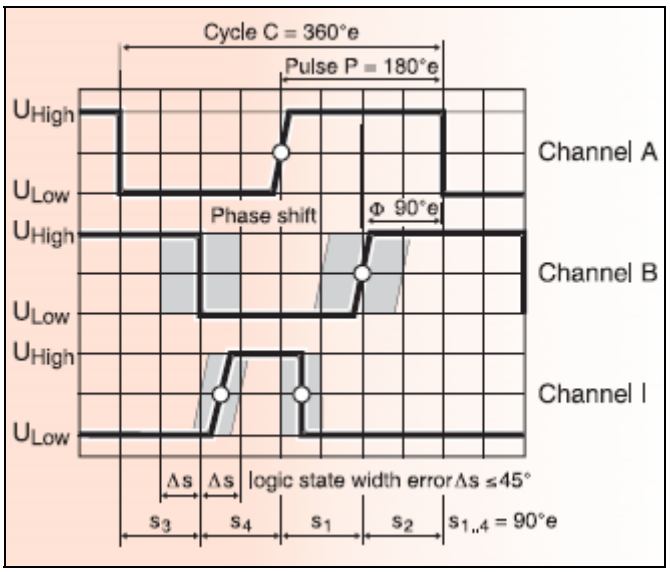

C.2 SELECTED ENCODERS FOR LAST THREE MINIMOTORS

SCANCON DIGITAL ENCODER

(Serial number: 2MCH)

Only 16mm in diameter and up to 5000 ppr. -True lines.

Option; ribbon cable + IDC. View sec. 20, p. 10

CHARACTERISTICS

ENCODER TYPE	Micro hollow shaft encoder
SMD - TECHNOLOGY	Strong compact electronics
HIGH IP-RATING	Std. IP 64 (with IDC; IP 50)
LOW CURRENT CONSUMPTION	To be connected directly to PLC'S and counters
SHORT CIRCUIT PROTECTION	Thermal shut down at 155°C
POWER SUPPLY	5V ± 10%
STRONG MEC. CONSTRUCTION	Based on 2 precision ball bearings for industrial environment

APPENDIX D

TECHNICAL DRAWINGS

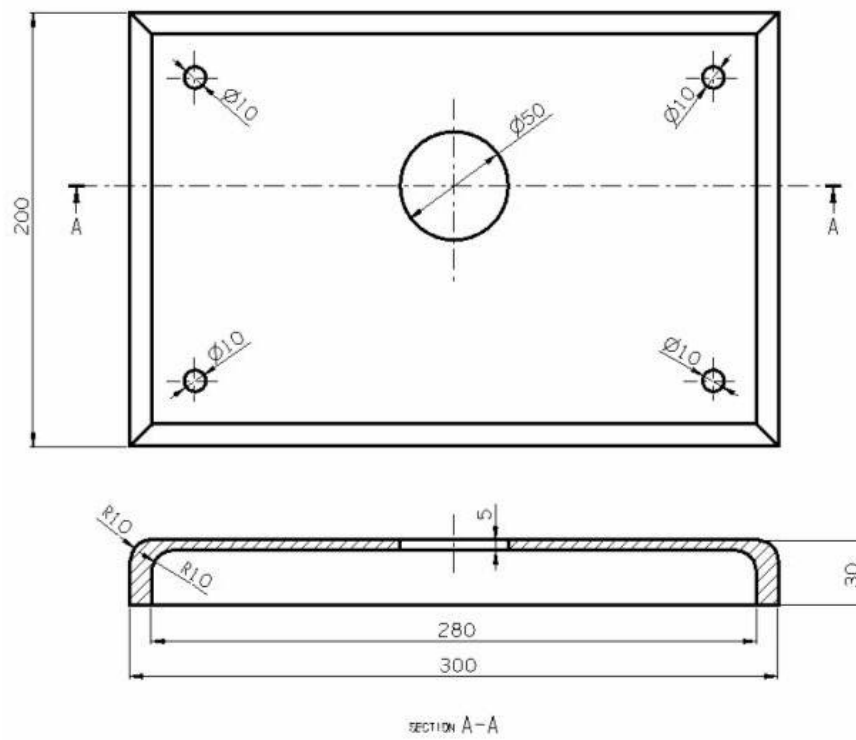

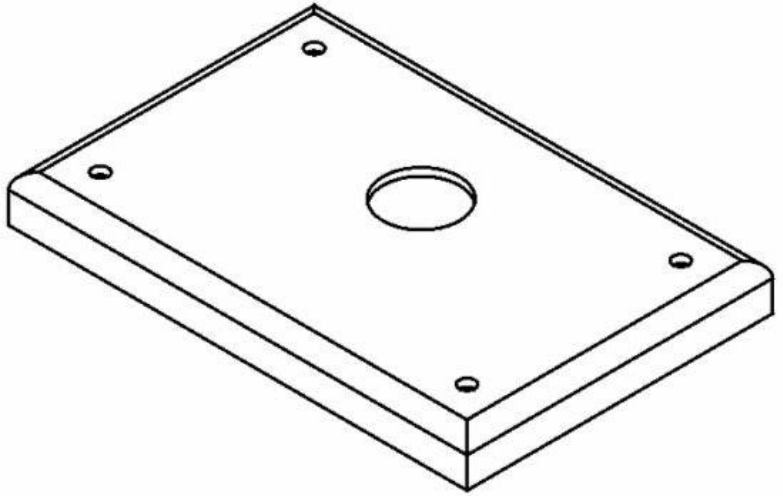

Middle East Technical University Mechanical Eng. Dept.		
Designer ÖZGÜR BAŞER	Size A4	Part Name: BASE 1
Approved İLHAN KONUKSEVEN	D 1	Mat. : Steel

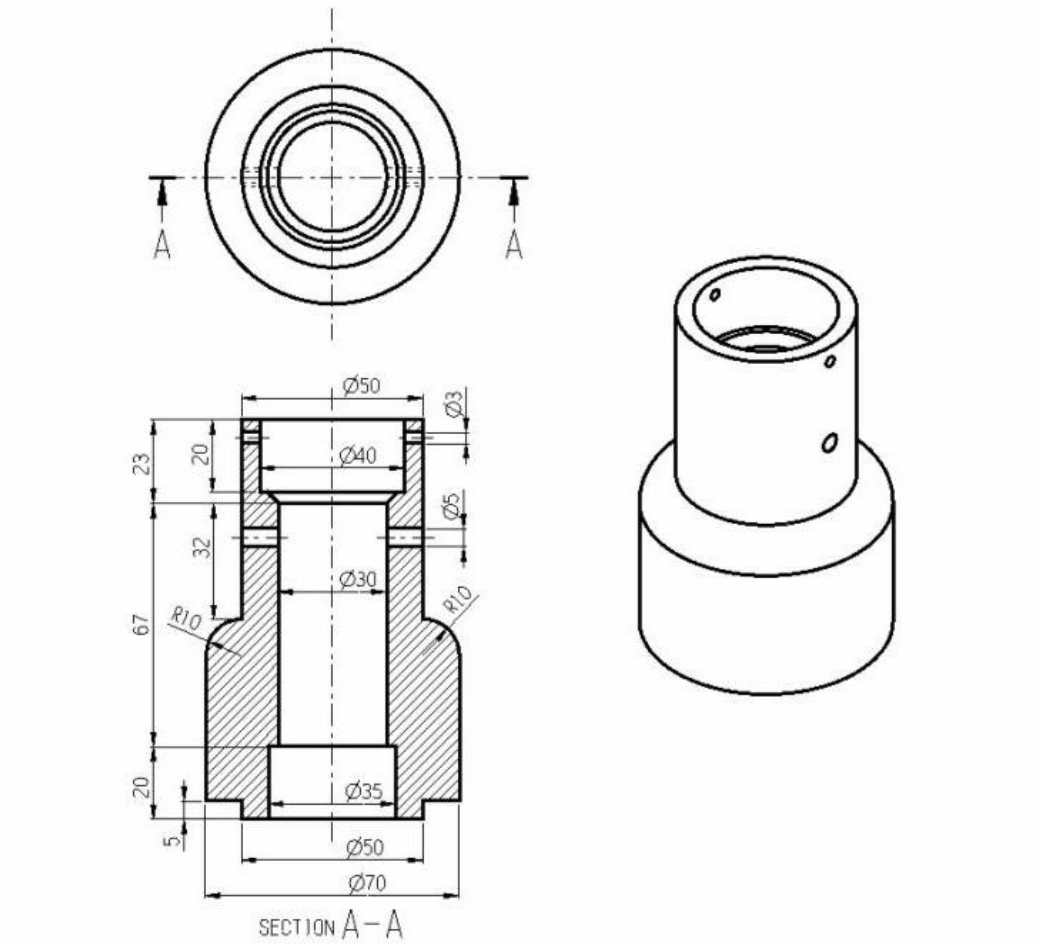

Middle East Technical University Mechanical Eng. Dept.		
Designer ÖZGÜR BAŞER	Size A4	Part Name: BASE 2
Approved İLHAN KONUKSEVEN	D 2	Mat. : Steel

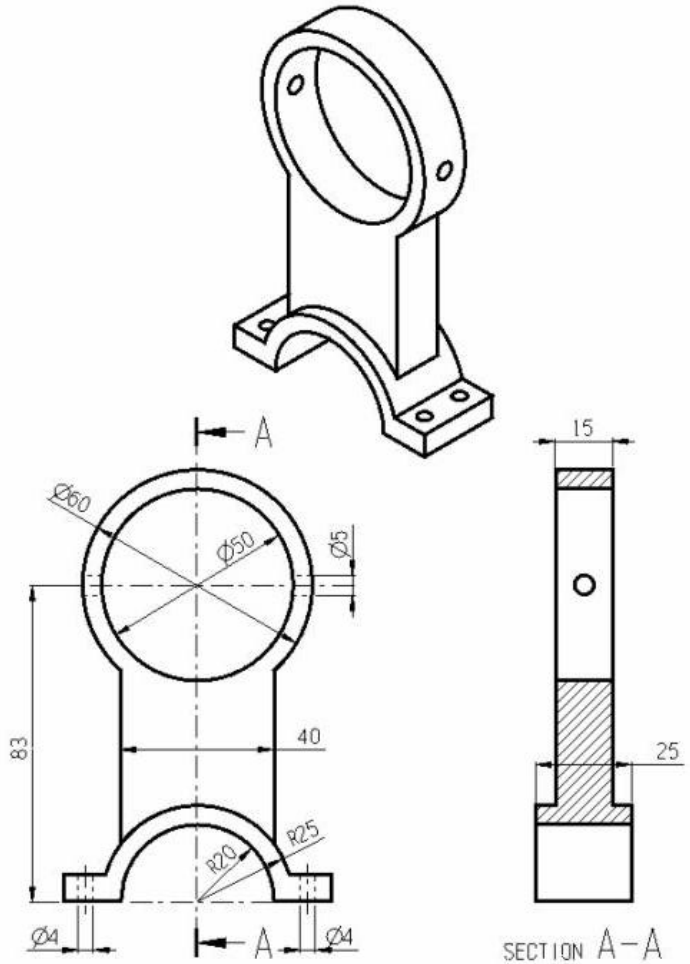

Middle East Technical University Mechanical Eng. Dept.		
Designer ÖZGÜR BAŞER	Size A4	Part Name: BASE 3
Approved İLHAN KONUKSEVEN	D 3	Mat. : Steel

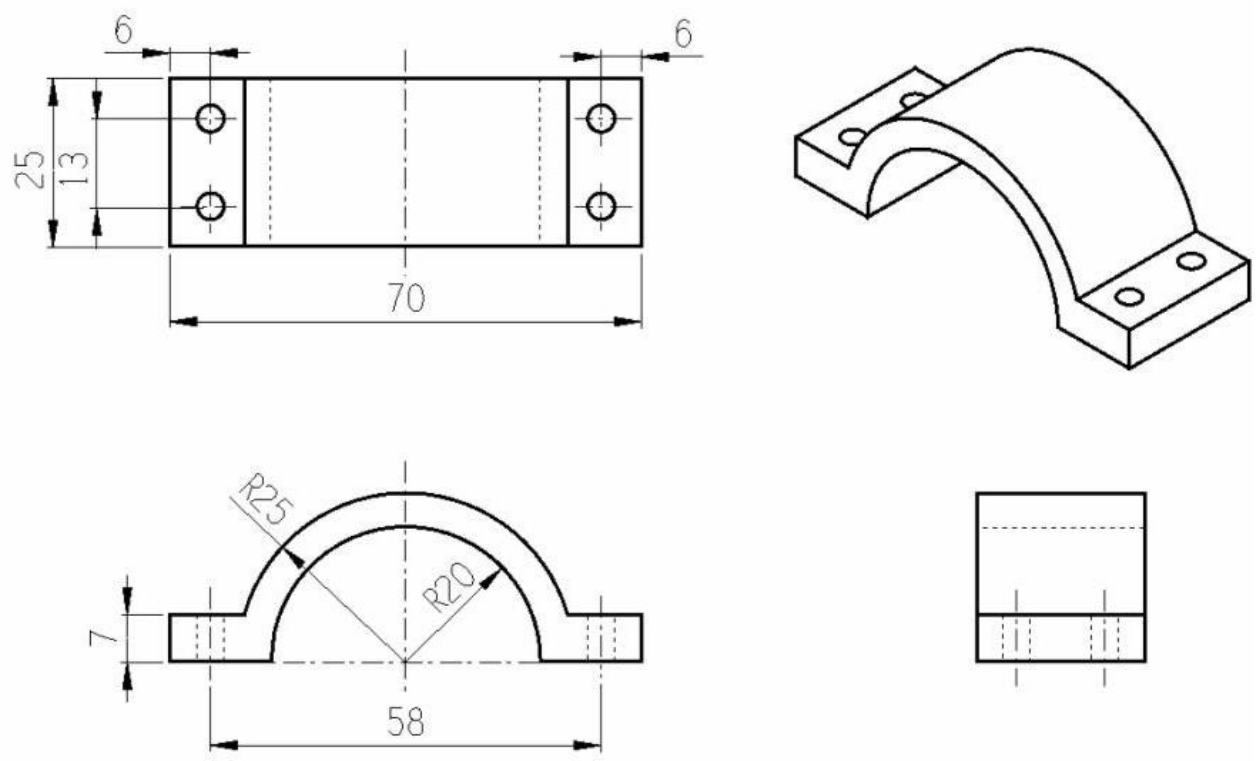

Middle East Technical University Mechanical Eng. Dept.		
Designer ÖZGÜR BAŞER	Size A4	Part Name: BASE 4
Approved İLHAN KONUKSEVEN	D 4	Mat. : Steel

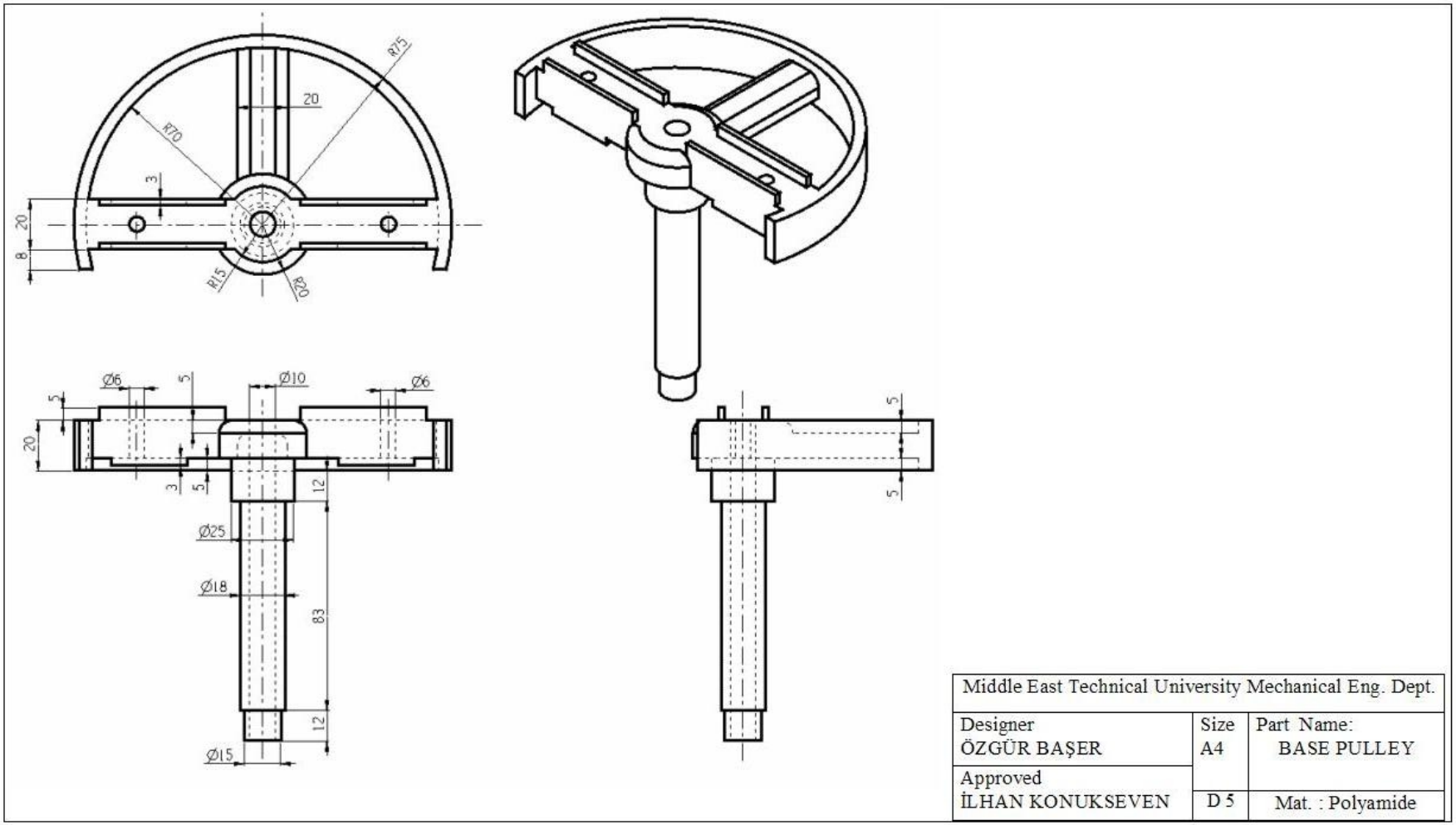

Middle East Technical University Mechanical Eng. Dept.		
Designer ÖZGÜR BAŞER	Size A4	Part Name: BASE PULLEY
Approved İLHAN KONUKSEVEN	D 5	Mat. : Polyamide

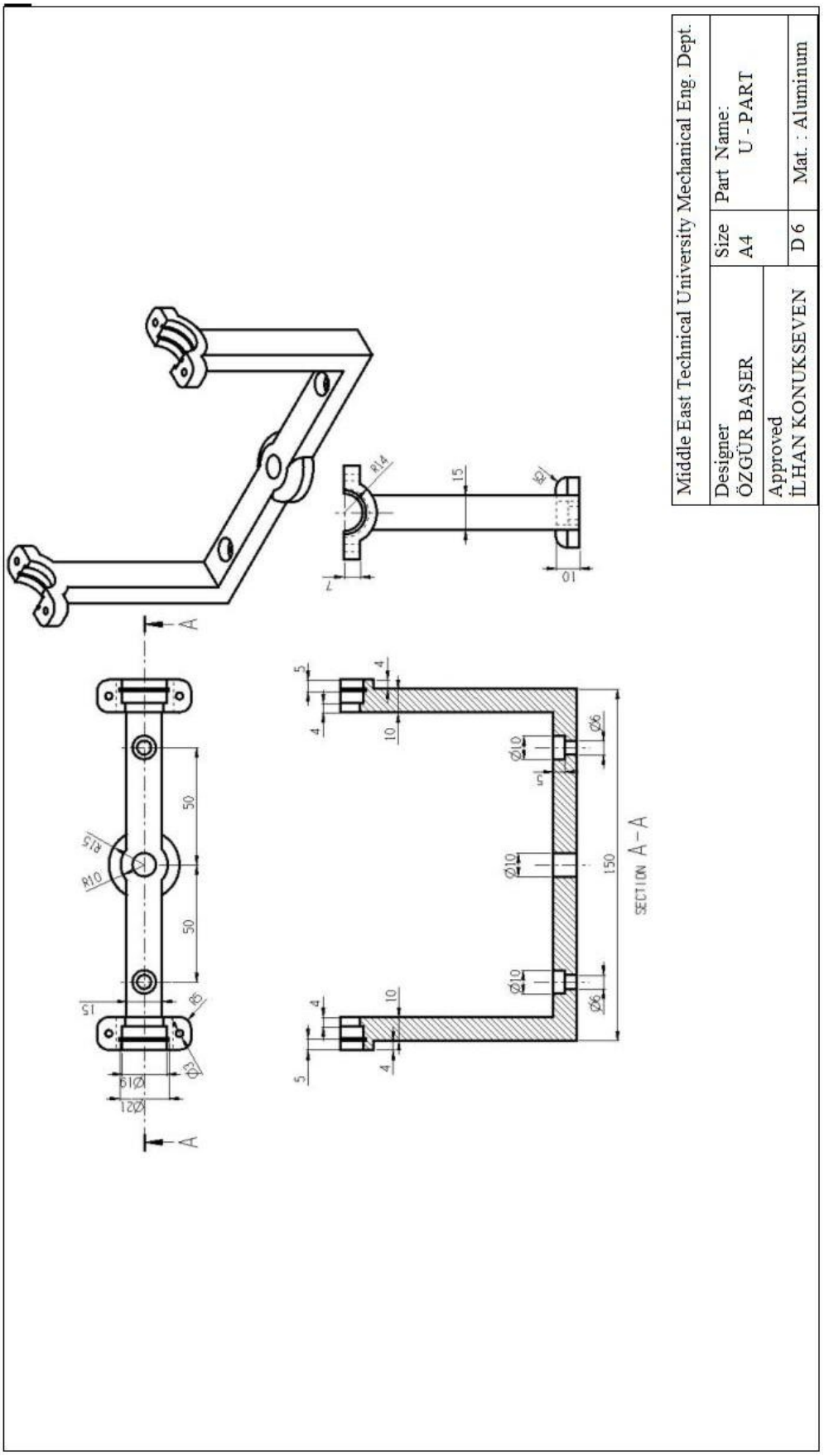
Middle East Technical University Mechanical Eng. Dept.
Designer
ÖZGÜR BAŞER
Size
A4
Part Name:
U - PART
Approved
İLHAN KONUKSEVEN
D 6
Mat. : Aluminum
SECTION A-A

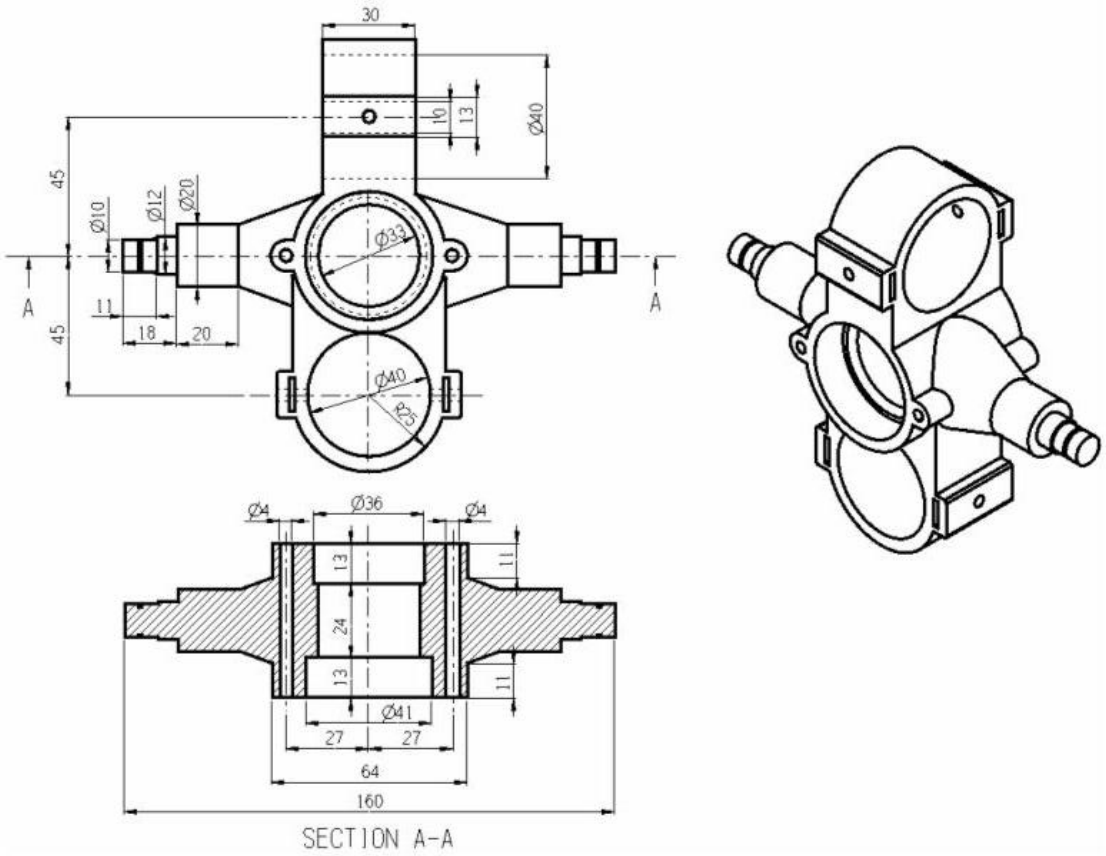

Middle East Technical University Mechanical Eng. Dept.		
Designer ÖZGÜR BAŞER	Size A4	Part Name: MIDDLE SHAFT
Approved İLHAN KONUKSEVEN	D 7	Mat. : Polyamide

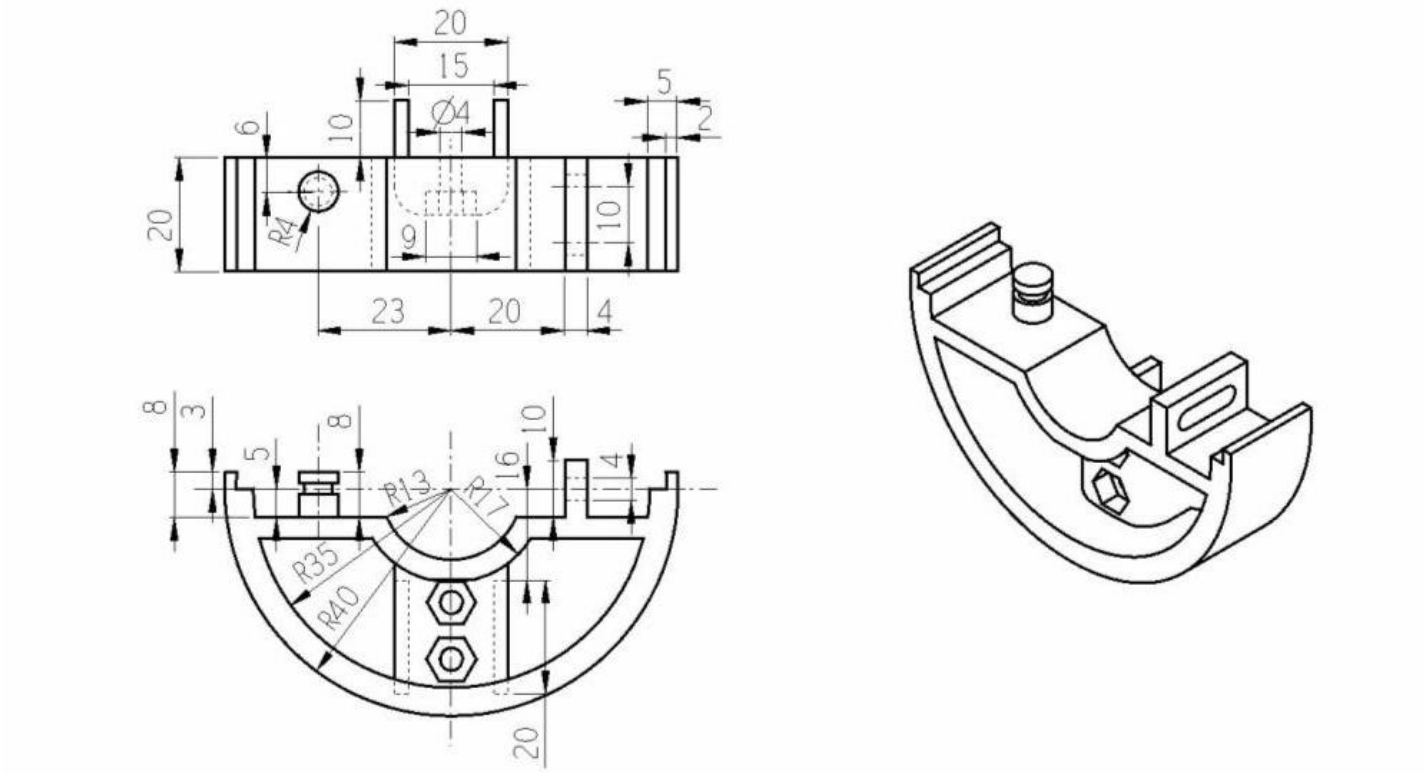

Middle East Technical University Mechanical Eng. Dept.		
Designer ÖZGÜR BAŞER	Size A4	Part Name: PULLEY 2
Approved İLHAN KONUKSEVEN	D 8	Mat. : Polyamide

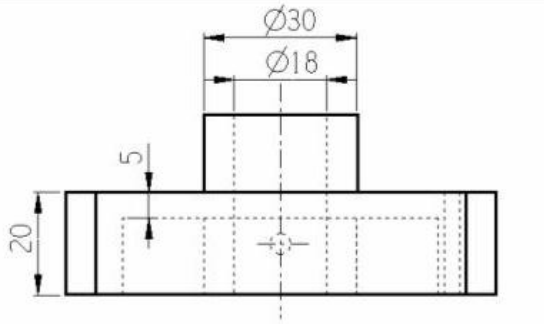

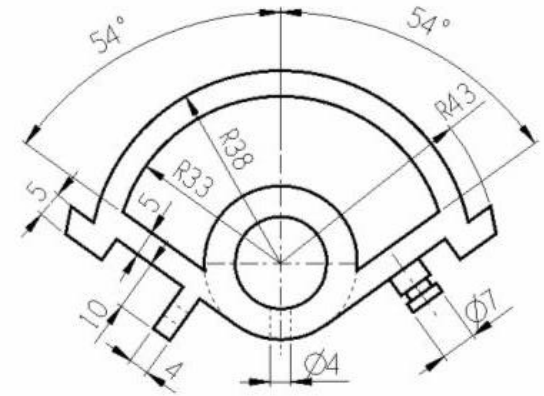

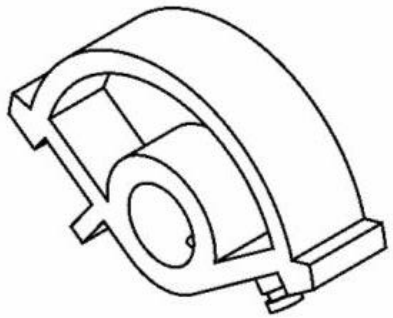

Middle East Technical University Mechanical Eng. Dept.		
Designer ÖZGÜR BAŞER	Size A4	Part Name: PULLEY 3
Approved İLHAN KONUKSEVEN	D 9	Mat. : Polyamide

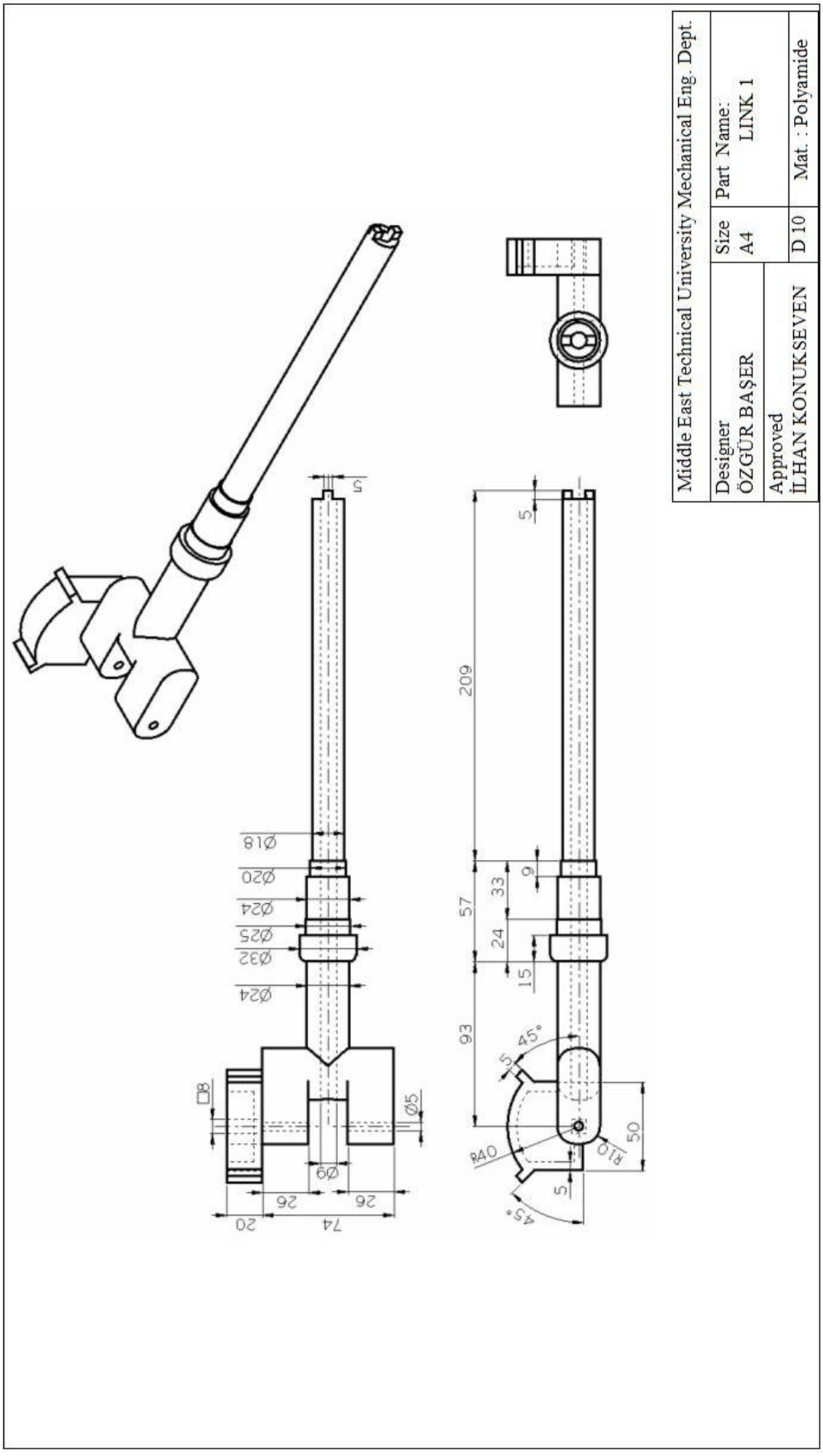
Middle East Technical University Mechanical Eng. Dept.
Designer
ÖZGÜR BAŞER
Size
A4
Part Name:
LINK 1
Approved
İLHAN KONUKSEVEN
D 10
Mat. : Polyamide
209
57
33
24
15
9
93
5
45°
50
R40
R10
74
26
20
Ø9
Ø5
Ø18
Ø20
Ø24
Ø25
Ø32

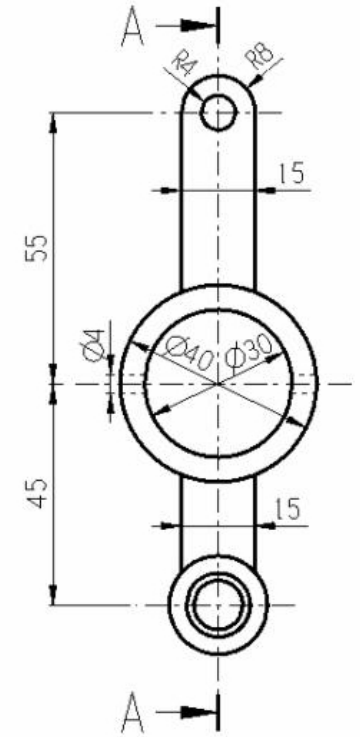

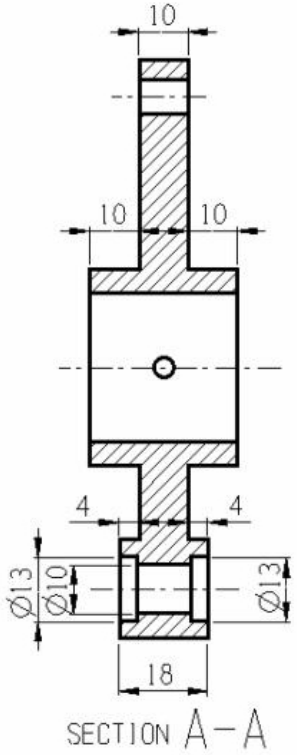

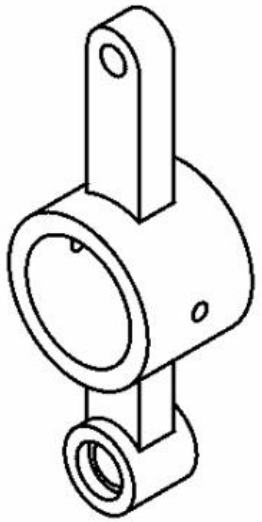

Middle East Technical University Mechanical Eng. Dept.		
Designer ÖZGÜR BAŞER	Size A4	Part Name: LINK 2
Approved İLHAN KONUKSEVEN	D 11	Mat. : Steel

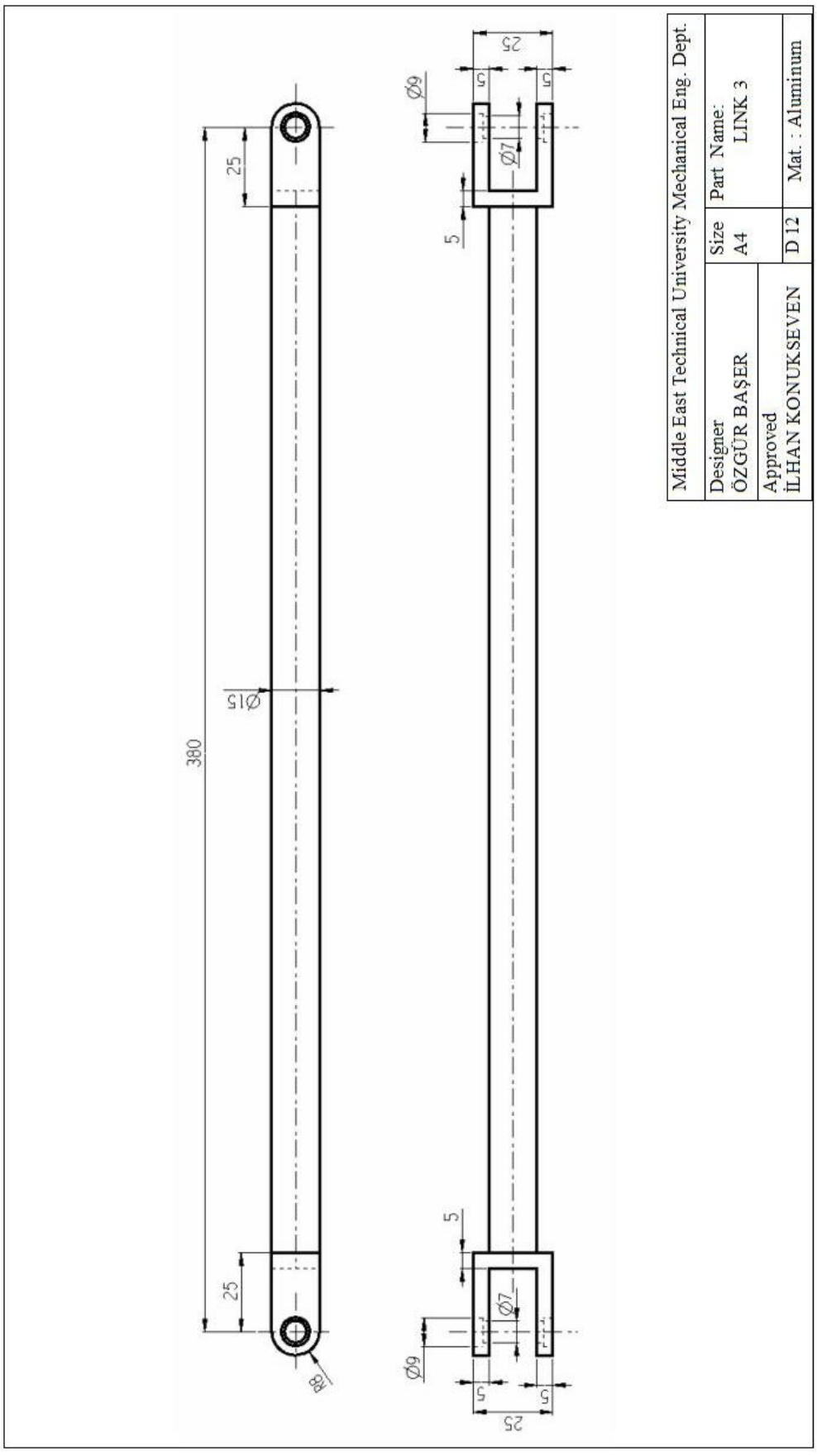
Middle East Technical University Mechanical Eng. Dept.
Designer
ÖZGÜR BAŞER
Approved
İLHAN KONUKSEVEN
Size
A4
D 12
Part Name:
LINK 3
Mat. : Aluminum
380
25
25
Ø15
Ø8
Ø9
Ø7
5
25

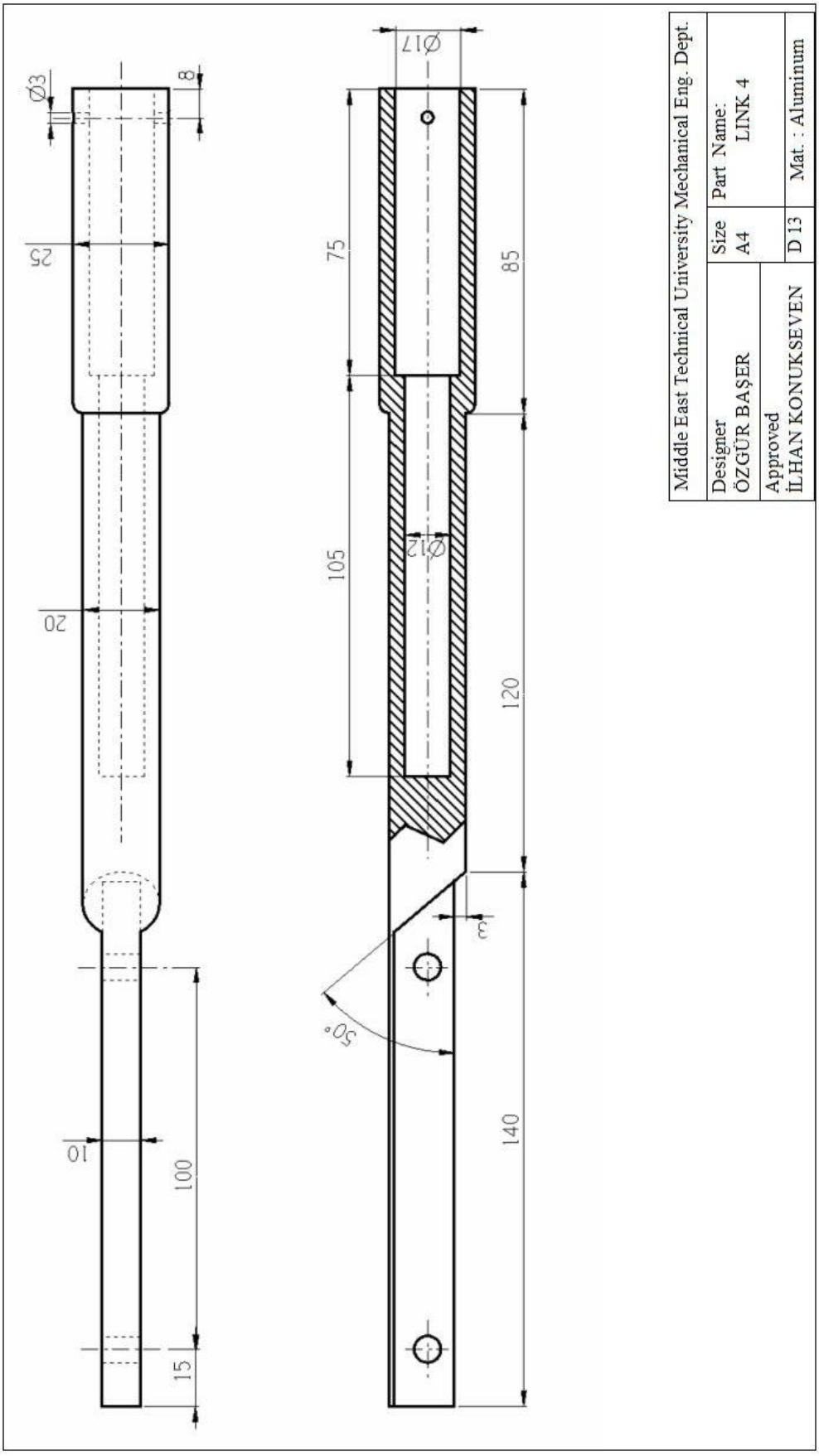
Ø3
8
25
20
10
100
15
Ø17
75
85
105
Ø12
120
3
50°
140
Middle East Technical University Mechanical Eng. Dept.
Designer
ÖZGÜR BAŞER
Approved
İLHAN KONUKSEVEN
Size
A4
D 13
Part Name:
LINK 4
Mat. : Aluminum

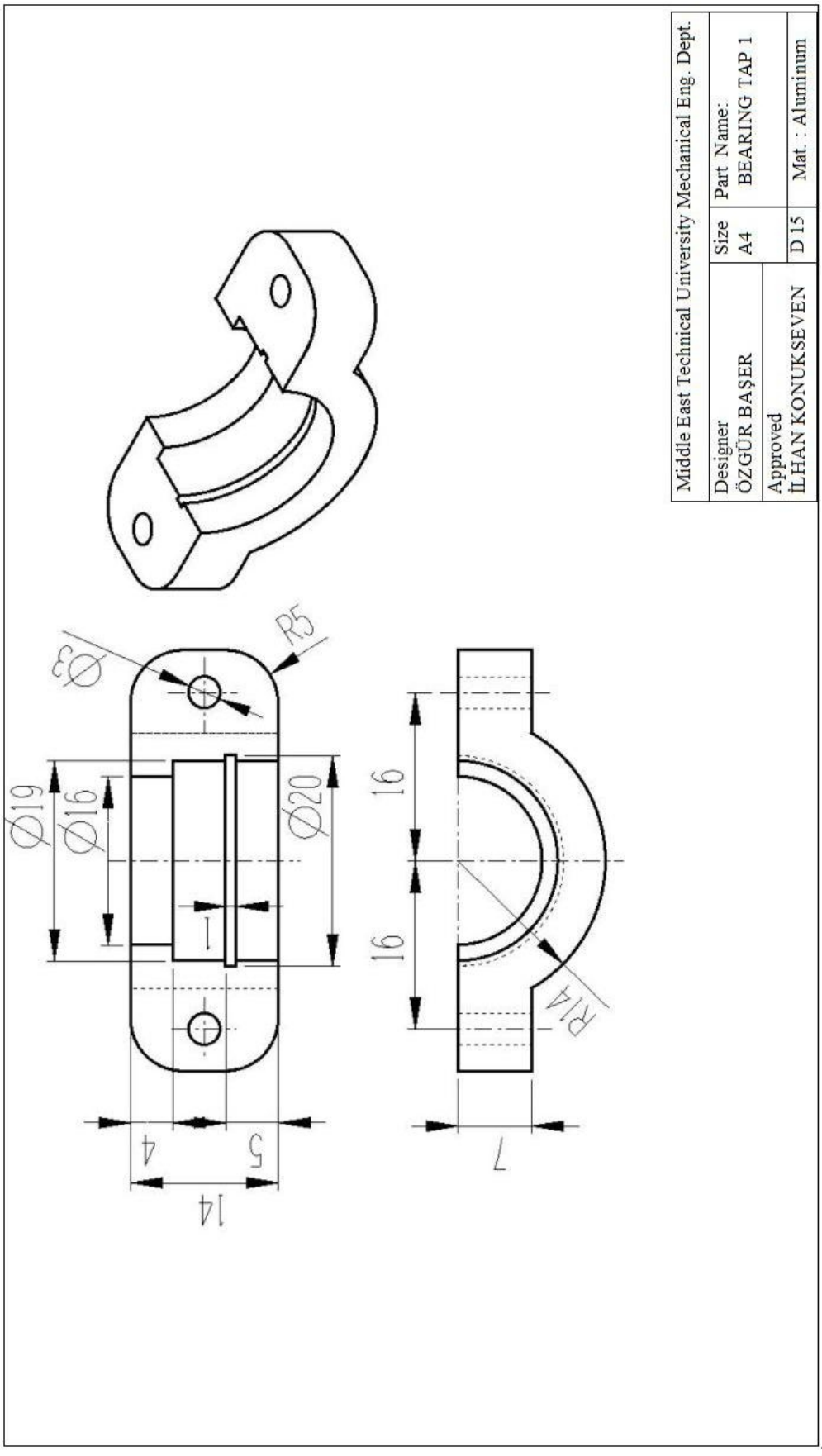
Middle East Technical University Mechanical Eng. Dept.
Designer ÖZGÜR BAŞER
Size A4
Part Name: BEARING TAP 1
Approved İLHAN KONUKSEVEN
D 15
Mat. : Aluminum
R5
Ø3
Ø19
Ø16
Ø20
16
16
R14
7
4
5
14

,

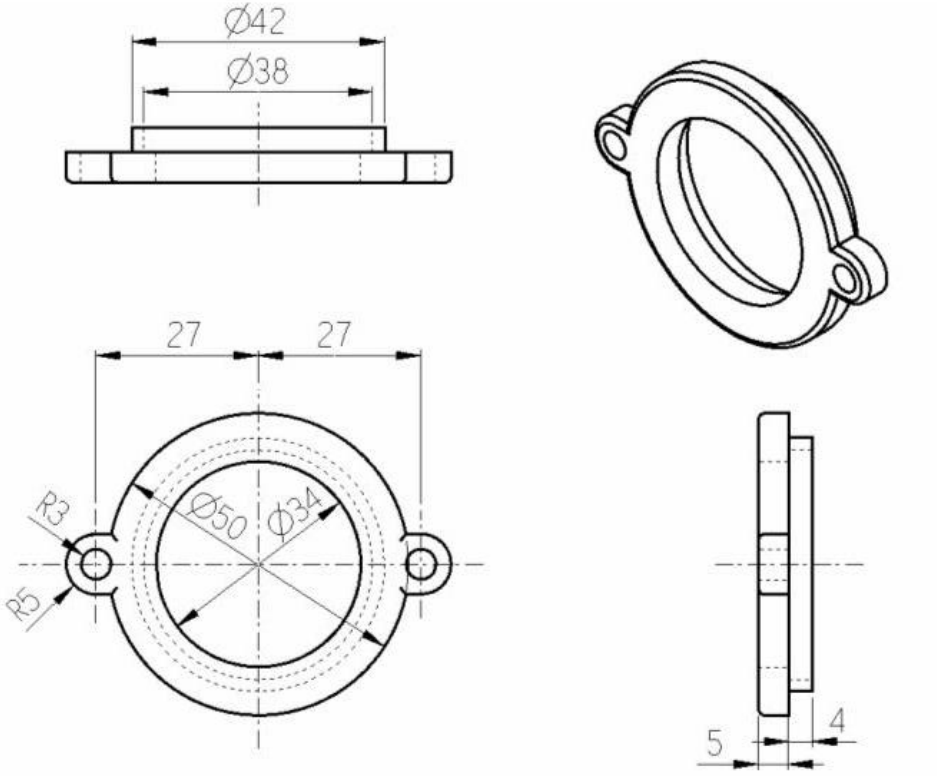

Middle East Technical University Mechanical Eng. Dept.		
Designer ÖZGÜR BAŞER	Size A4	Part Name: BEARING TAP 2
Approved İLHAN KONUKSEVEN	D 16	Mat. : Polyamide

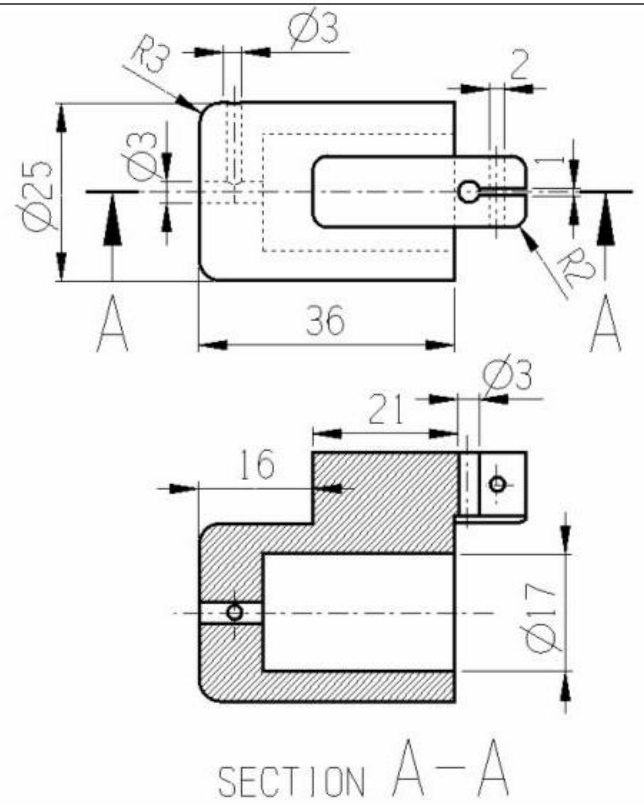

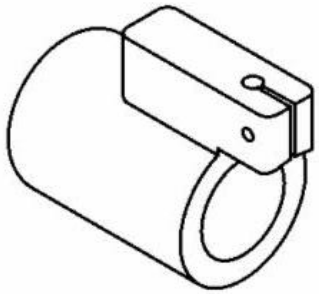

Middle East Technical University Mechanical Eng. Dept.		
Designer ÖZGÜR BAŞER	Size A4	Part Name: MINIMOTOR TAP 1
Approved İLHAN KONUKSEVEN	D 17	Mat. : Polyamide

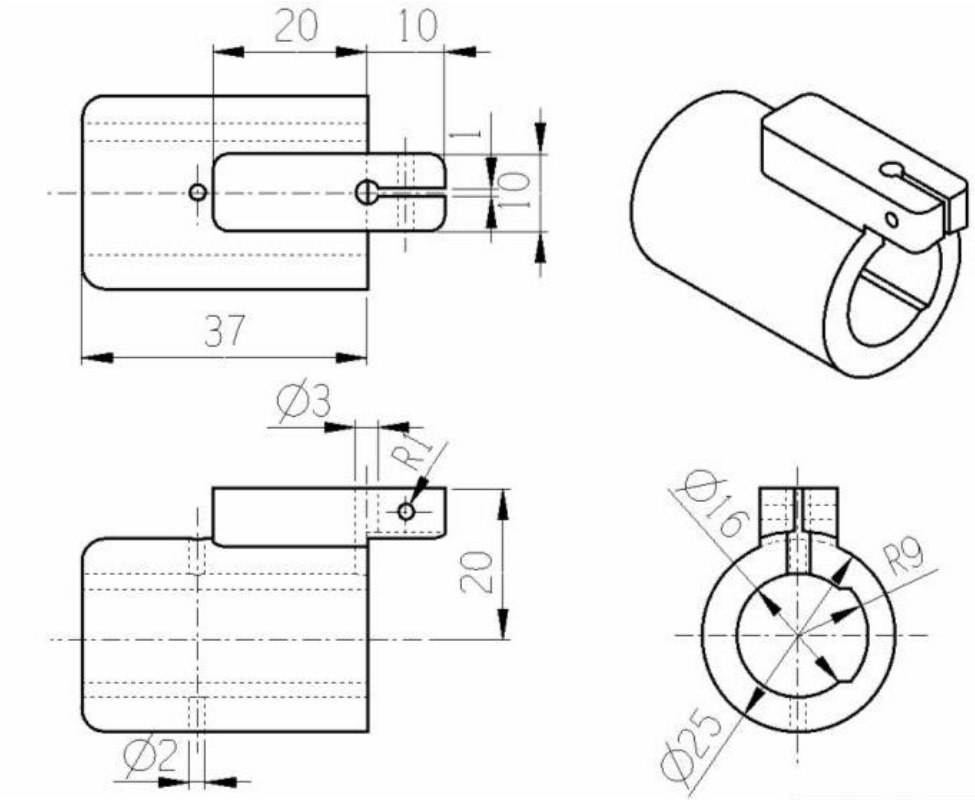

Middle East Technical University Mechanical Eng. Dept.		
Designer ÖZGÜR BAŞER	Size A4	Part Name: MINIMOTOR TAP 2
Approved İLHAN KONUKSEVEN	D 18	Mat. : Polyamide

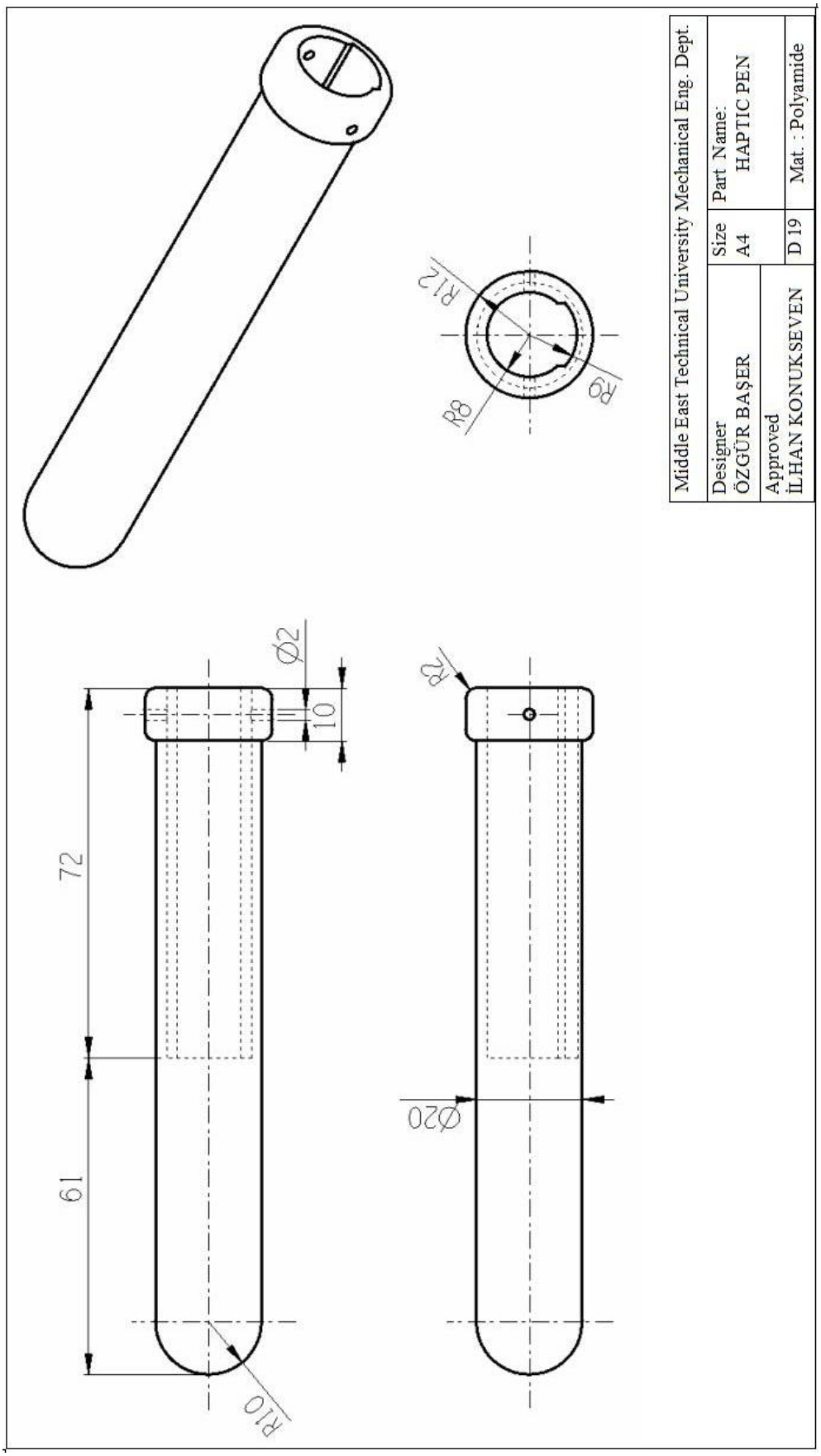
Middle East Technical University Mechanical Eng. Dept.
Designer
ÖZGÜR BAŞER
Approved
İLHAN KONUKSEVEN
Size
A4
D 19
Part Name:
HAPTIC PEN
Mat. : Polyamide
R12
R9
R8
Ø2
10
72
61
R10
R2
Ø20

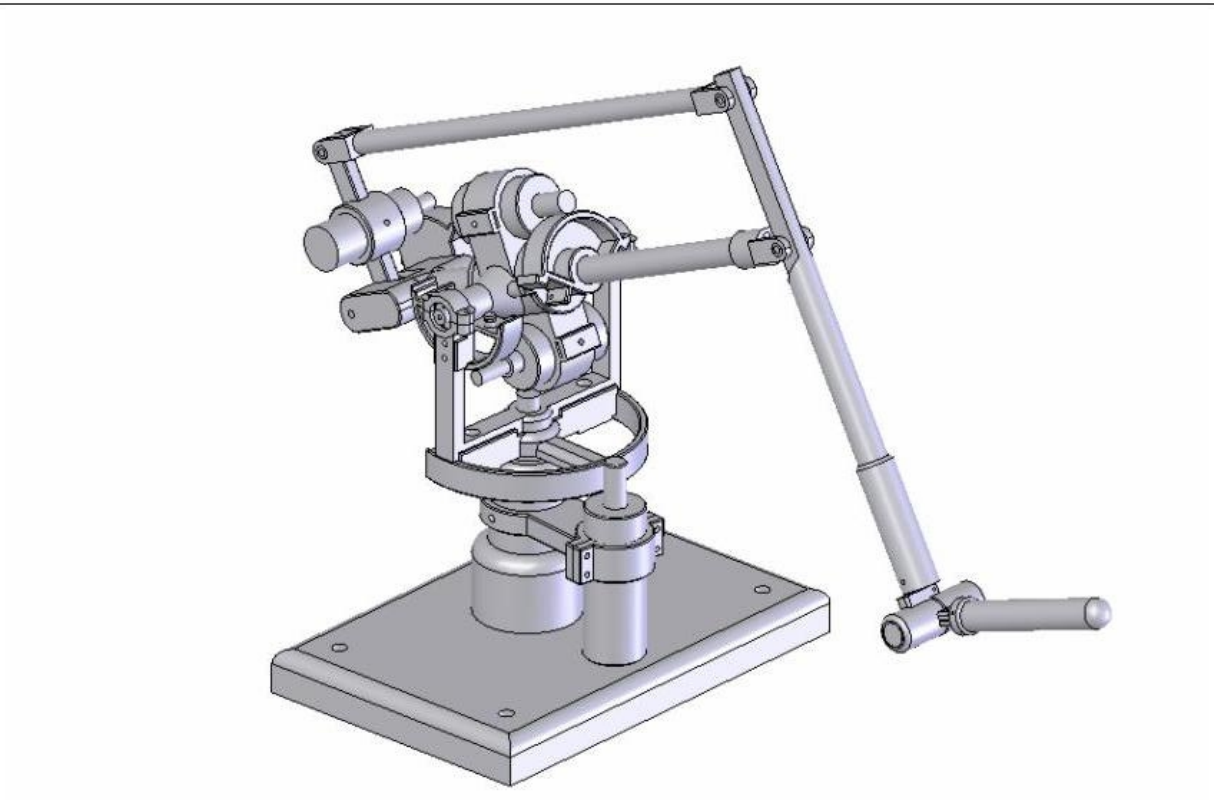

Middle East Technical University Mechanical Eng. Dept.		
Designer ÖZGÜR BAŞER	Size A4	Part Name: 7 DOF HAPTIC DEVICE
Approved İLHAN KONUKSEVEN	D 20	Mat. : Polyamide